

On the phase diagram of extensive-rank symmetric matrix denoising beyond rotational invariance

Jean Barbier^{1,*} Francesco Camilli^{1,†} Justin Ko^{2,‡} and Koki Okajima^{3,§}

¹*The Abdus Salam International Centre for Theoretical Physics
Strada Costiera 11, 34151 Trieste, Italy*

²*University of Waterloo*

Department of Statistics and Actuarial Science, 200 University Ave W, Waterloo, ON, N2L 3G1, Canada

³*The University of Tokyo*

Department of Physics, Graduate School of Science, 7-3-1 Hongo, Tokyo 113-0033, Japan

Matrix denoising is central to signal processing and machine learning. Its statistical analysis when the matrix to infer has a factorised structure with a rank growing proportionally to its dimension remains a challenge, except when it is rotationally invariant. In this case the information theoretic limits and an efficient Bayes-optimal denoising algorithm, called rotational invariant estimator [1, 2], are known. Beyond this setting few results can be found. The reason is that the model is not a usual spin system because of the growing rank dimension, nor a matrix model (as appearing in high-energy physics) due to the lack of rotation symmetry, but rather a hybrid between the two.

In this paper we make progress towards the understanding of Bayesian matrix denoising when the hidden signal is a factored matrix $\mathbf{X}\mathbf{X}^\top$ that is not rotationally invariant. Monte Carlo simulations suggest the existence of a *denoising-factorisation transition* separating a phase where denoising using the rotational invariant estimator remains Bayes-optimal due to universality properties of the same nature as in random matrix theory, from one where universality breaks down and better denoising is possible by exploiting the signal’s prior and factorised structure, though algorithmically hard. We also argue that it is only beyond the transition that factorisation, i.e., estimating \mathbf{X} itself, becomes possible up to sign and permutation ambiguities. On the theoretical side, we combine mean-field techniques in an interpretable multiscale fashion in order to access the minimum mean-square error and mutual information. Interestingly, our alternative method yields equations which can be reproduced using the replica approach of [3]. Using numerical insights, we then delimit the portion of the phase diagram where this mean-field theory is reliable, and correct it using universality when it is not. Our final ansatz matches well the numerics when accounting for finite size effects.

I. INTRODUCTION

Denoising a large matrix modelled as a product of two factors is a hard problem, both algorithmically, and from the viewpoint of theoretical analysis, especially if its rank is proportional to its dimension. Its applications range from signal processing and machine learning [4, 5], representation learning [6], sparse coding [7–9], robust principal components analysis [10, 11], sub-matrix localization [12], blind source separation [13], matrix completion [14, 15], community detection [16–18], video processing [4, 19], or recommender systems [20].

In this paper we focus on the symmetric version of matrix denoising for signal matrices which have a product structure. Denoising is formulated as a Bayesian inference problem over $\mathbf{X}\mathbf{X}^\top$ given a noisy data matrix $\mathbf{Y} \in \mathbb{R}^{N \times N}$ generated as

$$\mathbf{Y} = \sqrt{\frac{\lambda}{N}} \mathbf{X}\mathbf{X}^\top + \mathbf{Z}, \quad (1)$$

where the rectangular matrix $\mathbf{X} \in \mathbb{R}^{N \times M}$ is the hidden factor (also called signal, a terminology we will also

use for $\mathbf{X}\mathbf{X}^\top$ if there is no ambiguity), $\mathbf{Z} \in \mathbb{R}^{N \times N}$ is a noise matrix drawn from the Gaussian orthogonal ensemble (GOE), i.e. with Gaussian entries $Z_{ij} = Z_{ji} \sim \mathcal{N}(0, 1 + \delta_{ij})$ and all independent. The signal \mathbf{X} has i.i.d. components $(X_{i\mu})_{i \leq N, \mu \leq M}$ drawn from a sub-Gaussian symmetric prior distribution P_X with zero mean and unit variance. The rank of $\mathbf{X}\mathbf{X}^\top$ is thus at most $\min(N, M)$.

When the prior is different than centered Gaussian, the signal $\mathbf{X}\mathbf{X}^\top$ (and thus the data) is *not* rotationally invariant. Rotational invariance means in this context that the probability $P(\mathbf{X}\mathbf{X}^\top)$ would be equal to $P(\mathbf{O}\mathbf{X}\mathbf{X}^\top\mathbf{O}^\top)$ for any $N \times N$ orthogonal matrix \mathbf{O} . The setting where the prior P_X breaks this invariance, as well as the differences this induces w.r.t. the rotational invariant Gaussian prior $P_X = \mathcal{N}(0, 1)$, is the main focus of this paper.

The low rank version of matrix estimation ($M = O(1)$ while $N \rightarrow \infty$) is called the spiked Wigner model and was introduced as a statistical model for sparse principal components analysis (PCA) [21–24]. Spiked models are largely studied both in random matrix theory [25–27] and in high-dimensional inference [28–35]. As a matter of fact, both the replica analysis [29] and the rigorous proofs [17, 30, 36–42] heavily rely on the rank of the hidden matrix being finite. This, in turn, implies that from a thermodynamic point of view the system is controlled by the value of a finite number of order parameters, identifiable with the elements of a matrix overlap $\mathbf{X}^\top \mathbf{x} / N \in \mathbb{R}^{M \times M}$, where \mathbf{x} here is a sample from the posterior measure asso-

* jbarbier@ictp.it

† fcamilli@ictp.it

‡ justin.ko@uwaterloo.ca

§ darjeeling@g.ecc.u-tokyo.ac.jp

ciated to (1). Crucially the number of order parameters in these approaches is thus $O(M^2) = O(1)$, yielding to exact tractable formulas often derived by saddle point in the replica formalism.

However, when the rank M grows proportionally to N ,

$$\frac{M}{N} \rightarrow \alpha > 0,$$

as considered in the present paper, the saddle point does not apply anymore and the problem boils down to a matrix model. Matrix models appear frequently in high energy physics, in particular in Yang-Mills theories with internal symmetry groups of diverging dimension [43], in random matrix theory approaches to quantum gravity [44, 45], quantum chromo-dynamics [46], statistical mechanics models on planar random lattices [47–50] or counting planar diagrams [51, 52]. We refer the interested reader to the review [53]. A prototypical matrix model is a partition function of the type

$$\mathcal{Z}_{\text{MM}}(\mathbf{A}) := \int_{\mathbb{H}_N} d\mathbf{F} \exp(-\text{Tr}\mathbf{F}^2 + \text{Tr}V(\mathbf{A}\mathbf{F})), \quad (2)$$

where \mathbb{H}_N is the space of Hermitian $N \times N$ matrices, $d\mathbf{F}$ denotes the Lebesgue measure over it, the source $\mathbf{A} \in \mathbb{H}_N$ and V is a function applied only to each eigenvalue of its argument: $V(\mathbf{H}) = \mathbf{O} \text{diag}(V(d_i)_{i \leq N}) \mathbf{O}^\top$ whenever $\mathbf{H} = \mathbf{O} \text{diag}((d_i)_{i \leq N}) \mathbf{O}^\top$ with unitary \mathbf{O} . The *one-matrix integral* in (2) can be solved in the large N limit by the character expansion method [54, 55], or if V is sufficiently simple by means of the HarishChandra-Itzykson-Zuber (HCIZ) integral [56, 57]. Integration over real symmetric matrices instead of Hermitian can also be considered.

The HCIZ integral is defined as

$$\mathcal{Z}_{\text{HCIZ}}(\mathbf{A}, \mathbf{B}) := \int d\mu(\mathbf{O}) \exp\left(\frac{\beta N}{2} \text{Tr} \mathbf{O} \mathbf{A} \mathbf{O}^\top \mathbf{B}\right) \quad (3)$$

where $\beta = 2$ if \mathbf{A}, \mathbf{B} are $N \times N$ Hermitian, and $\beta = 1$ if they are real symmetric. Respectively the integral is over the unitary $\mathbb{U}(N)$ or orthogonal $\mathbb{O}(N)$ group, w.r.t. the corresponding uniform Haar measure μ . Remarkably, this integral is solved in closed form [57] for any N , and its asymptotics was also computed first by Matytsin [58] and then rigorously proved in [59, 60].

The approaches to the computation of these partition functions need Lebesgue measure over the matrix elements or a rotational invariant one. This is usually what allows to integrate away the $O(N^2)$ rotational degrees of freedom, leaving only N degrees of freedom for the eigenvalues or the corresponding spectral density. If, as it occurs for (3), the exponent of the integrand stays $O(N^2)$ then a saddle point over the eigenvalues is justified. In the present paper, however, we can no longer rely on this symmetry, because it is in general broken by the prior P_X as we shall see.

Organization of the paper. In Section II we introduce the main objects under investigation with the precise definition of the problem. We also give a preview of the

theoretical and numerical results of the paper. Given the number of conjectures revolving around matrix factorisation in the extensive-rank regime, we thoroughly review relevant results in the literature about the problem.

In Section III we present the observations obtained from numerical experiments based on parallel tempering [61, 62] and annealed importance sampling (AIS) [63], as well as simple arguments showing the existence of a regime where universality in the prior cannot hold. From these findings we draw a qualitative phase diagram and, in particular, we discuss a phase transition coined *denoising-factorisation transition*, separating two regions of the phase diagram of a very different nature.

Section IV presents an effective mean-field theory able to match the numerical observations, in particular the existence of the denoising-factorisation transition. The theory will provide an approximation for both the mutual information between observations and ground truth as well as the for the minimum mean-square error using a combination of the cavity method from statistical physics, a mean-field ansatz as well as known rigorous proofs of replica symmetric formulas in high-dimensional inference. Our theoretical insights are then discussed.

Section V elaborates around the possibility to carry out factorization, namely finding \mathbf{X} alone, up to unresolvable symmetries. The picture that emerges from our numerical results is consistent with the one of Section IV.

Notations. Symbol \sim expresses that a random variable is drawn from a certain law. $X_{i\mu} \stackrel{\text{iid}}{\sim} P$ means that $(X_{i\mu})_{i,\mu}$ are independent and identically distributed according to P . For a matrix $\mathbf{x} = (x_{i\mu})$ we denote $dP_X(\mathbf{x}) = \prod_{i,\mu} dP_X(x_{i\mu})$. Vectors are columns, their transpose are rows. We denote the inner product between vectors equivalently as $\mathbf{u} \cdot \mathbf{v} = \mathbf{u}^\top \mathbf{v} = \sum_i u_i v_i$. Symbol $\stackrel{\text{D}}{=}$ means equality in law. The norm $\|\mathbf{A}\| = (\sum_{ij} A_{ij}^2)^{1/2}$ is the Frobenius norm. The limit $\lim_{N \rightarrow \infty}$ means that both N, M diverge with $M = \alpha N + o_N(1)$ and we call it the *thermodynamic limit*. $\mathcal{N}(m, \sigma^2)$ is the density of a Gaussian with mean m and variance σ^2 .

Code repository. The Monte Carlo simulations used in this paper are accessible at the following link [64].

II. SETTING

Consider the channel (1). For the information theoretical analysis, one of the main goal is the computation of the mutual information (MI) density, i.e., per signal element:

$$\frac{I(\mathbf{X}\mathbf{X}^\top; \mathbf{Y})}{MN} = \frac{\mathcal{H}(\mathbf{Y})}{MN} - \frac{\mathcal{H}(\mathbf{Y} | \mathbf{X}\mathbf{X}^\top)}{MN} = \frac{\mathcal{H}(\mathbf{Y})}{MN} - \frac{\mathcal{H}(\mathbf{Z})}{MN}$$

where the Shannon entropy density of the data is

$$\begin{aligned} -\frac{\mathcal{H}(\mathbf{Y})}{MN} &= -\frac{1}{2MN} \sum_{i \leq j} \ln(2\pi(1 + \delta_{ij})) \\ &\quad + \frac{1}{MN} \mathbb{E} \ln \int dP_X(\mathbf{x}) e^{-\frac{1}{4} \text{Tr}(\mathbf{Y} - \sqrt{\frac{\lambda}{N}} \mathbf{x} \mathbf{x}^\top)^2} \\ &= -\frac{1}{2MN} \sum_{i \leq j} \ln(2\pi(1 + \delta_{ij})) - \frac{1}{4MN} \mathbb{E} \text{Tr} \mathbf{Y}^2 \\ &\quad + \frac{1}{MN} \mathbb{E} \ln \int dP_X(\mathbf{x}) e^{\frac{1}{2} \sqrt{\frac{\lambda}{N}} \text{Tr} \mathbf{Y} \mathbf{x} \mathbf{x}^\top - \frac{\lambda}{4N} \text{Tr}(\mathbf{x} \mathbf{x}^\top)^2} \end{aligned}$$

and the one for the noise

$$\begin{aligned} -\frac{\mathcal{H}(\mathbf{Z})}{MN} &= \frac{1}{MN} \mathbb{E} \ln \left(e^{-\frac{1}{4} \text{Tr} \mathbf{Z}^2} \prod_{i \leq j} \sqrt{2\pi(1 + \delta_{ij})}^{-1} \right) \\ &= -\frac{1}{2MN} \sum_{i \leq j} \ln(2\pi e(1 + \delta_{ij})) - \frac{1}{2M}. \end{aligned}$$

Therefore the MI reads

$$\begin{aligned} \frac{I(\mathbf{X} \mathbf{X}^\top; \mathbf{Y})}{MN} &= \frac{\lambda}{4MN^2} \mathbb{E} \text{Tr}(\mathbf{X} \mathbf{X}^\top)^2 \\ &\quad - \frac{1}{MN} \mathbb{E} \ln \int dP_X(\mathbf{x}) e^{\frac{1}{2} \sqrt{\frac{\lambda}{N}} \text{Tr} \mathbf{Y} \mathbf{x} \mathbf{x}^\top - \frac{\lambda}{4N} \text{Tr}(\mathbf{x} \mathbf{x}^\top)^2}. \end{aligned} \quad (4)$$

The first term in (4) is exactly computable:

$$\frac{1}{MN^2} \mathbb{E} \|\mathbf{X} \mathbf{X}^\top\|^2 = 1 + \alpha + O(N^{-1}). \quad (5)$$

Notice that its value does not depend on the prior chosen, as long as it is factorised over the elements of \mathbf{X} , centered and it has unit second moment.

We then isolate the so-called *free entropy*

$$\frac{1}{MN} \mathbb{E} \ln \int dP_X(\mathbf{x}) e^{\frac{1}{2} \sqrt{\frac{\lambda}{N}} \text{Tr} \mathbf{Y} \mathbf{x} \mathbf{x}^\top - \frac{\lambda}{4N} \text{Tr}(\mathbf{x} \mathbf{x}^\top)^2},$$

that is the non-trivial object to compute. This is the logarithm of the partition function of a matrix model like (2) where \mathbf{F} is replaced by $\mathbf{x} \mathbf{x}^\top$ which is symmetric positive semi-definite, with linear potential V and where the data \mathbf{Y} plays the role of the source \mathbf{A} . A major difference is that the reference measure of the integral is not rotational invariant in general. This makes it impossible to use methods from matrix models.

The posterior measure correctly exploits that the signal is factorised. It is thus a probability distribution over \mathbf{x} alone. For channel (1) it reads

$$dP(\mathbf{x} | \mathbf{Y}) = \frac{\exp\left(-\frac{1}{4} \|\mathbf{Y} - \sqrt{\frac{\lambda}{N}} \mathbf{x} \mathbf{x}^\top\|^2\right)}{C(\mathbf{Y})} dP_X(\mathbf{x}), \quad (6)$$

with $C(\mathbf{Y})$ a normalization. The noise being additive Gaussian, the MI is linked to the minimum mean-square error (MMSE) on $\mathbf{X} \mathbf{X}^\top$ via the I-MMSE relation [65]:

$$\frac{d}{d\lambda} \frac{I(\mathbf{X} \mathbf{X}^\top; \mathbf{Y})}{MN} = \frac{1}{4MN^2} \mathbb{E} \|\mathbf{X} \mathbf{X}^\top - \langle \mathbf{x} \mathbf{x}^\top \rangle\|^2 \quad (7)$$

where

$$\langle \cdot \rangle = \langle \cdot \rangle_{\mathbf{Y}} := \mathbb{E}[\cdot | \mathbf{Y}]$$

is the expectation w.r.t. the posterior measure. The object appearing on the r.h.s. of (7) is a fourth of the minimum mean square error $\text{MMSE} = \text{MMSE}_N$, i.e.,

$$\begin{aligned} \text{MMSE} &:= \frac{1}{MN^2} \mathbb{E} \|\mathbf{X} \mathbf{X}^\top - \langle \mathbf{x} \mathbf{x}^\top \rangle\|^2 \\ &= \frac{1}{M} \mathbb{E} \left\| \frac{\mathbf{X} \mathbf{X}^\top}{N} \right\|^2 - \frac{1}{M} \mathbb{E} \left\| \frac{\langle \mathbf{x} \mathbf{x}^\top \rangle}{N} \right\|^2. \end{aligned} \quad (8)$$

The posterior (6) is obtained via Bayes' rule and it is taking into account all the information related to the generating process of the data: P_X , the Gaussian nature of the noise, the value of λ . Such a setting where the posterior is known exactly to the statistician is said to be *Bayes-optimal*, and as a simple consequence of the tower rule for conditional expectations one can prove the Nishimori identities. With a little abuse of notation, we denote by $\langle \cdot \rangle$ also the infinite product measure $\bigotimes_{n=1}^{\infty} \mathbb{E}[\cdot | \mathbf{Y}]$. Hence, *replicas*, namely conditionally (on \mathbf{Y}) independent samples from the posterior (6), are averaged jointly by the measure $\langle \cdot \rangle$. Now we can state the following:

Proposition 1 (Nishimori identity). *Let f be a bounded function of the observations \mathbf{Y} , the ground truth factor \mathbf{X} and of replicas $(\mathbf{x}^{(k)})_{k \leq n}$ drawn independently from the posterior (6). Then*

$$\begin{aligned} \mathbb{E}_{\mathbf{X}, \mathbf{Y}} \langle f(\mathbf{Y}; \mathbf{X}, \mathbf{x}^{(2)}, \dots, \mathbf{x}^{(n)}) \rangle \\ = \mathbb{E}_{\mathbf{Y}} \langle f(\mathbf{Y}; \mathbf{x}^{(1)}, \mathbf{x}^{(2)}, \dots, \mathbf{x}^{(n)}) \rangle. \end{aligned} \quad (9)$$

We note that the diagonal part of the observations $(Y_{ii})_{i \leq N}$ does not contribute to the MI in the thermodynamic limit $N \rightarrow \infty$. In fact, $Y_{ii} = \sqrt{\lambda/N} \|\mathbf{X}_i\|^2 + Z_{ii}$ and if the prior is factorised $\|\mathbf{X}_i\|^2/N$ can be already estimated precisely thanks to the law of large numbers. Furthermore, its value is known to a Bayes-optimal statistician. This intuition is proved by a simple interpolation argument in Appendix A. Hence, from this moment on we shall work with the equivalent channel

$$Y_{ij} = Y_{ji} = \sqrt{\frac{\lambda}{N}} \mathbf{X}_i^\top \mathbf{X}_j + Z_{ij}, \quad 1 \leq i < j \leq N. \quad (10)$$

The MI for this channel then reads

$$\frac{I(\mathbf{X} \mathbf{X}^\top; \mathbf{Y})}{MN} = \frac{\lambda}{4} - \phi_N + O(N^{-1}) \quad (11)$$

with the new free entropy

$$\phi_N := \frac{1}{MN} \mathbb{E}_{\mathbf{Y}} \ln \mathcal{Z}_{N,M}(\mathbf{Y}), \quad (12)$$

where, using the language of statistical mechanics, we introduced the partition function of the model

$$\mathcal{Z}_{N,M}(\mathbf{Y}) := \int_{\mathbb{R}^{N \times M}} dP_X(\mathbf{x}) e^{-H_N(\mathbf{x}; \mathbf{Y})}$$

with Hamiltonian (which is minus the log-likelihood) given by

$$-H_N(\mathbf{x}; \mathbf{Y}) = \sqrt{\frac{\lambda}{N}} \sum_{i < j, 1}^N Y_{ij} \mathbf{x}_i^\top \mathbf{x}_j - \frac{\lambda}{2N} \sum_{i < j, 1}^N (\mathbf{x}_i^\top \mathbf{x}_j)^2. \quad (13)$$

The Gaussian case. If the prior $P_X = \mathcal{N}(0, 1)$ then $\mathbf{X}\mathbf{X}^\top$ is a rotational invariant matrix. In this case the MI is exactly computable by means of the HCIZ integral. In particular, the first integral in (4) becomes an integral over Wishart matrices. The rotational degrees of freedom are then integrated away with (3). Following the simplifications in [66], for Gaussian prior the MMSE reads

$$\text{MMSE} = \frac{1}{\lambda\alpha} \left(1 - \frac{4\pi^2}{3} \int \rho_Y(y)^3 dy \right) + o_N(1) \quad (14)$$

where ρ_Y is a.s. the limiting (as $N \rightarrow \infty$) spectral density of \mathbf{Y}/\sqrt{N} . Integrating the I-MMSE relation (7) one gets the MI:

$$\begin{aligned} \frac{I(\mathbf{X}\mathbf{X}^\top; \mathbf{Y})}{MN} &= \frac{1}{2\alpha} \int dx dy \rho_Y(x) \rho_Y(y) \ln |x - y| \\ &+ \frac{1}{8\alpha} + o_N(1). \end{aligned} \quad (15)$$

For the numerical computation of the limiting MI for Gaussian prior and SNR λ , the most convenient approach is to use the I-MMSE relation, i.e., to numerically integrate 4 times the MMSE (14) w.r.t. $\lambda' \in [0, \lambda]$ using ρ_Y given explicitly in [66] for a Wishart signal $\mathbf{X}\mathbf{X}^\top$.

The rotational invariant estimator (RIE). We briefly recall the construction of the RIE (which could be more appropriately called rotational equivariant estimator as noted in [67]) of Ledoit and P  ch   [1] and Bun et al. [2]. Given data as in equation (1), the RIE is the best estimator diagonalizing on the eigenbasis of the data, collected in an orthogonal matrix \mathbf{O}_Y . That given, it just remains to clean the eigenvalues by means of the *shrinkage formula*

$$\xi_i(\mathbf{Y}) := \frac{\gamma_{Y,i} - 2\pi \mathbf{H}[\rho_Y](\gamma_{Y,i})}{\sqrt{\lambda}}$$

where $(\gamma_{Y,i})$ are the eigenvalues of \mathbf{Y}/\sqrt{N} , ρ_Y is the corresponding asymptotic spectral density and \mathbf{H} is the Hilbert transform of the density:

$$\mathbf{H}[\rho_Y](x) := \frac{1}{\pi} \text{P.V.} \int \frac{d\rho_Y(y)}{x - y}.$$

The RIE is then composed as

$$\Xi(\mathbf{Y}) = \mathbf{O}_Y \text{diag}((\xi_i(\mathbf{Y}))_{i \leq N}) \mathbf{O}_Y^\top.$$

Optimal denoising and the RIE for the rectangular (non-symmetric) version of the problem was proposed recently in [68–71] based on the rectangular HCIZ integral [72].

A. Our contributions

The present paper gives both numerical insights and a consistent theoretical background that provide us with a thorough description of the phase diagram of matrix denoising in the extensive-rank regime, beyond the case of rotationally invariant signal usually considered.

First of all, using annealed importance sampling and replica exchange Monte Carlo sampling we carry out extensive finite size experiments, yielding values of relevant quantities, such as the MI between data and ground truth and the MMSE. In Section III we explore the phase diagram (α, λ) with these techniques and conclude that for structured enough priors, i.e. Rademacher $P_X = \frac{1}{2}\delta_1 + \frac{1}{2}\delta_{-1}$, there must be a phase transition that we call *denoising-factorisation* transition. Our numerical evidence supports the fact that the RIE is optimal for SNRs smaller than a critical value $\lambda_c(\alpha)$, and sub-optimal for larger values. This sub-optimality can actually be proven, discarding the strong version of the universality conjecture in [67] in a portion of the phase diagram. Yet, the conjecture empirically holds before the identified phase transition. The numerics also suggest that exploiting the factorised structure in order to achieve a better performance is possible but algorithmically hard for Monte Carlo beyond a certain SNR and that one cannot outperform the RIE without a sufficiently informative initialisation,

Prompted by these results, we built a *multiscale mean-field theory* to access the MI and MMSE. Our approach relies on an original combination of various methods from spin glasses. Firstly, the cavity method [73] will allow us to reduce the exponent of the partition function from $O(MN)$ to $O(N)$. The resulting expression will need to be simplified using a suitable mean-field ansatz. Then, the replica method [74] or known rigorous results will be applicable. The theory outlined in Section IV, though being an approximation, signals a phase transition in the SNR λ and proves to be accurate after it. A striking observation is that, despite being derived with a very different method, our mean-field equations can also be obtained through Sakata and Kabashima’s replica approach with Gaussian ansatz [3] once adapted to our setting. We apply their arguments in Appendix D. By comparison with numerics we then identify the portion of phase diagram where the mean-field equations are accurate, i.e., after the transition, and show how to correct them before it based on the universality of the solution in the prior.

In summary, we provide an accurate ansatz for the mutual information and minimum mean-square error for the denoising problem of a symmetric factorised matrix which is not rotationally invariant: under the hypothesis that the *denoising-factorisation transition* $\lambda_c(\alpha)$ is unique, $\lambda \in [0, \lambda_c(\alpha))$ corresponds to the *denoising phase*, with MI equal to (15) and the RIE attaining the MMSE performance despite it does not exploit the factorised structure of the signal nor the prior. Instead, $\lambda \in (\lambda_c(\alpha), +\infty)$ is the *factorisation phase* where the

MI and MMSE are captured by a mean-field theory in agreement with Sakata and Kabashima’s method [3], and the RIE is sub-optimal. There, exploiting the factorised structure and prior becomes essential to reach optimality.

B. Related works

The information theoretical limits of matrix estimation have been intensively studied in the past two decades. A setting that is now well understood is that of the low-rank spiked models [21]. As mentioned above, if M is finite several methods are available for the computation of MI between data and signal, e.g. the replica method [74] among the non-rigorous ones, and proofs based on the analysis of spatial coupling [38, 75], the adaptive interpolation [39], the cavity method [17, 76], or large deviation arguments [77].

In recent years an interest in the statistical analysis of the more challenging proportional scaling regime, $M/N \rightarrow \alpha$ as $N \rightarrow +\infty$, has grown. Among the first works in this direction we mention [3] which proposed a replica approach with an original “Gaussian ansatz” (see Appendix D) for dictionary learning in an optimisation setting, soon followed by the concurrent works [78–80] applying the same method in a Bayesian setting similar to ours. These works, however, seem not to take into account some correlations between variables that turn out to be relevant in the high-dimensional limit, as understood in [81, 82] and further detailed by some of the previous authors [83]. As mentioned in the last section, although it may be true that in [3, 78–80] some relevant correlations are neglected for Gaussian prior, our numerical evidence strongly suggests this is not true anymore in a factorisation phase. The latter only appears when testing with discrete priors, and has thus eluded the subsequent studies listed below, that aimed at matching the formulas in [3, 78–80] with the exact value of the MI predicted for Gaussian prior in [82] by means of the asymptotic expansion of Matytsin [58]. [82] was missing a justification of their final result, that was later provided in the concurrent works [83, 84], and rigorized in [66].

The authors of [83] provide a perturbative attempt to the computation of the MI based on Plefka-Georges-Yedidia (PGY) expansion [85, 86]. The PGY formalism yields a set of MN equations, that should play the role of an approximation to a certain perturbation order of the TAP equations [87]. When comparing the PGY estimator, truncated at order 2 and 3 of the perturbative expansion, with the exact solution for Gaussian prior given by the HCIZ integral, the authors still measure a significant discrepancy, a sign that higher perturbative orders may be non-negligible. The paper [84] attempted an innovative spectral replica symmetric ansatz, yet leading to an unsatisfactory solution as it is not possible to evaluate it and it is thus hard to extract predictions from it. In the rotational invariant case, the work [88] provided an interesting approach to the denoising problem based on

the RIE. In reference [89] the authors managed to exploit rotational invariance in order to analyse the dynamics of gradient flow for the denoising of a Wishart matrix.

A step towards the phase diagram for generic prior was done in the series of works [90–92], where the authors map the model into a sequence of neural networks for associative memory. They introduce a *decimation scheme*, greatly inspired by the replica computation for the Hopfield model [93] carried out by Amit, Gutfreund and Sompolinsky in [94], and by the unlearning mechanism [95–97]. [91] provides a phase diagram for the decimation scheme and numerical evidence that when the SNR is high, α is low and the prior is informative enough (such as Rademacher), decimation is able to outperform the RIE, despite requiring a computational time that is exponential in the size N of the system. The idea of decimation is that of retrieving the columns (\mathbf{X}_μ) (i.e., *patterns* in an associative memory interpretation) one at a time. In order to do this one needs to simplify the term $-\frac{\lambda}{2N} \text{Tr}(\mathbf{x}\mathbf{x}^\top)^2$ in the Hamiltonian (13). The latter favours posterior samples whose columns (\mathbf{x}_μ) remain quasi orthogonal to each others, a sort of “caging effect” where patterns influence each others in a way to not align in the same direction in order to have a chance to recover all the ground truth patterns jointly. This rigidity, which helps in the estimation, is completely given up on by decimation in favour of an analytically tractable model, paying the price of a brittle estimation: it works only for rather high SNR. On the contrary, in extensive-rank matrix denoising it is possible to give a non-trivial estimate of $\mathbf{X}\mathbf{X}^\top$ as soon as $\lambda > 0$ via the RIE. Therefore, a comprehensive theory should be able to take into account this caging effect.

More recently, [67] put forward a conjecture of *universality*, intended as independence of the MMSE on the prior P_X (as long as it is centered and with unit variance), which can be formulated in a weak and a strong version. The weak version states that the RIE is optimal among finite degree polynomial estimators, whereas the strong one would posit the universality to hold for all estimators. The strong version in particular would imply that, under Gaussian additive noise, the MI is the one corresponding to the Gaussian prior case of [59, 66, 83, 84]. However, this is in contrast with the evidence produced with decimation algorithms. From our analysis a richer picture emerges. We disprove the strong universality rigorously for any finite $\alpha > 0$. More precisely, we can prove that there exists an SNR beyond which the RIE cannot be optimal. Nevertheless, the conjecture is not to be completely discarded. In fact, we argue that universality of the MI and MMSE holds for low enough SNR, as supported by next Section’s numerical evidence. A possible explanation for the breaking of validity of the analysis in [67] showing universality in the whole phase diagram is the following. The argument is based on the careful analysis of the performance of low-degree polynomials [98]. The author is able to show that no algorithm based on degree- D polynomials of the data entries with $D \leq 3$ can

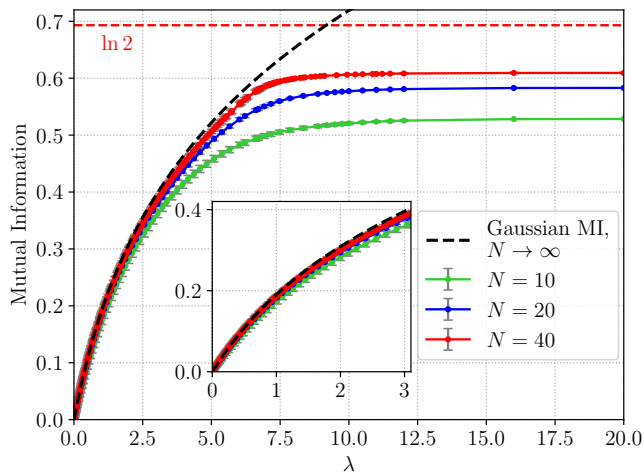


FIG. 1: Monte Carlo results for the mutual information with Rademacher prior for various sizes with $\alpha = 0.5$, i.e., $M = N/2$. Error bars represent the standard error of the mean. The curves are compared to the exact infinite size limit in the case of standard Gaussian prior computed using the HCIZ integral. The red dashed curve corresponds to the entropy of the Rademacher prior and it bounds the MI for all sizes from above.

improve w.r.t. the RIE in the large size limit $N \rightarrow \infty$. He also suggests that his argument extends to larger D . Then, *assuming that the $N \rightarrow +\infty$ and $D \rightarrow +\infty$ can be exchanged*, he concludes that no function of the data (approximated by a polynomial of arbitrary degree) can thus serve as estimator with better performance than the RIE. But commutation of limits can break at a phase transition (as mentioned by the author). Therefore, it may be that the argument is valid up to a critical SNR λ_c , a point beyond which more care should be taken with the large degree and size limits.

The value λ_c depends on α . In particular, recent literature supports the fact that when $\alpha \rightarrow 0$ the universality phase should shrink below $\lambda_c \rightarrow \lambda_c(\alpha = 0) =: \bar{\lambda}_c > 0$ (see FIG. 5). In [32] the authors prove that with a factorised prior, under some suitable hypothesis, the MI and MMSE reduce to those of the standard rank-1 formulas when $M = M_N$ grows sufficiently slowly, which is prior dependent and thus clearly not universal above the phase transition. Note that, for SNRs lower than the critical one, universality holds trivially at low rank, because the MMSE is that of the null estimator, i.e. 1. On top of it, here we show in Appendix C that the MSE of the RIE when $\alpha \rightarrow 0$ is that of naive PCA, which is worse than the Bayes-optimal performance for non rotational invariant priors beyond the transition. Furthermore, for $\alpha \rightarrow 0$ decimation's performance reduces to the one found via the low-rank formula for the MI [92], and is thus likely optimal in said limit. All this evidence supports that universality cannot hold in the $\alpha \rightarrow 0$ limit for all SNRs.

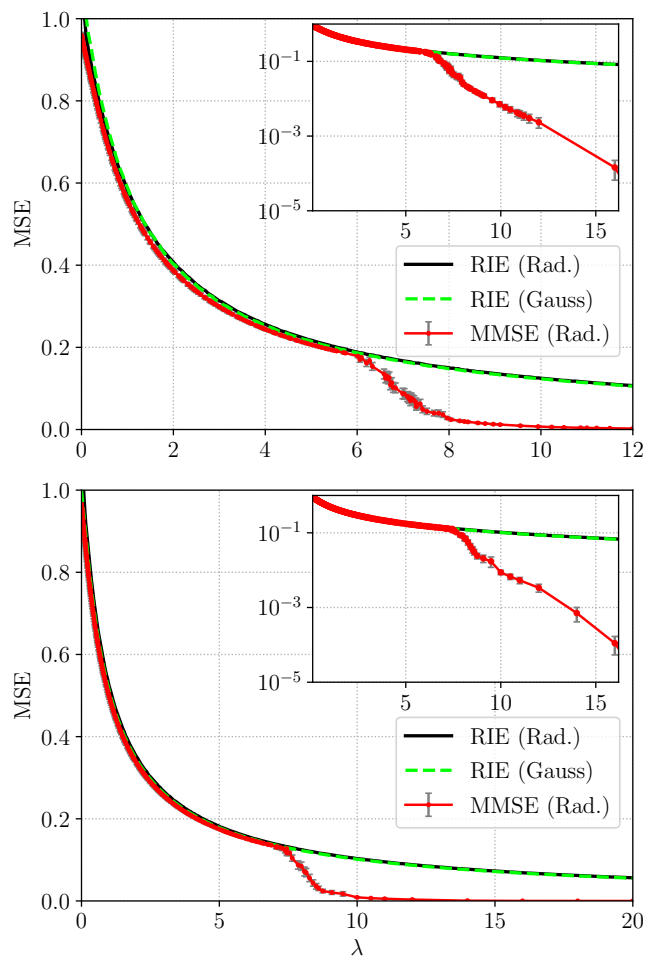


FIG. 2: Monte Carlo results for the MMSE for $N = 40$ with Rademacher prior (red) and $\alpha = 0.5$ (upper figure) and $\alpha = 0.7$ (lower figure). It is compared to the MSE of the RIE for both Rademacher and Gaussian priors. Error bars for the RIE are omitted since they are too small to be visible. Error bars for the MMSE represent standard errors of the mean.

III. EXPLORING THE PHASE DIAGRAM

We start by illustrating some important findings about the nature of matrix denoising in the extensive-rank regime that can already be probed using numerics and simple rigorous arguments. To do so we conducted replica-exchange Monte Carlo simulations, the details of which can be found in Appendix B. FIG. 1 are the results concerning the finite size value of the MI with $\alpha = 0.5$ in the case of Rademacher prior $P_X = \frac{1}{2}\delta_1 + \frac{1}{2}\delta_{-1}$, which will be our main running example of discrete prior with same mean and variance as the standard Gaussian prior. However, most of the conclusions we draw are not specific to Rademacher prior and apply to more generic discrete priors. Because in the Gaussian case we know the exact asymptotic solution, we use as comparison the curve

computed using the HCIZ integral corresponding to the $N, M \rightarrow \infty$ limit of the MI, see (14), (15) and text below.

According to the I-MMSE relation (7), the derivative of the MI w.r.t. to the SNR gives access to the MMSE. We plot it on FIG.2 (where it was computed by Monte Carlo, rather than by numerical differentiation of the MI). In addition, we plot the performance of the RIE for the same sizes. We recall that the RIE denoises the data \mathbf{Y} through eigenvalues shrinkage (keeping its eigenvectors untouched) in order to estimate $\mathbf{X}\mathbf{X}^\top$, but without ever exploiting its factorised structure. This procedure is Bayes-optimal when the matrix to denoise is rotationally invariant, which corresponds to the case of Gaussian prior $P_X = \mathcal{N}(0, 1)$ in the present setting, as the MSE of RIE matches the MMSE (14), see [66, 99].

A. Partial universality, a phase transition and a statistical-to-computational gap

As mentioned before, the recent strong conjecture from Semerjian [67] states that for any prior measure P_X for the i.i.d. entries of \mathbf{X} which is centered with unit variance, the MI and MMSE are universal in the sense that in the large system limit, their values match for all $\lambda \geq 0$ and $\alpha > 0$ the ones in the Gaussian case $P_X = \mathcal{N}(0, 1)$ (up to vanishing, non-universal corrections). Moreover, this MMSE performance should be reachable efficiently using the RIE. That this conjecture is wrong *in general* is clear from our finite size numerical experiments. Indeed, a striking observation is that beyond a certain SNR threshold, the MI curves for the Gaussian and discrete Rademacher priors display an evident discrepancy in the behavior of their respective slopes, a point beyond which the MI for Rademacher prior saturates quickly. This effect becoming sharper as the system size grows suggests a first order discontinuous phase transition in its λ -derivative and thus the MMSE. And indeed, this transition manifests itself in the MMSE too, which suddenly decreases beyond it. Based on our numerics and later on our theory (see Section IV E), we believe that in the thermodynamic limit this *denoising-factorisation transition* $\lambda_c(\alpha)$ is first order for $\alpha > 0$; instead for $\alpha \rightarrow 0$ which recovers the low-rank setting, the transition can be second order (continuous in the MMSE), like for the Rademacher prior.

Another important observation is the very good agreement before the transition between the asymptotic MI for Gaussian prior and the finite size MI for Rademacher prior. The numerics thus strongly suggest that despite the universality is not holding for all SNRs, it does before the transition. Also at the level of the MSE we observe an almost perfect matching already for $N = 40$ between the MMSE for Rademacher prior computed by Monte Carlo and the performance of the RIE, the latter being evaluated for both Rademacher and Gaussian priors. As it should, the RIE performance is independent of the prior details as long as mean and variance match.

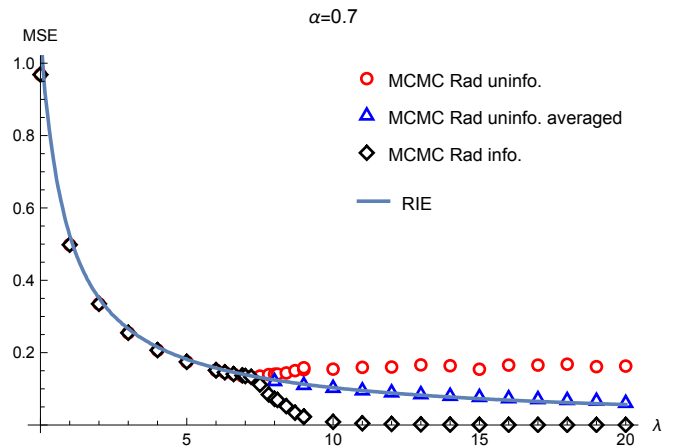


FIG. 3: MSE of the Metropolis algorithm for estimating $\mathbf{X}\mathbf{X}^\top$ with $(N, M) = (40, 28)$, so $\alpha = 0.7$, with an estimator obtained from a single uninformative random initialisation (red markers), with an estimator averaged over 32 independent random initialisations (blue markers), and with an estimator obtained from informative initialisation (i.e., on the ground truth, black markers). Before the transition all markers overlap. These are compared to the RIE performance in the large system limit (blue line). Experimental curves are averaged over 36 instances of the problem (\mathbf{X}, \mathbf{Z}) .

But while the RIE is Bayes-optimal for all SNR in the Gaussian case, beyond λ_c it becomes sub-optimal in the Rademacher case, as expected if universality breaks down given that it cannot exploit the prior.

A natural question is then whether in the region $\lambda > \lambda_c$ there is a statistical-to-computational gap that not only prevents the RIE to reach the MMSE performance, but also a larger class of efficient algorithms including Bayesian ones like Monte Carlo algorithms. Monte Carlo simulations in FIG. 3 (where we run a standard Metropolis algorithm) indicate that without a strongly informative initialisation about the signal, outperforming the RIE is not possible. We observe that, beyond the transition where the informative factorisation state appears (black markers), the performance of an estimator constructed from an empirical average over Monte Carlo samples, all obtained from a single random initialisation, is worse than the RIE. This is probably due to a dynamical glass phase transition [100] where exponentially many metastable states appear [101], preventing Monte Carlo to properly sample the equilibrium corresponding to the informative factorisation state beyond ≈ 7.5 , recall FIG.2. The metastable states are, however, correlated due to the data. Therefore, an additional average over random initialisations (and thus over associated metastable states) should somehow “clean” the effect of glassiness. In order to test this hypothesis we have run, for each SNR and realisation of the problem, 32 Monte Carlo chains initialised independently and randomly. The final estimator is then computed as an

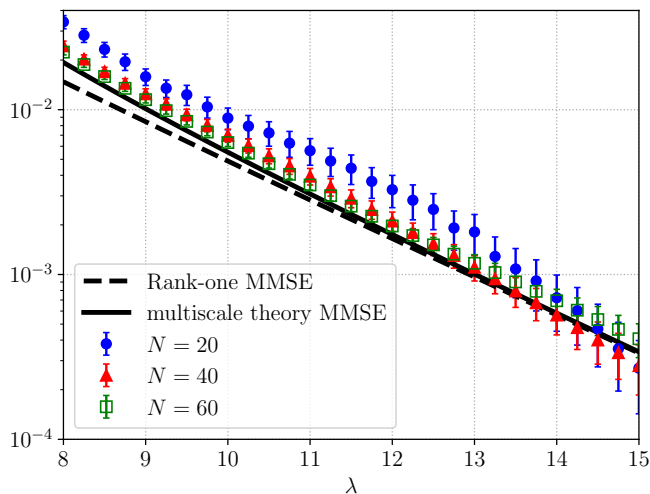


FIG. 4: Monte Carlo results for the MMSE for $N \in \{20, 40, 60\}$ with Rademacher prior, with $\alpha = 0.5$ and SNR λ in the factorisation phase. We also plot the rank-1 MMSE and the MMSE obtained from our multiscale theory (see Section IV) for comparison. Error bars represent standard errors of the mean.

empirical average over the outputs of these independent runs. The performance reached in this way matches precisely that of the RIE, so the aforementioned cleaning takes place, and suggesting that the dynamical glass corresponds to a shattering of the RIE state. Yet, the equilibrium informative state is not reached, which would require instead averaging over an exponentially (in N) large number of Monte Carlo samples (or a smarter sampling procedure, like the replica exchange Monte Carlo algorithm used for FIG. 2, which is *not* an inference algorithm). We conclude that the dynamical glass phase can be cleaned in polynomial time but the final outcome cannot outperform the RIE, which supports the existence of a hard phase. Algorithmic hardness was hypothesized in [67] as a possible consequence of the validity of the weak universality conjecture but not of the strong one. To summarize, the picture that emerges is that of universality of the information theoretic quantities effectively holding at low SNR, which suggests the alternative name of *universal phase*. It then breaks down at larger SNR through a phase transition marking the starting point of a *hard phase* for Monte Carlo algorithms.

The hard phase for Monte Carlo has already been called multiple times *factorisation phase*. The name comes from the fact that in order to denoise \mathbf{XX}^\top optimally, exploiting the factorised structure together with the prior becomes necessary; in other words, the RIE is not optimal. In addition, in this region there is a close match between the MMSE with the one in the low-rank (rank-1) setting where factorisation occurs, see FIG. 4. Factorisation means that the discrete nature of \mathbf{X} when combined with a higher quality data (i.e., higher SNR), strong enough to allow for inference of the patterns them-

selves (as we shall see in Section V), yields an overall much better denoising performance than the RIE. Quantitatively, this translates into an exponential decay of the MMSE as a function of the SNR (similarly to what happens in dictionary learning, see FIG. 5 of [80]), whose exponent is the same as in rank-1 matrix estimation, see FIG. 4. We also stress the even better agreement of our theory with the $N = 60$ points in FIG. 4. In particular, despite the gap between the green points and the rank-1 curve is very small, our theory can explain it. In contrast, in the denoising phase the MMSE decay in λ is polynomial, see inset of FIG. 2. This change of polynomial to exponential decay of the MMSE will be captured by the theory, as well as the fact that the MMSE is close to the rank-1 curve in the factorisation phase, see FIG. 8. In this phase universality breaks down due to the discreteness of the prior. We can thus also alternatively call it the *non-universal phase*.

B. Breaking of universality beyond the transition

With all these observations in mind we thus agree with the strong universality conjecture of [67] when the SNR is sufficiently low, but we can rigorously discard it beyond a threshold using a simple argument based on the definition of the MI. Consider a discrete prior P_X with same mean and variance as $\mathcal{N}(0, 1)$. The MI can be written as

$$\frac{I(\mathbf{XX}^\top; \mathbf{Y})}{MN} = \frac{\mathcal{H}(\mathbf{XX}^\top)}{MN} - \frac{\mathcal{H}(\mathbf{XX}^\top | \mathbf{Y})}{MN} \leq \frac{\mathcal{H}(\mathbf{XX}^\top)}{MN},$$

where the upper bound follows from the fact that for discrete priors both entropies are non-negative. That is it: the MI cannot grow indefinitely as a function of the SNR for a discrete prior (the upper bound remains finite for any size), while it does so for the Gaussian prior (black dashed curve in FIG. 1). This discards the possibility of universality at least beyond the point where the MI density for the Gaussian case crosses the entropy density associated with the matrix \mathbf{XX}^\top . We are going to show below that $|\mathcal{H}(\mathbf{XX}^\top) - \mathcal{H}(\mathbf{X})| = o(MN)$. Therefore, we have a bound on the denoising-factorisation transition. Let $X \sim P_X$, a centered discrete prior of unit variance, \mathbf{Z} the same GOE noise as before and $\tilde{X}_{i\mu} \stackrel{\text{iid}}{\sim} \mathcal{N}(0, 1)$ for $i \leq N, \mu \leq M$. Define the limiting mutual information for the model with Gaussian prior as

$$\iota^G(\alpha, \lambda) := \lim_{N \rightarrow \infty} \frac{1}{MN} I\left(\tilde{\mathbf{X}}\tilde{\mathbf{X}}^\top; \sqrt{\frac{\lambda}{N}} \tilde{\mathbf{X}}\tilde{\mathbf{X}}^\top + \mathbf{Z}\right). \quad (16)$$

We have the following upper bound on the domain of possible prior universality:

$$\lambda_c(\alpha) \leq \inf \{ \lambda \geq 0 : \iota^G(\alpha, \lambda) \geq \mathcal{H}(X) \}. \quad (17)$$

Because $\iota^G(\alpha, \lambda)$ is known using the HCIZ integral via (14), (15) the bound is explicit (we have used that the prior is factorised over the signal matrix entries to get

$\mathcal{H}(\mathbf{X})/MN = \mathcal{H}(X)$ but a similar bound can be written even if there is no such factorisation). In the case of Rademacher prior its entropy equals $\ln 2$. We indeed see in FIG. 1 that the bound holds but it does not look sharp.

Interestingly, we can also explain the apparent gap between the value towards which the finite size MI saturates and the entropy of the prior. In fact, the observations \mathbf{Y} are informed about the ground truth \mathbf{X} only through the combination $\mathbf{X}\mathbf{X}^\top = \sum_{\mu \leq M} \mathbf{X}_\mu \mathbf{X}_\mu^\top$. Hence for large λ we shall have $I(\mathbf{X}\mathbf{X}^\top; \mathbf{Y}) \approx \mathcal{H}(\mathbf{X}\mathbf{X}^\top)$ at leading order, which is smaller than $\mathcal{H}(\mathbf{X})$ by the data processing inequality. The inequality in this case is strict: $\mathcal{H}(\mathbf{X}\mathbf{X}^\top) < \mathcal{H}(\mathbf{X})$ because $\mathbf{X}\mathbf{X}^\top$ is a non-invertible function of \mathbf{X} . The degeneracy of the mapping $\mathbf{X} \mapsto \mathbf{X}\mathbf{X}^\top$ explains accurately the gap. Specifically, for each $\mathbf{X}\mathbf{X}^\top$ there can be $M!$ permutations of the columns of \mathbf{X} that leave it invariant. Furthermore, if the prior is also symmetric like in the Rademacher prior case of FIG. 1, we must add possible sign flips of these $M!$ to the invariance group of $\mathbf{X}\mathbf{X}^\top$. Of these $2^M M!$, some are actually redundant, because columns of \mathbf{X} can match. The probability that any two columns match with a factorised Rademacher prior, however, is $O(M^2 2^{-N})$, which is negligible for large enough N with respect to the leading order corrections that we are going to compute. The probability of more columns matching is of even lower order. Hence we can finally say that

$$\mathcal{H}(\mathbf{X}) = \mathcal{H}(\mathbf{X}\mathbf{X}^\top) + \ln(2^M M!) - o_N(1). \quad (18)$$

Putting these considerations together, we readily get

$$\frac{I(\mathbf{X}\mathbf{X}^\top; \mathbf{Y})}{MN} \xrightarrow{\lambda \rightarrow \infty} \frac{\mathcal{H}(\mathbf{X})}{MN} - \frac{\ln(2^M M!)}{MN} + o_N(1), \quad (19)$$

where the remainder can be estimated to be of order $O(M \ln M 2^{-N})$. It is now manifest that as $M, N \rightarrow \infty$, despite the degeneracy induced by signed permutations, the contributions yielded by the second and third terms on the r.h.s. vanish. This explains why increasing N and $M = \alpha N + o_N(1)$ in FIG. 1 is sufficient to reduce the gap with the saturation value $\ln 2$. E.g., for $N = 20, M = 10$ the contribution of the signed permutations is ≈ 0.1102 which summed to the saturation value of the blue curve ≈ 0.5826 yields ≈ 0.6928 , which is remarkably close to $\ln 2 \approx 0.6931$. The same holds for the other gaps. Note that we do not claim that beyond the transition point the thermodynamic limit of the MI should saturate strictly to the prior entropy. Indeed, FIG. 2 shows that a small gap survives whose size decreases exponentially fast with the SNR.

The right hand side of (17) is a rigorous bound above which universality of the MI and MMSE cannot hold for discrete priors in any possible scenario. We note that given the extensive set of works on universality in random matrices [102–108], it may come as a surprise that universality breaks down. E.g., at the level of the asymptotic spectrum of $\mathbf{X}\mathbf{X}^\top$ and thus of \mathbf{Y} , or even at the level of more local statistics, the previous papers show universality. But the mutual information depends on all the

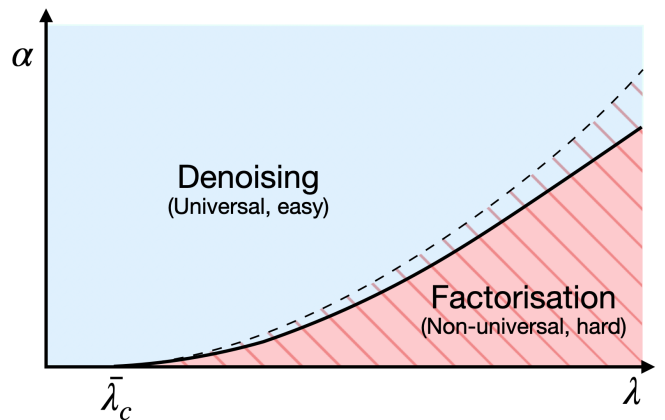


FIG. 5: Qualitative phase diagram for matrix denoising with discrete (Rademacher) prior. The thermodynamic phase transition $\lambda_c(\alpha)$ or equivalently $\alpha_c(\lambda)$ (solid line) is of first order for $\alpha > 0$. It is preceded by a spinodal transition where the informative state appears but is not yet the equilibrium (dashed line). The blue region is the denoising phase where prior universality holds, and optimal denoising is algorithmically easy using the RIE. The shaded region corresponds to the dynamical glass phase (we cannot assess whether this region starts precisely at the spinodal transition as displayed). The red region is the factorisation phase where universality breaks. There, it is possible but hard to denoise better than the RIE. The line $\alpha = 0$ recovers the results for the rank-1 version of the problem and is thus special: $\bar{\lambda}_c = \lambda_c(0)$ is second order and there is no hard phase for Rademacher prior.

fine statistical properties of the data such as the potential discrete nature of \mathbf{X} , which become manifest at high enough SNR.

We also remark that the reasoning leading to the existence of a threshold beyond which universality w.r.t. the base measure of the matrix to infer cannot hold can be extended to a much broader set of matrix inference/learning models. In any such model, if the signal \mathbf{X} is discrete the MI between data and signal cannot exceed the entropy of \mathbf{X} (as a function of the SNR, number of data, etc). This establishes an upper bound on the region of possible validity of prior universality in models where replacing the signal by a Gaussian equivalent with matching moments yields an unbounded MI. We foresee that this fact can have implications on other relevant models of matrix inference/learning such as neural networks.

Summary. Our findings are condensed into a phase diagram in the (α, λ) plane, see FIG. 5. We have identified two phases for matrix denoising with discrete prior. In the *denoising or universal phase*, we conjecture that it is information theoretically not possible to outperform the RIE for denoising $\mathbf{X}\mathbf{X}^\top$ despite it does not exploit its factorised structure, nor prior. It is therefore *algorithmically easy* to reach MMSE performance (i.e., in polynomial

complexity in N). Universality in the prior may be linked to the quasi uniformity of the eigenvectors of $\mathbf{X}\mathbf{X}^\top$ [109–112] and the universality of its spectrum [102, 105, 106] when \mathbf{X} is made of i.i.d. entries. Beyond the transition point we find the *factorisation or non-universal phase*. In this phase both the discrete nature of the prior and the factorised form of the signal matrix come into play. If exploited properly, these ingredients become crucial: information theoretically, they can allow a Bayesian algorithm, such as Monte Carlo sampling, to outperform the spectral RIE algorithm. This is however *algorithmically hard* due to the presence of a dynamical glass phase appearing through a spinodal transition.

The denoising-factorisation transition is the natural extensive-rank generalisation of the famous Baik-Ben Arous-Péché transition (as well as its Bayesian counterpart) happening in the rank-1 version of the model [17, 38, 113], and the phenomenology described here with a universal phase at low SNR (where denoising is trivially bad in the rank-1 case) followed by a prior-dependent informative phase is also reminiscent of it.

Finally, we can also interpret the transition as marking the starting point of a *feature learning regime*, where it becomes information theoretically possible to detect and exploit fine features in the data for achieving better denoising. In the denoising phase, on the contrary, even knowing in advance the features (factorised and discrete structure) does not yield any improvement compared to assuming no particular structure (i.e., a Gaussian prior).

IV. MULTISCALE MEAN-FIELD THEORY

The goal is now to develop an effective theory able to predict the numerical observations discussed earlier, in particular the denoising-factorisation transition. As already mentioned, we cannot employ the methods from matrix models such as spherical integrals. Instead, we will rely on set of spin glass techniques concatenated in an original way. The proposed approach is called multiscale mean-field theory. The reason is that it will use multiple mean-field techniques in a multiscale fashion. What we mean by “multiscale” is the following. The free entropy ϕ_N in (11) can be thought as a matrix model but with a base measure breaking the rotational invariance. Another viewpoint is that of a non-standard spin system made of N spins (the rows of \mathbf{x} , $(\mathbf{x}_i)_{i \leq N}$) which are M -dimensional (i.e., have extensive dimensionality instead of being scalar or low-dimensional variables) or, instead, M spins (the columns of \mathbf{x} , $(\mathbf{x}_\mu)_{\mu \leq M}$) which are N -dimensional. The two viewpoints are perfectly equivalent. Yet, the first view of N spins living in M dimensions will turn out to be much more convenient for calculations, as it shall be clear from the following discussion.

The starting point of the approach is the expression

(8) for the MMSE:

$$\text{MMSE} = \frac{1}{N^2 M} \mathbb{E} \|\mathbf{X}\mathbf{X}^\top\|^2 - \frac{1}{N^2 M} \sum_{i,j=1}^N \mathbb{E} \langle \mathbf{x}_i \cdot \mathbf{x}_j \rangle^2.$$

By exchangeability among rows, one can also select an arbitrary index, say $j = N$, and re-write it as

$$\text{MMSE} = \frac{1}{NM} \left(\sum_{i=1}^{N-1} \mathbb{E} (\mathbf{X}_i \cdot \mathbf{X}_N)^2 - \sum_{i=1}^{N-1} \mathbb{E} \langle \mathbf{x}_i \cdot \mathbf{x}_N \rangle^2 \right).$$

The diagonal element $i = j = N$ cancels by the Nishimori identity. The above formula is crucial to realize that the MMSE of matrix denoising is linked to the so-called YMMSE of a random linear regression problem with noisy design. In linear regression, the YMMSE corresponds to the MMSE of the projection of the regressor onto the covariates (i.e., the responses), see [114]. In the mapping onto a regression problem, $\mathbf{x} = (\mathbf{x}_i)_{i \leq N-1}$ can be seen as an estimator for an uncertain covariates matrix \mathbf{X} (with a slight abuse of notation we denote $\mathbf{x}, \mathbf{X} \in \mathbb{R}^{N-1 \times M}$ as for the whole $N \times M$ matrices), while \mathbf{x}_N is the estimator of the regressor \mathbf{X}_N . From now on we denote $\boldsymbol{\eta} := \mathbf{x}_N$ and $\mathbf{H} := \mathbf{X}_N$ to distinguish regressor from covariates in the linear regression interpretation. The YMMSE in this case reads $\mathbb{E} \|\mathbf{X}\mathbf{H} - \langle \mathbf{x}\boldsymbol{\eta} \rangle\|^2 / (NM) = (\mathbb{E} \|\mathbf{X}\mathbf{H}\|^2 - \mathbb{E} \|\langle \mathbf{x}\boldsymbol{\eta} \rangle\|^2) / (NM)$ with $\langle \mathbf{x}\boldsymbol{\eta} \rangle$ the Bayes-optimal estimator of the responses. This is precisely the MMSE for matrix denoising and the main goal is thus to evaluate it.

Mapping the problem onto a linear regression has the advantage of converting a matrix model into a vector inference problem potentially tractable using known approaches. To this end, we isolate row $\mathbf{x}_N = \boldsymbol{\eta}$ using the cavity method. This has the effect of “reducing the scale of the problem”: we go from a partition function associated with an Hamiltonian of order $O(MN)$ to one with Hamiltonian of $O(M)$. This $O(MN) \rightarrow O(M)$ reduction by the cavity method corresponds to the first scale. Contrary to standard spin or inference models (like the Hopfield model or the perceptron treated with the cavity method in [73, 115], where there are two possible ways to dig a cavity as in the present problem), the effective inference problem appearing here remains high-dimensional (because $M \rightarrow \infty$ with N). Yet, the scale reduction is helpful, as it will allow us to integrate away the $N - 1$ bulk rows using a mean-field approximation.

To further reduce dimensionality and get tractable low-dimensional formulas, we will then employ rigorous replica formulas [116], yielding finally an effective scalar inference problem. This $O(M) \rightarrow O(1)$ reduction of the order of the Hamiltonian treated corresponds to the second scale in the problem.

A comment on row and column cavities. The cavity method is a powerful technique for analysing the order parameters of a model, as we will do in this paper. It can also be employed to directly compute the free energy, e.g.,

of spin glasses [73, 76, 115, 117, 118]. In our model there are two possible ways to dig a cavity: extracting a row or a column. It turns out that, as far as the free entropy ϕ_N is concerned, each of the two cavity approaches yields the same limit, provided it exists.

Proposition 2 ([32] Equivalence of cavity representations). *Let*

$$\begin{aligned}\Delta_{\text{row}}(N) &:= \mathbb{E} \ln \mathcal{Z}_{N+1, M_{N+1}} - \mathbb{E} \ln \mathcal{Z}_{N, M_{N+1}}, \\ \Delta_{\text{col}}(N) &:= \mathbb{E} \ln \mathcal{Z}_{N, M_{N+1}} - \mathbb{E} \ln \mathcal{Z}_{N, M_N}.\end{aligned}$$

Suppose that $\lim_{N \rightarrow \infty} \frac{\Delta_{\text{row}}(N)}{M_N}$ and $\lim_{N \rightarrow \infty} \frac{\Delta_{\text{col}}(N)}{M_N}$ exist and they are respectively equal to L_{row} and L_{col} . Then $L_{\text{row}} = L_{\text{col}}$.

This result implies that if the limit of the row and column cavity contributions exist, then

$$\lim_{N \rightarrow \infty} \phi_N = \lim_{N \rightarrow \infty} \frac{\Delta_{\text{row}}(N)}{M_N}.$$

This may provide a viable alternative to compute the MI (11) without having to carry out both cavity computations. This proposition is general and applies to any sequence with two growing dimensions. It shows that despite there are two possible cavities, it is a-priori sufficient to consider a single one in order to access all relevant thermodynamic quantities in the problem. We will show that this is indeed the case.

Even if equivalent in theory, one of the two cavities may be more convenient for computations. In the present case, the row cavity is easier because the part of the Hamiltonian depending on row $\mathbf{x}_i \in \mathbb{R}^M$ carries a noise variable $\mathbf{Z}_i \in \mathbb{R}^N$ independent from the rest. This, in turn, allows us to identify a well-defined inference problem at scale $O(M)$ for the cavity (linear regression with noisy design).

More precisely, the posterior can be decomposed in terms of rows \mathbf{x}_i and $\mathbf{Y}_i = (Y_{ij})_{j \leq i-1}$, $i = 1, \dots, N$, as

$$\begin{aligned}P(\mathbf{x} | \mathbf{Y}) &\propto P_X(\mathbf{x}_N) P(\mathbf{Y}_N | \mathbf{x}_N, (\mathbf{x}_j)_{j \leq N-1}) \\ &\quad \times \prod_{i \leq N-1} P_X(\mathbf{x}_i) P(\mathbf{Y}_i | \mathbf{x}_i, (\mathbf{x}_j)_{j \leq i-1}) \\ &\propto P(\mathbf{x}_N | \mathbf{Y}_N, (\mathbf{x}_j)_{j \leq N-1}) \\ &\quad \times P((\mathbf{x}_j)_{j \leq N-1} | (\mathbf{Y}_j)_{j \leq N-1}),\end{aligned}\quad (20)$$

where we have dropped normalisations. This decomposition which follows from (10) emphasizes that, conditional on the ‘‘bulk’’ $(\mathbf{x}_j)_{j \leq N-1}$, the ‘‘cavity’’ \mathbf{x}_N depends on a single data row \mathbf{Y}_N , and the bulk marginal posterior measure is independent of the cavity. Note that, even if not apparent, the same argument holds when extracting any other cavity row after a proper permutation of row indices. This decomposition will be crucial as, firstly, this is how we will recognize that the posterior of the cavity conditional on the bulk corresponds to a lower dimensional Bayes-optimal inference problem. And secondly, the bulk measure can be simplified without having to modify the cavity measure. Such a decomposition cannot be written if performing a column cavity.

A. First scale: $O(MN) \rightarrow O(M)$ reduction by the cavity method

As anticipated, we now aim at computing the YMMSE of a random linear estimation (RLE) problem with uncertain design (as studied in [119]). This will in turn yield a formula for the MI too. The RLE we are interested in is obtained via a row cavity extraction as follows.

Recall the Hamiltonian (13) with N rows and M columns and where Y_{ij} has been expanded in signal and noise contributions:

$$\begin{aligned}-H_{N,M}(\mathbf{x}; \mathbf{Z}, \mathbf{X}) &= \sum_{i < j}^N \left[\sqrt{\frac{\lambda}{N}} Z_{ij} \mathbf{x}_i \cdot \mathbf{x}_j \right. \\ &\quad \left. + \frac{\lambda}{N} (\mathbf{X}_i \cdot \mathbf{X}_j) \mathbf{x}_i \cdot \mathbf{x}_j - \frac{\lambda}{2N} (\mathbf{x}_i \cdot \mathbf{x}_j)^2 \right]\end{aligned}\quad (21)$$

with $\mathbf{x}_i \cdot \mathbf{x}_j = \sum_{\mu \leq M} x_{i\mu} x_{j\mu}$. Recall also that we denote the cavity \mathbf{x}_N by $\boldsymbol{\eta} \in \mathbb{R}^M$, \mathbf{X}_N by $\mathbf{H} \in \mathbb{R}^M$ and the bulk (i.e., all but the cavity) variables as $\mathbf{x}, \mathbf{X} \in \mathbb{R}^{N-1 \times M}$. Now we segregate the contribution of $\boldsymbol{\eta}$ from the Hamiltonian:

$$-H_{N,M}(\mathbf{x}, \boldsymbol{\eta}; \lambda) = -H'_{N,M}(\mathbf{x}; \lambda) - H_{N,M}^{\text{row}}(\boldsymbol{\eta}; \mathbf{x}, \lambda),$$

with bulk Hamiltonian

$$\begin{aligned}-H'_{N,M}(\mathbf{x}; \lambda) &= \sum_{i < j}^{N-1} \left[\sqrt{\frac{\lambda}{N}} Z_{ij} \mathbf{x}_i \cdot \mathbf{x}_j \right. \\ &\quad \left. + \frac{\lambda}{N} (\mathbf{X}_i \cdot \mathbf{X}_j) \mathbf{x}_i \cdot \mathbf{x}_j - \frac{\lambda}{2N} (\mathbf{x}_i \cdot \mathbf{x}_j)^2 \right],\end{aligned}\quad (22)$$

and cavity Hamiltonian

$$\begin{aligned}-H_{N,M}^{\text{row}}(\boldsymbol{\eta}; \mathbf{x}, \lambda) &= \sum_{i=1}^{N-1} \left[\sqrt{\frac{\lambda}{N}} Z_{iN} \mathbf{x}_i \cdot \boldsymbol{\eta} \right. \\ &\quad \left. + \frac{\lambda}{N} (\mathbf{X}_i \cdot \mathbf{H}) \mathbf{x}_i \cdot \boldsymbol{\eta} - \frac{\lambda}{2N} (\mathbf{x}_i \cdot \boldsymbol{\eta})^2 \right].\end{aligned}\quad (23)$$

In order to lighten the notation we have dropped dependencies on the ground truth and the noise. From $-H_{N,M}^{\text{row}}$ we recognize (up to a constant) the log-likelihood of an RLE problem over both (\mathbf{X}, \mathbf{H}) with (i) data $\tilde{\mathbf{Y}}(\lambda) = \mathbf{Y}_N = (\tilde{Y}_i = Y_{Ni})_{i \leq N-1}$ obtained as

$$\tilde{\mathbf{Y}}(\lambda) = \sqrt{\frac{\lambda}{N}} \mathbf{X} \mathbf{H} + \tilde{\mathbf{Z}}$$

with Gaussian noise $\tilde{\mathbf{Z}} = (Z_{Ni})_{i \leq N-1}$, \mathbf{Y}_N the last data row, as well as (ii) additional side information $\mathbf{Y}' = (Y_{ij} = Y_{ij}^{\zeta=\lambda})_{i < j \leq N-1}$ about the bulk $\mathbf{X} = (\mathbf{X}_i)_{i \leq N-1}$, where

$$Y_{ij}^{\zeta} = \sqrt{\frac{\zeta}{N}} \mathbf{X}_i \cdot \mathbf{X}_j + Z_{ij}, \quad 1 \leq i < j \leq N-1. \quad (24)$$

ζ is an auxiliary SNR that should be taken equal to λ , but we consider a more general model where it may differ, in

which case we denote the data $\mathbf{Y}'(\zeta) = (Y'_{ij})_{i < j \leq N-1}$ (so $\mathbf{Y}' = \mathbf{Y}'(\lambda)$). All the noises appearing in the above equations are independent. $\tilde{\mathbf{Y}}$ can more generally be thought as coming from a generalised linear model (GLM)

$$\tilde{Y}_i \sim P_{\text{out}}\left(\cdot \mid \frac{\mathbf{X}_i \cdot \mathbf{H}}{\sqrt{N}}\right), \quad i \leq N, \quad (25)$$

with output channel

$$P_{\text{out}}(y \mid x) := \frac{1}{\sqrt{2\pi}} e^{-\frac{1}{2}(y - \sqrt{\lambda}x)^2}. \quad (26)$$

We are going to work in this more general setting and specialise to the Gaussian linear channel (26) at the end.

The mutual information $I(\tilde{\mathbf{Y}}(\lambda), \mathbf{Y}'(\zeta); \mathbf{X}, \mathbf{H})$ is nothing but the original one (11) when $\zeta = \lambda$. Because we have that $I(\tilde{\mathbf{Y}}(\lambda), \mathbf{Y}'(\zeta); \mathbf{X}, \mathbf{H}) = \mathcal{H}(\tilde{\mathbf{Y}}(\lambda) \mid \mathbf{Y}'(\zeta)) + C$ with C independent of λ , the contribution to the MI that is sufficient in order to access

$$\text{YMMSE} := \frac{\mathbb{E}\|\mathbf{X}\mathbf{H} - \langle \mathbf{x}\boldsymbol{\eta} \rangle\|^2}{NM} = 1 - \frac{\mathbb{E}\|\langle \mathbf{x}\boldsymbol{\eta} \rangle\|^2}{NM} \quad (27)$$

by an I-MMSE relation is the free entropy, which is the conditional entropy $\mathcal{H}(\tilde{\mathbf{Y}}(\lambda) \mid \mathbf{Y}'(\zeta))$ up to a constant:

$$\begin{aligned} \phi_N^{\text{RLE}}(\lambda, \zeta) &= \phi_N^{\text{RLE}} \\ &:= \frac{1}{M} \mathbb{E}_{\tilde{\mathbf{Y}}(\lambda), \mathbf{Y}'(\zeta)} \ln \int_{\mathbb{R}^M} dP_X(\boldsymbol{\eta}) \left\langle e^{-H_{N,M}^{\text{row}}(\boldsymbol{\eta}; \mathbf{x}, \lambda)} \right\rangle' \end{aligned} \quad (28)$$

where we introduce the bulk measure

$$\langle \cdot \rangle' = \frac{1}{\mathcal{Z}'(\mathbf{Y}'(\zeta))} \int_{\mathbb{R}^{N-1 \times M}} dP_X(\mathbf{x}) e^{-H_{N,M}(\mathbf{x}; \zeta)}(\cdot)$$

with proper normalisation \mathcal{Z}' . $\langle \cdot \rangle'$ is the posterior measure associated to the side channel (24) with SNR ζ . From ϕ_N^{RLE} one can define the MI for the RLE problem

$$\begin{aligned} \iota_N^{\text{RLE}}(\lambda, \zeta) &:= \frac{1}{M} I(\mathbf{X}, \mathbf{H}; \tilde{\mathbf{Y}}(\lambda) \mid \mathbf{Y}'(\zeta)) \\ &= \frac{\lambda}{2} - \phi_N^{\text{RLE}}(\lambda, \zeta). \end{aligned} \quad (29)$$

The connection with the YMMSE is then realized through a derivative w.r.t. the SNR λ . By integration by parts one gets the I-MMSE relation

$$\left. \frac{d}{d\lambda} \iota_N^{\text{RLE}}(\lambda, \zeta) \right|_{\zeta=\lambda} = \frac{1}{2} \text{YMMSE}. \quad (30)$$

B. Second scale: $O(M) \rightarrow O(1)$ reduction by bulk approximation and replica formulas

The new Hamiltonian $H_{N,M}^{\text{row}}$ is of $O(M)$. Until now everything is exact and rigorous: *we have not introduced any approximation yet*. If we could integrate out the bulk \mathbf{x} we would have a drastic cut in the number of degrees of freedom, with only the cavity row remaining,

leaving us with a standard vector problem. However, an explicit integration w.r.t. the measure $\langle \cdot \rangle'$ is in general not feasible without a simplifying ansatz.

Before implementing this simplification let us make an important remark. We could have tried to simplify the problem using an ansatz earlier in the computation, i.e. directly at the level of the original Hamiltonian/problem in order to go directly from the scale of $O(MN)$ degrees of freedom to $O(1)$ effective ones, e.g. using the replica method as in the previous works [80, 83, 84]. Having already reduced the scale down to $O(M)$ by the cavity method *in an exact manner*, our approximations will only be at the level of the bulk through the simplification of $\langle \cdot \rangle'$: the ‘‘direct’’ interaction between the cavity and the bulk captured by $H_{N,M}^{\text{row}}$, which defines the first conditional posterior in (20), is kept untouched, with approximations only made on the bulk law $H'_{N,M}$, i.e., the second posterior law in (20). In essence our simplification assumes that the interactions among bulk variables have a lower order effect on the free entropy ϕ_N^{RLE} computed by cavity when compared to the direct cavity-bulk interaction. This intuition is vindicated by the fact that the theory predicts the denoising-factorisation transition and the good quantitative agreement with experiments.

Besides being physically meaningful, the approximation we make should also yield a tractable problem, namely it should allow us to integrate explicitly and ideally without further approximations the bulk degrees of freedom. We achieve this by replacing the channel (24) by an effective, more manageable, one:

$$\mathbf{Y}'_{\text{eff}}(\sigma) = \sqrt{\sigma} \mathbf{X} + \mathbf{Z}'_{\text{eff}}, \quad (31)$$

where $\mathbf{Z}'_{\text{eff}} = (Z'_{i\mu})_{i \leq N-1, \mu \leq M}$ is a matrix of i.i.d. Gaussian variables, \mathbf{X} is the ground truth bulk as before, σ is a tunable SNR for the effective observations $\mathbf{Y}'_{\text{eff}}(\sigma) = (\mathbf{Y}'_i \in \mathbb{R}^M)_{i \leq N-1} = (Y'_{i\mu})_{i \leq N-1, \mu \leq M}$. This is nothing but a mean-field ansatz for the problem, i.e., a parametrization of the bulk measure in terms of marginals only. Its potential validity in this extensive-rank setting will be thoroughly discussed later. For now, let us just notice that this form of marginal is asymptotically exact for standard (low rank) models [17, 38, 116].

Within this factorised mean-field ansatz the simplified bulk measure, still denoted with the same bracket, reads

$$\langle \cdot \rangle' = \prod_{i,\mu=1}^{N-1,M} \frac{1}{\mathcal{Z}'(Y'_{i\mu})} \int dP_X(x_{i\mu}) e^{\sqrt{\sigma} Y'_{i\mu} x_{i\mu} - \frac{1}{2} \sigma x_{i\mu}^2}(\cdot)$$

with again a proper normalisation that we continue denoting \mathcal{Z}' . Under this simplified bulk measure, we define the free entropy ψ_N^{RLE} similarly as (28):

$$\begin{aligned} \psi_N^{\text{RLE}}(\lambda, \sigma) &= \psi_N^{\text{RLE}} \\ &:= \frac{1}{M} \mathbb{E}_{\tilde{\mathbf{Y}}(\lambda), \mathbf{Y}'_{\text{eff}}(\sigma)} \ln \int_{\mathbb{R}^M} dP_X(\boldsymbol{\eta}) \left\langle e^{-H_{N,M}^{\text{row}}(\boldsymbol{\eta}; \mathbf{x}, \lambda)} \right\rangle'. \end{aligned} \quad (32)$$

The idea will be to find a $\sigma_* = \sigma_*(\lambda)$ such that the free entropy for the RLE with noisy design $\phi_N^{\text{RLE}}(\lambda, \lambda)$ is well

approximated by $\psi_N^{\text{RLE}}(\lambda, \sigma_*)$. There is an immediate simplification due to the factorisation of the bulk measure. Using the channel (26) we can recast the free entropy as

$$\begin{aligned} \psi_N^{\text{RLE}} &= -\frac{1}{\alpha} \mathbb{E} \ln P_{\text{out}}(\tilde{Y}_1 | 0) \\ &+ \frac{1}{M} \mathbb{E}_{\tilde{\mathbf{Y}}(\lambda), \mathbf{Y}'_{\text{eff}}(\sigma)} \ln \int dP_X(\boldsymbol{\eta}) \prod_{i=1}^{N-1} \left\langle P_{\text{out}}\left(\tilde{Y}_i \mid \frac{\mathbf{x}_i \cdot \boldsymbol{\eta}}{\sqrt{N}}\right) \right\rangle' \end{aligned}$$

where we were able to factorise the i -product. For the first term we have used the fact that $P_{\text{out}}(\tilde{\mathbf{Y}} | 0)$ factorises over the elements of $\tilde{\mathbf{Y}}$, giving a sum of contributions that are all equal in average.

Under the factorised measure $\langle \cdot \rangle'$, the rescaled sums $\mathbf{x}_i \cdot \boldsymbol{\eta} / \sqrt{N}$ behave as Gaussians by the central limit theorem, for any fixed $\boldsymbol{\eta}$. Therefore, it is now equivalent to think of the $x_{i\mu}$'s as independent Gaussians with mean and variance

$$m(Y'_{i\mu}) := \langle x_{i\mu} \rangle', \quad V(Y'_{i\mu}) := \langle x_{i\mu}^2 \rangle' - \langle x_{i\mu} \rangle'^2,$$

or equivalently

$$x_{i\mu} \stackrel{\text{D}}{=} m(Y'_{i\mu}) + \xi_{i\mu} \sqrt{V(Y'_{i\mu})}, \quad (33)$$

with $\xi_{i\mu} \stackrel{\text{iid}}{\sim} \mathcal{N}(0, 1)$ the new annealed bulk degrees of freedom. For later convenience we also introduce the overlap for the bulk variables

$$\begin{aligned} J &= J(\sigma) := \mathbb{E} m(Y'_{i\mu}) X_{i\mu} \\ &= \mathbb{E}_{X, Z'} X \frac{\int dP_X(x) x e^{(\sqrt{\sigma} Z' + X\sigma)x - \frac{1}{2}\sigma x^2}}{\int dP_X(x) e^{(\sqrt{\sigma} Z' + X\sigma)x - \frac{1}{2}\sigma x^2}} \end{aligned} \quad (34)$$

with $Z' \sim \mathcal{N}(0, 1)$, $X \sim P_X$. By the Nishimori identity it is also equal to $J = \mathbb{E} m(Y'_{i\mu})^2$, and thus we have, using the properties of the prior, that $(m(Y'_{i\mu}))_{i, \mu}$ are i.i.d. sub-Gaussian random variables with

$$\mathbb{E} m(Y'_{i\mu}) = 0, \quad \mathbb{E} m(Y'_{i\mu})^2 = J. \quad (35)$$

Rewriting ψ_N^{RLE} by means of (33) we get

$$\begin{aligned} \frac{1}{M} \mathbb{E}_{\tilde{\mathbf{Y}}, \mathbf{Y}'_{\text{eff}}} \ln \int dP_X(\boldsymbol{\eta}) \prod_{i=1}^{N-1} \mathbb{E}_{\xi_i} P_{\text{out}}\left(\tilde{Y}_i \mid \frac{m(\mathbf{Y}'_i) \cdot \boldsymbol{\eta}}{\sqrt{N}}\right) \\ + \frac{(\sqrt{V(\mathbf{Y}'_i)} \circ \boldsymbol{\xi}_i) \cdot \boldsymbol{\eta}}{\sqrt{N}} \Big) - \frac{1}{\alpha} \mathbb{E} \ln P_{\text{out}}(\tilde{Y}_1 | 0) + o_N(1) \end{aligned}$$

with $\boldsymbol{\xi}_i = (\xi_{i\mu})_{\mu \leq M}$, $m(\mathbf{Y}'_i) = (m(Y'_{i\mu}))_{\mu}$ and similarly for $V(\mathbf{Y}'_i)$, and \circ denotes component-wise product. The

remainder is due to the fact that i runs to $N-1$ and not to N . It will be dropped in the following.

Being in a Bayes-optimal setting, strong concentration effects allow us to simplify $((\sqrt{V(\mathbf{Y}'_i)}/N \circ \boldsymbol{\xi}_i) \cdot \boldsymbol{\eta})_i$. Indeed, these are conditionally on $\boldsymbol{\eta}$ independent centered Gaussian random variables with variance

$$\frac{1}{N} \sum_{\mu=1}^M V(Y'_{i\mu}) \eta_{\mu}^2 = \alpha \mathbb{E} V(\sqrt{\sigma} X + Z') + o_N(1)$$

where the equality holds with overwhelming probability when $N, M \rightarrow \infty$. We stress that we have used $\|\boldsymbol{\eta}\|^2/M = 1 + o_N(1)$. $\boldsymbol{\eta}$ is a sample from a posterior, so this replacement is a priori not guaranteed, but thanks to Bayes-optimality $\|\boldsymbol{\eta}\|^2/M$ concentrates onto its mean which is the same as for the ground truth by the Nishimori identity. Still using the Nishimori identity one gets directly that $\mathbb{E} V(Y'_{i\mu}) = 1 - J$. Therefore, by defining the more noisy channel

$$\tilde{P}_{\text{out}}^{(\sigma, \alpha)}(y | x) := \mathbb{E}_{\xi \sim \mathcal{N}(0, 1)} P_{\text{out}}(y | x + \xi \sqrt{\alpha(1 - J(\sigma))})$$

and collecting all the above observations, up to negligible corrections the free entropy rewrites as

$$\begin{aligned} \psi_N^{\text{RLE}} &= -\frac{1}{\alpha} \mathbb{E} \ln P_{\text{out}}(\tilde{Y}_1 | 0) \\ &+ \frac{1}{M} \mathbb{E}_{\tilde{\mathbf{Y}}, \mathbf{Y}'_{\text{eff}}} \ln \int dP_X(\boldsymbol{\eta}) \prod_{i=1}^{N-1} \tilde{P}_{\text{out}}^{(\sigma, \alpha)}\left(\tilde{Y}_i \mid \frac{m(\mathbf{Y}'_i) \cdot \boldsymbol{\eta}}{\sqrt{N}}\right). \end{aligned}$$

The first contribution is simple to compute since $\tilde{Y}_1 \sim P_{\text{out}}(\cdot | \mathbf{X}_1 \cdot \mathbf{H} / \sqrt{N})$ is asymptotically equal in law to $\tilde{Y}_1 \sim P_{\text{out}}(\cdot | \sqrt{\alpha} Z')$. A final simplification is to replace the i.i.d. centered sub-Gaussian variables $(m(Y'_{i\mu}))$ playing the role of quenched covariates by Gaussians $(\sqrt{J} \tau_{i\mu})$ with $\tau_{i\mu} \stackrel{\text{iid}}{\sim} \mathcal{N}(0, 1)$, using (35). This leaves the free entropy unchanged at leading order because the replica computation for the GLM and its rigorous proof simply leverage on the fact that $(m(\mathbf{Y}'_i) \cdot \boldsymbol{\eta} / \sqrt{N})_{i \leq N}$ behave as Gaussian random variables under the quenched expectation w.r.t. \mathbf{Y}' , and these have the same law in the large system limit as $(\tau_i \cdot \boldsymbol{\eta} \sqrt{J/N})_i$. It thus become

$$\begin{aligned} \psi_N^{\text{RLE}} &= -\frac{1}{\alpha} \mathbb{E} \ln P_{\text{out}}(\tilde{Y}_1 | 0) \\ &+ \frac{1}{M} \mathbb{E}_{\tilde{\mathbf{Y}}, \boldsymbol{\tau}} \ln \int dP_X(\boldsymbol{\eta}) \prod_{i=1}^{N-1} \tilde{P}_{\text{out}}^{(\sigma, \alpha)}\left(\tilde{Y}_i \mid \sqrt{J} \frac{\boldsymbol{\tau}_i \cdot \boldsymbol{\eta}}{\sqrt{N}}\right) \end{aligned}$$

at leading order. It is finally in the familiar form of free entropy of a GLM with quenched Gaussian covariates matrix, whose rigorous limiting value is found in [116]:

$$\begin{aligned} \psi^{\text{RLE}} &= \lim_{N \rightarrow \infty} \psi_N^{\text{RLE}} = \text{extr}_+ \left\{ -\frac{rq}{2} + \mathbb{E}_{\xi, H} \ln \int dP_X(\eta) e^{(\xi\sqrt{r} + Hr)\eta - \frac{1}{2}r\eta^2} - \frac{1}{\alpha} \mathbb{E}_{\xi} \int dy P_{\text{out}}(y | \sqrt{\alpha}\xi) \ln P_{\text{out}}(y | 0) \right. \\ &\quad \left. + \frac{1}{\alpha} \mathbb{E}_{\xi, u_0} \int dy \tilde{P}_{\text{out}}^{(\sigma, \alpha)}(y | \sqrt{\alpha J(\sigma)(1-q)} u_0 + \sqrt{\alpha J(\sigma)q} \xi) \ln \mathbb{E}_u \tilde{P}_{\text{out}}^{(\sigma, \alpha)}(y | \sqrt{\alpha J(\sigma)(1-q)} u + \sqrt{\alpha J(\sigma)q} \xi) \right\} \quad (36) \end{aligned}$$

where extremization is intended w.r.t. (r, q) , and (ξ, u_0, u) are i.i.d. standard Gaussian variables, $H \sim P_X$. extr_+ selects the solution of the saddle point equations, obtained by equating to zero the gradient of the replica potential $\{\dots\}$, which maximizes it.

In the Bayes-optimal setting the extremizer q_* corresponds to the asymptotic overlap between the ground truth row \mathbf{H} and a sample $\boldsymbol{\eta}$ from the posterior associated to the RLE with noisy covariates problem (24), (25), or between two conditionally independent posterior samples by the Nishimori identity, which concentrate onto their mean given by

$$q_* = \lim_{N \rightarrow \infty} \mathbb{E} \frac{1}{M} \mathbf{H} \cdot \mathbb{E}[\boldsymbol{\eta} | \tilde{\mathbf{Y}}(\lambda), \mathbf{Y}'_{\text{eff}}(\sigma)] \quad (37)$$

$$= \lim_{N \rightarrow \infty} \mathbb{E} \frac{1}{M} \|\mathbb{E}[\boldsymbol{\eta} | \tilde{\mathbf{Y}}(\lambda), \mathbf{Y}'_{\text{eff}}(\sigma)]\|^2, \quad (38)$$

where $\mathbb{E}[\boldsymbol{\eta} | \tilde{\mathbf{Y}}, \mathbf{Y}'_{\text{eff}}]$ equals the posterior mean of the cavity given direct observations $\tilde{\mathbf{Y}}$ about it, and the effective observations for the bulk. Instead, the extremizer r_* corresponds to the effective SNR which controls the cavity fields underlying the marginals of the cavity coordinates: asymptotically, the unnormalised random marginal probability density function of any of the η_i reads

$$dP(\eta_i \in [\eta, \eta + d\eta]) \propto dP_X(\eta) e^{(\xi\sqrt{r_*} + Hr_*)\eta - \frac{1}{2}r_*\eta^2} \quad (39)$$

with randomness $\xi \sim \mathcal{N}(0, 1)$ and $H \sim P_X$. In other words, in the thermodynamic limit a cavity coordinate has marginal corresponding to a random posterior distribution $P(H \in \cdot | \sqrt{r_*}H + \xi)$ associated with the effective scalar observation $\sqrt{r_*}H + \xi$ with prior P_X .

If we specify the above to the Gaussian output channel (26) we obtain

$$\begin{aligned} \psi^{\text{RLE}} &= \text{extr}_+ \left\{ \mathbb{E}_{\xi, H} \ln \int dP_X(\eta) e^{(\xi\sqrt{r} + Hr)\eta - \frac{1}{2}r\eta^2} - \frac{rq}{2} \right. \\ &\quad \left. + \frac{\lambda}{2} - \frac{1}{2\alpha} \ln(1 + \lambda\alpha(1 - J(\sigma)q)) \right\}. \quad (40) \end{aligned}$$

C. Saddle point equations and mutual information

The saddle point equations are obtained by equating the gradient of $\{\dots\}$ in (40) to zero:

$$q = \mathbb{E}_{\xi, H} H \langle \eta \rangle_r, \quad (41)$$

$$r = \frac{\lambda J(\sigma)}{1 + \lambda\alpha(1 - J(\sigma)q)}, \quad (42)$$

where

$$\langle \cdot \rangle_r := \frac{1}{Z_r} \int dP_X(\eta) e^{(\xi\sqrt{r} + Xr)\eta - \frac{1}{2}r\eta^2}(\cdot)$$

with $\xi \sim \mathcal{N}(0, 1)$, $H \sim P_X$ and Z_r is the normalisation. The solutions (q_*, r_*) depend on α, λ , and $J(\sigma)$.

The main question now is how to set the effective bulk SNR σ . We argue that it can be determined with a consistency argument. σ , which enters the problem through (31), controls the cavity fields acting on the bulk $(X_{i\mu})$. J is then the overlap that any row of \mathbf{x} has with the corresponding ground truth row in \mathbf{X} , by definition (34). Rows are completely exchangeable. Therefore the random cavity marginals (39) should have the same law as the bulk marginals. This is achieved by matching the SNRs in the effective scalar observation channels for the cavity coordinates $\sqrt{r_*}(\sigma)H + \xi$ and bulk coordinates $\sqrt{\sigma}X + Z'$. This yields the third missing consistency equation needed for $\sigma_*(\lambda)$ in addition to the two we already have for (q, r) :

$$r_* = \frac{\lambda J(\sigma_*)}{1 + \lambda\alpha(1 - J(\sigma_*)q_*)} = \sigma_*. \quad (43)$$

As intuition may suggest, fixing the cavity fields in this way also equates the two overlaps J and q_* . To see this, it is sufficient to realize that the function $F(r) = \mathbb{E}H \langle \eta \rangle_r$ is monotonic in $r \geq 0$, and thus invertible. Then, by a simple application of it to both sides of (43) we readily get $q_* = J(\sigma_*)$ as predicted. The two conditions $\sigma_* = r_*$ and $J(\sigma_*) = q_*$ are thus equivalent.

Using this knowledge, we recast (41), (42) as

$$q = \mathbb{E}_{\xi, H} H \langle \eta \rangle_r, \quad (44)$$

$$r = \frac{\lambda q}{1 + \lambda\alpha(1 - q^2)}. \quad (45)$$

These are solved via fixed point iterations. Their solutions shall be denoted by $q_*(\alpha, \lambda), r_*(\alpha, \lambda)$. Using the relation (30) but with ψ^{RLE} , and that the solution is extremizing ψ^{RLE} , we can finally approximate the MMSE:

$$\begin{aligned} \text{MMSE} &= 2 \frac{\partial}{\partial \lambda} \left(\frac{\lambda}{2} - \psi^{\text{RLE}}(\lambda, \sigma_*) \right) \\ &= \frac{1 - q_*(\alpha, \lambda)^2}{1 + \lambda\alpha(1 - q_*(\alpha, \lambda)^2)}. \quad (46) \end{aligned}$$

Note that $q_* = r_* = \sigma_* = 0$ is always a solution of the system of equations for any (α, λ) . We call it the *paramagnetic solution* as it corresponds to no alignment

between posterior sample and ground truth. However, the MMSE for this solution,

$$\text{MMSE}_{\text{para}} = \frac{1}{1 + \alpha\lambda}, \quad (47)$$

is a non-trivial decreasing function of the SNR. This is because denoising is still possible, for any $\lambda > 0$, when the matrix \mathbf{X} has no macroscopic overlap with a posterior sample ($q_* = 0$ which is both the row or column overlap under ansatz (31)). We have checked that apart from very low SNR, this solution is unstable in the sense that any small positive initialisation for the iterative solution of the saddle point equations will yield another solution.

Given the MMSE, one could be tempted to integrate it w.r.t. the SNR λ to obtain the MI of matrix denoising. However, there could be multiple solutions $q_*(\alpha, \lambda)$ associated to given values of λ and α , which impeaches this naive reasoning. A more careful approach is required. Given the two equations, we thus look for the *mutual information potential* that generates them, and we shall always choose solutions that minimize it. Indeed, it turns out that there is a unique potential $\iota(r, q; \alpha, \lambda)$ that yields (44), (45) and is at the same time consistent with the I-MMSE relation (7) which, using (46), must be

$$\frac{d}{d\lambda} \iota(r_*, q_*; \alpha, \lambda) = \frac{1}{4} \frac{1 - q_*(\alpha, \lambda)^2}{1 + \lambda\alpha(1 - q_*(\alpha, \lambda)^2)}. \quad (48)$$

We observe that (44), (45) define a vector field

$$v_r(r, q) := q - \mathbb{E}H\langle\eta\rangle_r, \quad (49)$$

$$v_q(r, q) := r - \frac{\lambda q}{1 + \lambda\alpha(1 - q^2)}. \quad (50)$$

It is conservative, because it is irrotational on a simply connected domain:

$$\frac{\partial}{\partial q} v_r(r, q) = 1 = \frac{\partial}{\partial r} v_q(r, q). \quad (51)$$

Therefore, any line integral of this vector field starting from $(0, 0)$ and ending at an arbitrary point (r, q) will yield the potential. We choose $(0, 0) \rightarrow (r, 0) \rightarrow (r, q)$:

$$\begin{aligned} \iota(r, q; \alpha, \lambda)K + C &= \int_0^r v_r(s, 0)ds + \int_0^q v_q(r, p)dp \\ &= -2\mathbb{E}_{\xi, H} \ln \int dP_X(\eta) e^{(\xi\sqrt{r} + Hr)\eta - \frac{1}{2}r\eta^2} + rq \\ &\quad + \frac{1}{2\alpha} \ln(1 + \lambda\alpha(1 - q^2)) \end{aligned}$$

where we have introduced two constants K and C to be fixed later. The term $\mathbb{E}H\langle\eta\rangle_s = 1 - \text{mmse}(H | \sqrt{s}H + \xi)$ has been integrated w.r.t. s using the I-MMSE relation for a scalar Gaussian channel [65]. It is easy to check that this potential generates the correct saddle point equations. Now we evaluate it at their solutions. This will yield a MI whose basic properties will help us to fix K and C . In particular, at $\lambda = 0$ one has $q_* = r_* = 0$, and

$\iota(r_*, q_*; \alpha, 0) = 0$, which directly entails $C = 0$. In order to fix K we compute the derivative

$$\frac{d}{d\lambda} \iota(r_*, q_*; \alpha, \lambda) = \frac{1}{2K} \frac{1 - q_*(\alpha, \lambda)^2}{1 + \lambda\alpha(1 - q_*(\alpha, \lambda)^2)}. \quad (52)$$

The I-MMSE relation (48) then requires $K = 2$. Hence, we can finally write the MI of matrix denoising as

$$\iota(\alpha, \lambda) := \text{extr}_- \{ \iota(r, q; \alpha, \lambda) \} \quad (53)$$

with MI potential

$$\begin{aligned} \iota(r, q; \alpha, \lambda) &:= \frac{rq}{2} + \frac{1}{4\alpha} \ln(1 + \lambda\alpha(1 - q^2)) \\ &\quad - \mathbb{E}_{\xi, H} \ln \int dP_X(\eta) e^{(\xi\sqrt{r} + Hr)\eta - \frac{1}{2}r\eta^2}. \end{aligned} \quad (54)$$

Extremization is w.r.t. (r, q) . extr_- selects the solution of the saddle point equations minimizing the potential.

As it should, this formula recovers the known rank-1 replica symmetric potential [17, 38] when $\alpha \rightarrow 0$:

$$\begin{aligned} \iota(r, q; 0, \lambda) &= \frac{rq}{2} + \frac{\lambda}{4}(1 - q^2) \\ &\quad - \mathbb{E}_{\xi, H} \ln \int dP_X(\eta) e^{(\xi\sqrt{r} + Hr)\eta - \frac{1}{2}r\eta^2}. \end{aligned}$$

As manifest from the derivation, our multiscale mean-field theory can handle generic observation channels as long as the observations remain independent conditionally on the signal, namely $Y_{ij} \sim P_{\text{out}}(\cdot | \mathbf{X}_i \cdot \mathbf{X}_j / \sqrt{N})$. The fixed point equation $q = \mathbb{E}H\langle\eta\rangle_r$ is unchanged, whereas $r = g_{\text{out}}(q)$ with a channel-dependent g_{out} is obtained by canceling the derivative of (36) w.r.t. q . The consistency $r = \sigma$ still holds, as well as $J(\sigma) = q$.

Relation to the Sakata and Kabashima replica method with Gaussian ansatz. The same formula for the MI (53), (54) can be produced using the approach of [3], also used in [78–80] in a Bayesian context. We have adapted their method to our model in Appendix D for completeness, which is close to what is done in [80]. This alternative derivation does not go through a cavity computation but instead uses directly the replica method at the scale $O(MN)$. From our understanding, the first ‘‘Gaussian ansatz’’ they use is to approximate $(z_{ij}^a = \mathbf{x}_i^a \cdot \mathbf{x}_j^a / \sqrt{N})_{i,j=1,\dots,N, a=0,\dots,n}$, where a is the replica index, as a jointly Gaussian family. The second ansatz is on their covariance. Somewhat counter intuitively, they consider them independent. Overall, this is equivalent to consider $(z_{ij}^a)_{i,j}$ as a GOE matrix, with a semicircular spectral density. This is hard to justify a-priori, given that this matrix is of Wishart type, whose spectrum follows the Marcenko-Pastur law. This approximation may however be more justifiable as $\alpha = M/N$ gets large because in this case, a Wishart matrix resembles more a GOE one with a mean. As discussed in [83], this approximation is indeed supposedly more accurate in this case (as confirmed by our numerics), and even possibly exact in the $\alpha \rightarrow \infty$ limit. Interestingly, (54) also

yields the low rank formula in the limit $\alpha \rightarrow 0$, which signals the approach is actually taking into account both α limits.

As mentioned in Section II B, equations (44), (45) were deemed incorrect for a long time. In fact, in the past they were tested against the exact MI for Gaussian prior only [83]. But this is precisely the case in which they are not supposed to hold, because the denoising phase never ends for Gaussian prior and so the HCIZ integral is the right tool. With our contribution we redeem the replica equations found in [3, 78–80], and show that they actually yield excellent results in the factorisation phase (and suprisingly good ones in the denoising phase too for sufficiently large α), a phase which exists only for non-rotationally invariant priors. Despite leading to the same equations, the multiscale theory we propose is based on different, interpretable, hypotheses.

D. Complete ansatz taking into account the prior universality in the denoising phase

We have confirmed numerically that the prior universality conjecture of [67] holds before the denoising-factorisation transition. This should be considered in order to improve the mean-field theory as it is inaccurate in this region. Indeed, the MMSE predicted by the multiscale theory does not match the exact one for Gaussian prior, nor for the Rademacher case in the denoising phase. This is somehow expected. The reason is that our ansatz for the bulk measure, corresponding to taking the posterior associated with the channel $\mathbf{Y}'_{\text{eff}} = \sqrt{\sigma} \mathbf{X} + \mathbf{Z}'_{\text{eff}}$, breaks an “effective rotational symmetry” that seems to hold in the denoising phase as we argue in Section V. The rotational symmetry breaking comes from the fact that this channel corresponds to a direct observation of \mathbf{X} . Therefore there is no reason for the theory to be quantitatively correct in the denoising phase which is fundamentally different from the factorisation phase. Yet, beyond the transition our ansatz is an excellent approximation (if not exact), because of the strong alignment between posterior “patterns” $(\mathbf{x}_\mu)_{\mu \leq M}$ and the planted ones $(\mathbf{X}_\mu)_{\mu \leq M}$ (see Section V). This implies that the behavior of the cavity $\boldsymbol{\eta}$ is dominated by its direct interaction with the associated planted row \mathbf{H} (mediated by $H_{N,M}^{\text{row}}$) while the effect of the bulk simplifies greatly and is captured by a mean-field linked to channel (31). We conclude that the denoising phase is a sort of “random matrix theory regime” which needs to be analyzed by its own set of techniques (i.e., proofs of universality and the HCIZ integral). In contrast, the factorisation phase is a “mean-field regime” more amenable to statistical physics methods and we are thus confident that the proposed approach is accurate in this region, as backed up by the numerics and the robustness of our ansatz to attempts at improving it, see Section IV F.

From FIG. 3 and the related discussion, we deduce that there are always only three possible thermody-

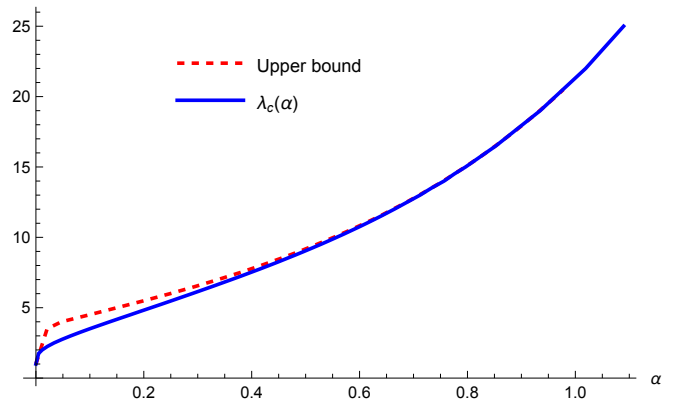


FIG. 6: Thermodynamic denoising-factorisation phase transition $\lambda_c(\alpha)$ given by (55) and its upper bound given by the r.h.s. of (17), for Rademacher prior.

amic states: one corresponds to the “universal RIE branch”, another to the “non-universal factorisation branch” reached from informative initialisation, and finally the dynamical glass state. Given our numerical evidence as well as the work of Semerjian [67], for low SNRs we select the RIE branch as equilibrium state, which corresponds to the Gaussian MI ι^G . After the transition, that will be properly defined below, we instead select the factorisation state described correctly by the multiscale theory with informative initialisation, see Section IV E.

The question now is how to locate the denoising-factorisation phase transition, assuming there is only one transition (which is verified in our numerical experiments). Considering a discrete prior, we know from (19) that the asymptotic MI must saturate to $\mathcal{H}(X)$ when the SNR diverges. In addition, the MI has to be continuous. It is not difficult to see that if we select ansatz (53) for too low SNRs, then the MI would saturate at a lower value than it should, given the exponential saturation for large SNRs predicted by (53). Therefore, the only alternative remaining is to locate the thermodynamic transition in the large system limit as

$$\lambda_c(\alpha) := \sup \{ \lambda \geq 0 : \iota^G(\alpha, \lambda) \leq \iota(\alpha, \lambda) \}. \quad (55)$$

As we show in the next section this is in good agreement with our finite size experiments once we take properly into account finite size effects. Consistently, our final ansatz ι^* for the MI is then

$$\iota^*(\alpha, \lambda) := \min \{ \iota^G(\alpha, \lambda), \iota(\alpha, \lambda) \}. \quad (56)$$

Note that the choice of selecting the Gaussian MI in the denoising phase for an informative prior like Rademacher (i.e., a prior which is not rotational invariant) is somewhat intuitive. The MMSE associated with an informative prior cannot be larger than in the Gaussian case. Therefore, ι cannot be correct in the region where its prediction of the MMSE (46) is larger than the one of the RIE (14). The Gaussian MMSE is thus necessarily

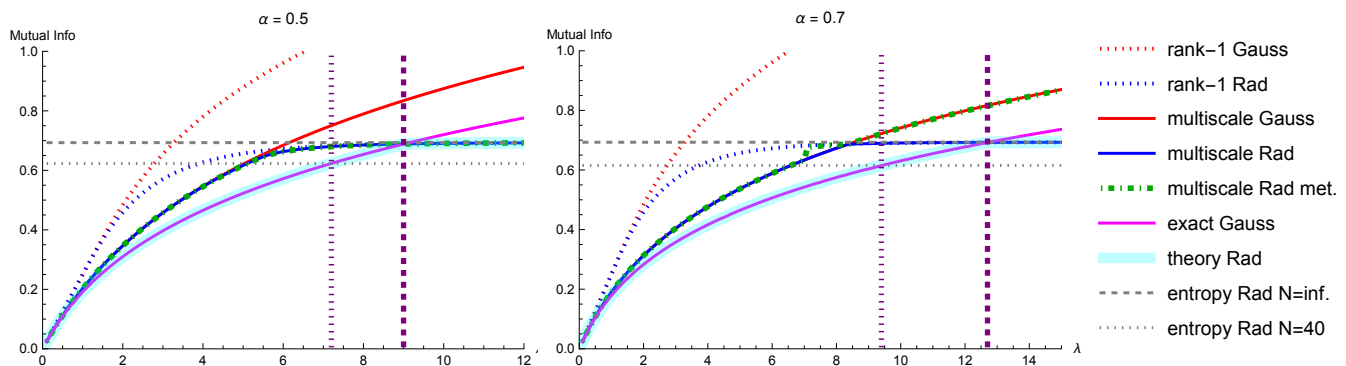


FIG. 7: Thermodynamic limit of the mutual information as function of the SNR for $\alpha \in \{0.5, 0.7\}$ with Gaussian and Rademacher priors. We plot *i*) the rank-1 MIs, *ii*) the “multiscale” curves referring to $\iota(\alpha, \lambda)$ (53) with the equilibrium solution selected, *iii*) the “multiscale met.” curve corresponds to the metastable solution (which only exists for Rademacher prior), *iv*) the “exact Gauss” curve is the exact MI for Gaussian prior $\iota^G(\alpha, \lambda)$ (16), *v*) the “theory Rad” is the complete ansatz $\iota^*(\alpha, \lambda)$ (56) for Rademacher prior once taking into account universality in the denoising phase, *vi*) the entropy density $\mathcal{H}(\mathbf{X}\mathbf{X}^\top)/(NM)$ for $N \rightarrow +\infty$, equal to $\ln 2$, and its finite-size approximation (18) given by $\ln 2 - \ln(2^M M!)/(MN)$ with $N = 40$, $M = \alpha N$. Finally *vii*) the right most vertical line pinpoints the crossing of the exact Gaussian MI with the multiscale prediction, i.e., the infinite size transition λ_c (55), while the left most vertical line shows the crossing of the Gaussian MI with $\ln 2 - \ln(2^M M!)/(MN)$ which approximates the location of the denoising-factorisation transition taking into account finite size effects.

at least a better approximation to the true one, and we claim that in the denoising phase they actually match, in agreement with the analysis of [67]. On the other hand, as discussed in the following section, the choice of our ansatz in the factorisation phase is validated by the good agreement with our numerical experiments, see for instance FIG. 4.

E. Theoretical phase diagram and consistency with the numerical observations

Iterating (44), (45) we obtain the MMSE predicted by the mean-field theory, which we provide in FIG. 8. We also plot the associated asymptotic MI (53) in FIG. 7. When solving (44), (45) by fixed point iteration, we call the initialisation $q^{t=0} = 1$ *informative*. The *uninformative* initialisation is instead $q^{t=0} = \varepsilon \ll 1$ but non-zero. From these two obtained solutions, the *equilibrium* (q_* , r_*) is the one that minimizes (54). The other solution (we always observed at most two) is called *metastable*. It matches the equilibrium solution if unique, as for $\alpha = 0.5$ in FIG. 7, while they differ beyond a point for $\alpha = 0.7$.

The complete ansatz taking into account universality at low SNR is $\iota^*(\alpha, \lambda)$ (56). We display the associated MI and MMSE on the plots in cyan. For all plots displayed, ι^* catches the key features of the problem evidenced by our numerical findings. We stress again the extremely good agreement between four times the λ -derivative of ι^* and the finite size MMSEs in the factorisation phase, see also FIG. 4. Hereby we describe our theoretical findings focusing on the complete ansatz ι^* if not specified otherwise, comparing them with those of Section III.

i) Agreement with the mutual information upper bound. We have verified that our prediction for the MI for Rademacher prior remains upper bounded by the entropy $\mathcal{H}(X)$ as it should, see FIG. 6. The transition predicted by (55) is thus always in agreement with the bound (17), which becomes tighter as α increases as seen from the figure. This is a non-trivial consistency check, entailing in particular that for high SNRs the MMSE decays exponentially with the SNR, as supported by finite size numerical experiments, see FIG. 4 and 8. The exponential decay of our MMSE prediction in the factorisation phase, which is asymptotically in λ the same as for the rank-1 case with Rademacher prior, hints at the fact that in the factorisation phase there is essentially decoupling between the posterior patterns (\mathbf{x}_μ), and the problem resembles M independent rank-1 problems with properly tuned SNRs.

ii) Universality at low SNR. Despite the mean-field solution ι being approximate in the denoising “random matrix regime”, at low values of the SNR the curves $\iota(\alpha, \lambda)$ for Gaussian and Rademacher prior, which should be identified with the RIE curve, do match; it is also evident at the level of the MMSE, see FIG. 8. This is a signature of universality holding in a regime of SNRs captured by the mean-field theory, in agreement with FIG. 1 and 2. When α increases, the matching lasts until very close to the crossing of ι and the Rademacher prior entropy, thus the universality signature becomes more pronounced. It shows that ι becomes more accurate and consistent at larger α (but it also is exact at $\alpha = 0$). Obviously, ι^* is universal before the transition by construction.

iii) Denoising-factorisation transition. The theory correctly predicts the existence of the denoising-factorisation

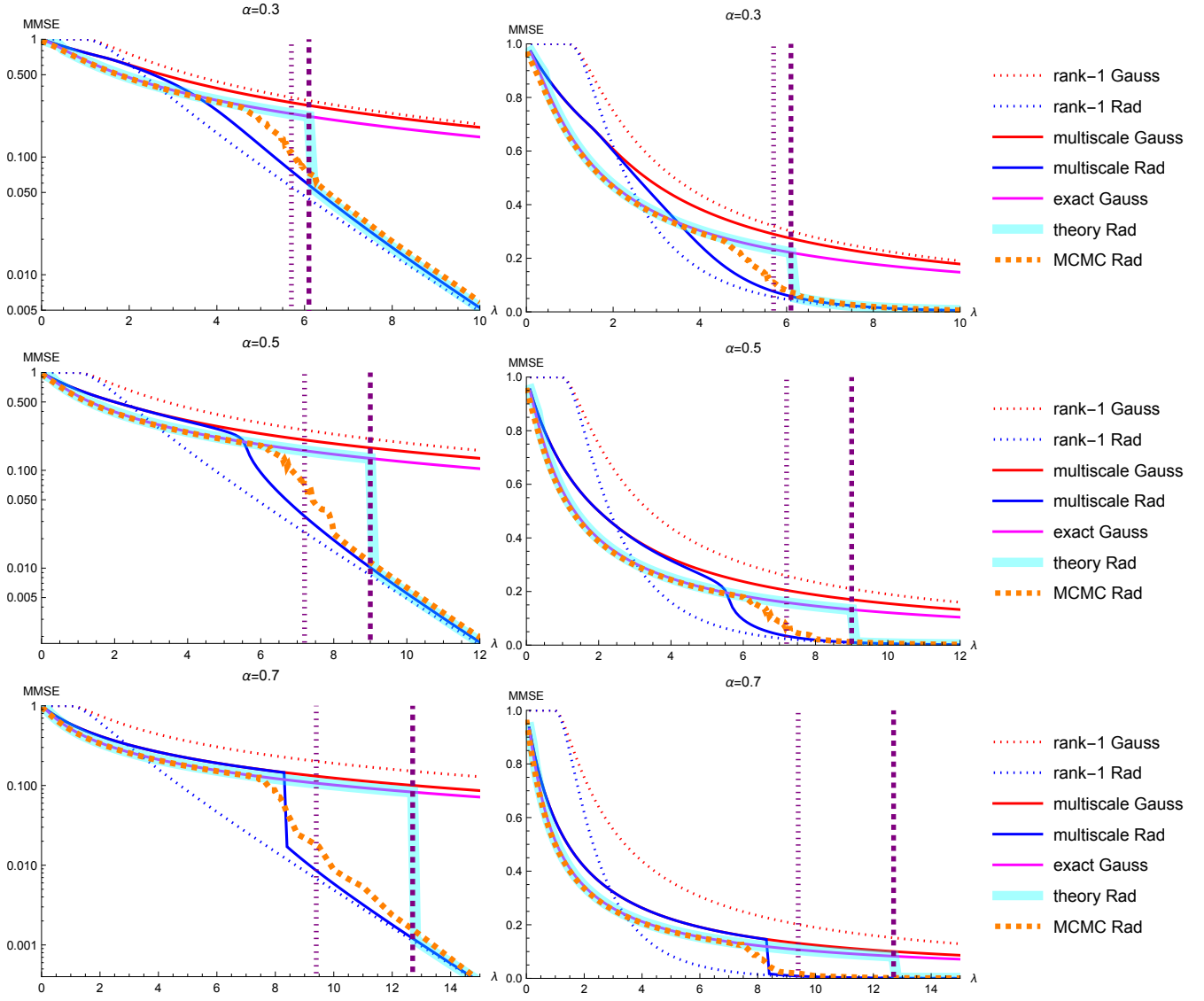


FIG. 8: Thermodynamic limit of the MMSE as function of the SNR for $\alpha \in \{0.3, 0.5, 0.7\}$ and Gaussian and Rademacher priors. Logarithmic scale on the left, linear scale on the right. We plot *i*) the rank-1 MMSEs, *ii*) the “multiscale” curves correspond to the prediction (46) with the equilibrium solution selected, *iii*) the “exact Gauss” curve is the true Gaussian MMSE obtained via (14), which also corresponds to the performance of the RIE for any prior with zero mean and unit variance, *iv*) the cyan “theory Rad” is our theoretical prediction for the MMSE with Rademacher prior corresponding to four times the derivative of $\iota^*(\alpha, \lambda)$ (56) w.r.t. λ , and *v*) “MCMC Rad” are the Monte Carlo results with Rademacher prior (see Tables I and II for details). Finally *vi*) the right vertical line pinpoints the location of the infinite N transition λ_c (55), while the one on the left is its approximate location once taking into account finite size effects, see caption of FIG. 7 and text.

transition observed in our numerical experiments. Indeed, for all α 's tested we see a change of behaviour in the λ -derivative of the MI $\iota^*(\alpha, \lambda)$ separating the regime where the MI is prior independent, from the factorisation phase where the MI for the Rademacher prior approaches the entropy of the prior exponentially fast in λ . The MI for the Gaussian prior instead continues to increase smoothly as it should. The transition as well as the algebraic versus exponential decay of the MMSE in

the SNR observed numerically is caught by the theory, see FIG. 8. Interestingly, this is also the case for the mean-field solution ι alone.

For what concerns the quantitative prediction of the transition location, it seems from FIG. 8 that there is a non-negligible gap with what $\iota^*(\alpha, \lambda)$ predicts (blue cyan curve). We argue here that this is due to the finite size of the simulated system, and can be accounted for. In fact, our arguments in Section III make it clear that

for finite sizes the MI for Rademacher prior must not saturate to $\ln 2$ due to the degeneracy induced by column permutations and signs, which explains precisely the gap with $\ln 2$ in FIG. 1. Since the empirical MI curves follow $\iota^G(\lambda, \alpha)$ rather closely at low SNR, they must saturate earlier, namely at a smaller λ than the asymptotic one λ_c , and at a lower value than $\ln 2$. For instance, for $\alpha = 0.5$ and $N = 40$ saturation occurs at $\text{MI} \approx 0.6228$, which is also reported as the lowest dotted horizontal line in the left panel of FIG. 7. The curve ι^G crosses that value at $\lambda \approx 7.2$, which gives us an estimate of the transition location for that size (even if formally we cannot talk about phase transition at finite size). But we see that the change in the behaviour of the derivative of the finite size MI is not sudden and starts even before 7.2. This is consistent with FIG. 8 for $\alpha = 0.5$, where the MCMC curve detaches from the Gaussian MI around $\lambda \approx 6.5$. Nevertheless, observe that the finite-size-corrected approximation to the transition at 7.2 falls nicely in the middle of the “crossover region” between the two phases for the MMSE. The same correcting approach works for the other values of α .

Let us explain in more detail the way we computed corrections to the transition location. The procedure starts by computing the finite size entropy $\mathcal{H}(\mathbf{X}\mathbf{X}^\top)/(NM)$ using (18). Then we find the SNR where ι^G attains this value: this gives an upper bound on the finite size transition, which we expect to be close to it given the numerical and theoretical evidence. This implies that the larger α , the smaller the slope of $\iota^G(\alpha, \lambda)$ in λ , and thus the larger the gap between the asymptotic transition point λ_c and its approximate location for finite size, see FIG. 7.

On top of this gap increasing with α , the crossover region for the transition should also get wider. To see it we notice that the finite size corrections to the MI, estimated through (19) as $\ln(2^M M!)/(MN)$ ($\approx 5 \cdot 10^{-2}$ in all our experiments), are large given the size of the system ($MN \approx 1000$ in all our experiments). As comparison, in the low rank spiked Wigner model (our model with $M = 1$), finite size corrections to the MI instead vanish as $1/N$ which is faster relatively to the system size. For size 1000, this yields a correction of around 10^{-3} for a low rank model, which is roughly two orders of magnitude smaller than here. Notice also that finite size corrections increase in α , since they are directly linked to the number of column permutations. In summary, thanks to the aforementioned correction procedure, the predicted finite size “transition” does fall in the middle of the crossover region for the MMSE, which gets wider with larger α .

iv) Spinodal transition and statistical-to-computational gap. Our theory $\iota^*(\alpha, \lambda)$ predicts the presence of a thermodynamic first order phase transition $\lambda_c(\alpha)$ with a discontinuity in the MMSE for any $\alpha > 0$. We have already discussed based on FIG. 3 that at low SNR, the only thermodynamic state present is the universal RIE state. This implies that before the first order transition, there must be a spinodal transition linked to the appearance of the informative factorisation state in addition to

the RIE state, a point around which the RIE state seems to shatter into a dynamical glassy state as observed on FIG. 3. A spinodal transition followed by the coexistence of an informative and glassy states is a typical mechanism at the root of algorithmic hardness in high-dimensional inference [100, 120]. This connection should however be considered with some precaution, as it has been noticed in various settings that the onset of glassiness does not always prevent inference algorithms, including sampling-based, to perform well [100, 121, 122]. ι^* is unable to detect the location of the spinodal transition given that it is a pure equilibrium theory. One would need to modify it in order to take into account out-of-equilibrium glassy effects linked to replica symmetry breaking [100, 123], which is out of the scope of the present paper. Given that we are in the Bayes-optimal setting, the thermodynamic equilibrium can anyway be described by a replica symmetric theory [124–126].

It is worth noting that even though the mean-field prediction $\iota(\alpha, \lambda)$ is not exact in the denoising phase, the potential (54) does capture the presence of a spinodal transition for $\alpha \geq 0.7$, see FIG. 3 and the green curve in FIG. 7. Indeed, when $\alpha = 0.7$ the multiscale theoretical curve exhibits a metastable branch around $\lambda \approx 7$, see the discontinuity in green curve in FIG. 7. It detaches from the equilibrium curve through a spinodal transition where the informative fixed point appears. We thus interpret the mean-field theory as an approximation valid over the whole range of SNR (while ι^* may be exact), in the sense of the critical phenomenology it implies and that cannot be probed from our final ansatz alone.

F. Can the mean-field theory $\iota(\alpha, \lambda)$ be improved?

We have shown that the mean-field prediction (53) based on the bulk approximation (31) produces excellent results in the factorisation phase where an MMSE lower than the Gaussian one is possible (but is approximative in the denoising phase where ι^* corrects it). One may wonder if it possible to do better by generalizing ansatz (31). We have performed several attempts keeping the bulk measure factorised over the indices (i, μ) as needed to justify the computation of the RLE free entropy.

As first trial, one may think that each entry (i, μ) comes with a different SNR $\sigma_{i\mu}$, whose values are i.i.d. drawn from a certain distribution which becomes the new order parameter. In that case, equations (41), (42) simply contain $\mathbb{E}_\sigma J(\sigma)$ in place of $J(\sigma)$. In particular, (41) forces the distribution of σ to be a δ_{σ_*} where again $\sigma_* = r_*$, since the r.h.s. is deterministic. Hence this approach recovers the proposed solution.

Another approach is to introduce an SNR profile (σ_μ) such that $Y'_{i\mu} = \sqrt{\sigma_\mu} X_{i\mu} + Z'_{i\mu}$, only labeled by μ to detect possible inhomogeneities at equilibrium in the “column index space”. The (σ_μ) are then assumed to be divided in an arbitrary number C of blocks to be sent to $+\infty$ after the thermodynamic limit, in a similar fashion to spatial

coupling, see [127, 128] for similar computations. Specifically $\sigma_\mu = \sigma_c$ if $\mu \in \Lambda_c \subset \{1, \dots, M\}$. The computation in Section IV B still works, except that this time we need to introduce more order parameters $(r_c, q_c)_{c=1, \dots, C}$, where q_c corresponds to the overlap $\frac{C}{M} \sum_{\mu \in \Lambda_c} \eta_\mu H_\mu$. These order parameters then satisfy the equations

$$q_c = \mathbb{E}H\langle \eta \rangle_{r_c},$$

$$r_c = \frac{\lambda J(\sigma_c)}{1 + \lambda \alpha \left(1 - \frac{1}{C} \sum_{c=1}^C J(\sigma_c) q_c\right)},$$

together with the cavity-bulk consistency equation $\sigma_c = r_c$. This system always admits the paramagnetic solution $\sigma_c = r_c = q_c = 0$ for any given set of c 's, and the homogeneous solution $(\sigma_c, r_c, q_c) = (\sigma_*, r_*, q_*)$ for all c 's, which also coincides with the solution given by the ansatz (31). No other solution seems to exist. Interestingly, the latter seems to be always the most convenient in terms of MMSE, since we see numerically that in that case all the SNR values σ_c get attracted to a higher SNR σ_* w.r.t. the case when some σ_c are set to 0. Furthermore, if one interprets the above system of equations as a fixed point equation for σ_c ,

$$\sigma_c = \frac{\lambda J(\sigma_c)}{1 + \lambda \alpha \left(1 - \frac{1}{C} \sum_{c=1}^C J(\sigma_c)^2\right)},$$

the solutions where some $\sigma_c = 0$ are unstable under such iteration which discards them. One can also run a population dynamics [101] using the above equation interpreted as a distributional fixed point equation, which thus looks for a solution where the law of the (σ_μ) is the same for all μ , rather than to look for solutions for the ordered profile (σ_c) shared by all rows. And, again, the final histogram of (σ_μ) ends up peaked around the value of the homogeneous solution σ_* .

A final attempt we made consists in admitting a block structure also in the i -index, i.e. the row index: $\sigma_{i\mu} = \sigma_{\ell c}$ for $i \in \Lambda_\ell, \mu \in \Lambda_c$, with $\ell = 1, \dots, L$ and c as before. With this block structure, one can recast the fixed points equations in terms of the same order parameters as above with some slight differences:

$$q_{\ell'c} = \mathbb{E}H\langle \eta \rangle_{r_{\ell'c}},$$

$$r_{\ell'c} = \frac{1}{L} \sum_{\ell=1}^L \frac{\lambda J(\sigma_{\ell c})}{1 + \lambda \alpha \left(1 - \frac{1}{C} \sum_{c=1}^C J(\sigma_{\ell c}) q_c\right)},$$

where ℓ' corresponds to the index of the row-block from which the cavity was extracted. They are completed with the cavity-bulk consistency $\sigma_{\ell'c} = r_{\ell'c}$. All this must be true for all $\ell' \in \{1, \dots, L\}$ as the cavity can be extracted from any block. Because the r.h.s. of the $r_{\ell'c} = \dots$ equation is ℓ' -independent, solutions must be homogeneous in the row-block indices and we are back to the previous case.

In conclusion, none of these possible generalizations of (31) yields an improvement w.r.t. our current ansatz.

This suggests that the solution we found is robust as long as the bulk measure is assumed to be factorised, which we think is exact in the factorisation phase.

V. PROBING THE PHASES THROUGH THE OVERLAP MATRIX, AND FACTORISATION

In this section we consider only a Rademacher distributed \mathbf{X} for simplicity. So far, we have focused on the denoising task of recovering $\mathbf{X}\mathbf{X}^\top$. We have divided the phase diagram in two thermodynamic phases: the universal denoising phase where the RIE is optimal, and the factorisation phase where it is not, because exploiting the prior and *factorised* structure is needed there to denoise. It is thus natural to wonder if optimal denoising is related to the *factorisation task*, namely estimating the single factor \mathbf{X} non-trivially. Non-trivial estimation means here finding an estimator $\hat{\mathbf{X}}(\mathbf{Y})$ verifying

$$\lim_{N \rightarrow \infty} \frac{1}{NM} \max_{\mathbf{\Pi} \in \pi_M} \text{Tr}(\mathbf{X}^\top \hat{\mathbf{X}} \mathbf{\Pi}) > 0, \quad (57)$$

where π_M is the set of $M \times M$ signed permutation matrices. It is not clear that it is possible given the numerous symmetries and invariances of the model. In this section we explore this question by getting a more detailed description of the phases through the analysis of a richer order parameter than the MMSE, namely the *overlap*:

$$\mathbf{Q} := \frac{\mathbf{X}^\top \mathbf{x}}{N} = \left(\frac{\mathbf{X}_\mu^\top \mathbf{x}_\nu}{N} \right)_{\mu, \nu \leq M} \in \mathbb{R}^{M \times M}, \quad (58)$$

where $\mathbf{x} \sim P(\cdot | \mathbf{Y})$ is a posterior sample, and (\mathbf{x}_μ) are the columns/patterns of \mathbf{x} . The MMSE can be written directly in terms of the overlap:

$$\text{MMSE} = \frac{1}{M} \mathbb{E} \left\| \frac{\mathbf{X}\mathbf{X}^\top}{N} \right\|^2 - \frac{1}{M} \mathbb{E} \langle \|\mathbf{Q}\|^2 \rangle, \quad (59)$$

which follows from the Nishimori identity. From (57), a posterior sample \mathbf{x} is a non-trivial estimator if $\frac{1}{M} \text{Tr}(\mathbf{Q}\mathbf{\Pi}^*) > o_N(1)$ for a \mathbf{x} -dependent permutation $\mathbf{\Pi}^*$.

A. Behavior of the overlap in the two phases: can \mathbf{X} be inferred?

It is insightful to distinguish between the diagonal and off-diagonal contributions of the overlap to the MMSE. Note that from the permutation and sign invariance, columns of posterior samples \mathbf{x} obtained from the Monte Carlo sequence must be sorted appropriately to match the ones of the ground truth in order to access a meaningful overlap. In other words, we need an efficient way to approximate the solution of the optimisation problem (57). Numerically, this is achieved via iteration with respect to the columns of \mathbf{X} . In the first iteration, one finds the column of \mathbf{x} showing the largest absolute inner product with \mathbf{X}_1 , labeling its index as $\pi(1)$.

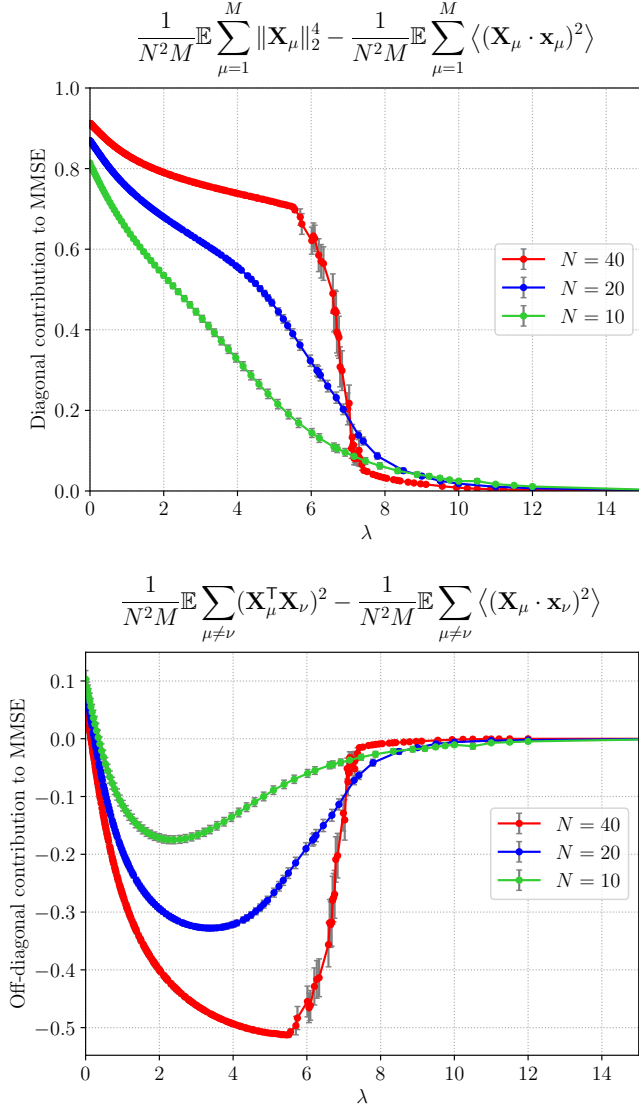


FIG. 9: Monte Carlo results for the diagonal (upper figure) and off-diagonal (lower one) contributions to the MMSE (59) after reordering of each sample columns, with Rademacher prior, for various N with $\alpha = 0.5$. Error bars represent standard errors of the mean.

For subsequent iterations $\mu = 2, \dots, M$, choose $\pi(\mu)$ as $\pi(\mu) = \operatorname{argmax}_{\nu \in S_\mu} |\mathbf{X}_\mu^\top \mathbf{x}_\nu|$, where S_μ is the set of indices from 1 to M excluding $\pi(1), \dots, \pi(\mu - 1)$. By executing this column reordering procedure for *each* posterior sample, we can distinguish between diagonal and off-diagonal contributions to the MMSE, with the diagonal one representing the error made from misalignment between matched patterns, and the off-diagonals representing the contributions from alignment between unmatched patterns. For all the rest of this section, every time a posterior sample \mathbf{x} appears, it is assumed that its columns have already been permuted according to the

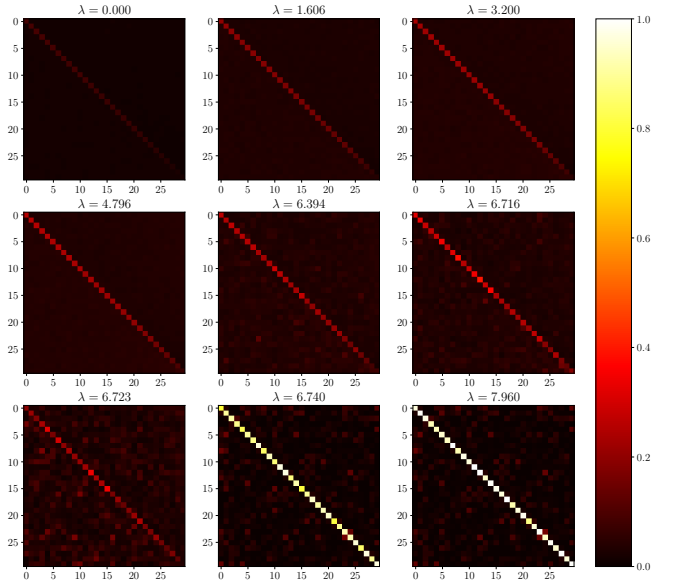


FIG. 10: Average squared overlap $N^{-2} \langle (\mathbf{X}^\top \mathbf{x})^{\odot 2} \rangle$ (the square applies entrywise) for various SNRs obtained by Monte Carlo after reordering of each sample columns, for a single instance (\mathbf{X}, \mathbf{Z}) with Rademacher prior and $(N, M) = (60, 30)$.

above greedy procedure as $\mathbf{x} \leftarrow \mathbf{x} \mathbf{\Pi}^{\text{greedy}}(\mathbf{x})$, and the Monte Carlo approximations of expectations $\langle \cdot \rangle$ are taking into account this per-sample columns reordering.

FIG. 9 shows the diagonal and off-diagonal contributions to the MMSE (59) for finite sizes computed by Monte Carlo. First, looking at the diagonal contribution to the MMSE for SNRs in the denoising phase (λ less than ~ 6 for this size), the curve seems to get closer to $1 = \mathbb{E} \sum_{\mu=1}^M \|\mathbf{X}_\mu\|^2 / (N^2 M)$ as N increases. Looking at the bottom part of FIG. 9 we observe that in this phase the off-diagonal overlap entries contribute greatly in decreasing the MMSE in FIG. 2. The strong negative values of $(\mathbb{E} \sum_{\mu \neq \nu} (\mathbf{X}_\mu^\top \mathbf{X}_\nu)^2 - \mathbb{E} \sum_{\mu \neq \nu} \langle (\mathbf{X}_\mu^\top \mathbf{x}_\nu)^2 \rangle) / (N^2 M)$ indicate that the $(Q_{\mu\nu})_{\mu \neq \nu}$ fluctuate more around 0 than in the case of i.i.d. patterns $(\mathbf{X}_\mu^\top \mathbf{X}_\nu / N)_{\mu \neq \nu}$. This is even more evident when plotting the histogram of the overlap entries in the denoising phase, see FIG. 11. The broader distributions compared to the gray one indicate larger fluctuations than in the random case (where \mathbf{X} and \mathbf{x} are i.i.d. from the prior). This plot illustrates that each \mathbf{x}_μ has small projection on most $(\mathbf{X}_\nu)_{\nu \leq M}$ of order $O(1/\sqrt{N})$; yet, as λ increases a large fraction of these projections become typically larger than between independent patterns (but of the same order).

Beyond the transition, however, the diagonal contribution to the MMSE drops quickly to zero, meaning that posterior patterns pair with ground truth patterns which are *retrieved* in a synchronized way (lower part of FIG. 10). Consistently, the off-diagonal contribution approaches 0, as posterior patterns “orthogonalize” w.r.t.

to the planted patterns, except for matched pairs that contribute to the reduction in the diagonal MMSE contribution. This already shows that in the factorisation phase, non-trivial estimation of \mathbf{X} is possible, up to the unavoidable signs and permutation ambiguity of the columns. The answer is less clear in the denoising phase and requires more care.

The averaged entrywise squared overlap is displayed in FIG. 10 for various SNRs, and in particular close to the crossover region (three plots at the bottom). The homogeneous background and weaker diagonal before the transition (upper part) signals that the information about the ground truth patterns is somehow diluted in all the posterior patterns, consistently with the bottom panel of FIG. 9. The diagonal then gets suddenly stronger and the background much smaller around the transition, indicating again a strong pattern-to-pattern matching between posterior samples and the signal in the factorisation phase. Overall these figures illustrate a clear change of behavior between the two phases, where the quasi basis of posterior patterns (\mathbf{x}_μ) (i.e., a set of N -dimensional vectors whose pairwise inner products are approximately \sqrt{N}) “aligns” much more with the quasi basis of planted patterns (\mathbf{X}_μ) beyond the transition (the latter were drawn i.i.d. and are thus almost orthogonal and linearly independent with high probability).

We have made two empirical observations that may suggest at first sight that factorisation is possible in the denoising phase, too: *i*) the diagonal contribution to the MMSE (upper part of FIG. 9) seems bounded away from one, and *ii*) the diagonals displayed in FIG. 10 seem $O(1)$ in the denoising phase. The question we thus aim at elucidating is whether these are artefacts of finite size effects combined with the column reordering procedure applied to the posterior samples (which necessarily amplifies the overlap diagonal), or if these effects survive to the thermodynamic limit. In other words, is the overlap $\mathbf{x}_\mu \cdot \mathbf{X}_\mu/N$ between matched pairs vanishing or not in the thermodynamic limit in the denoising phase (still assuming the permutation ambiguity is resolved)?

In order to answer this question, we can heuristically estimate finite size corrections, helping ourselves with the histograms at the top in FIG. 11. Similar histograms were obtained from overlap matrices to which we removed the diagonal for a fair comparison (even if the histogram almost does not change if keeping the diagonal, which is not true anymore beyond the transition as clear from the bottom one in FIG. 11). The diagonal is removed since it has different statistical properties than the off-diagonal entries, and we need to understand the statistics of the complement of the diagonal in order to assess if such random variables can induce the observed diagonal just through the reordering procedure. From FIG. 11 we deduce that the marginal law of off-diagonal elements rescaled by \sqrt{N} behave as centered Gaussian variables with variance $\sigma^2(\lambda)$ tuned by the SNR, evaluated numerically from the histograms. We thus make the simplifying assumption that the correlations among the

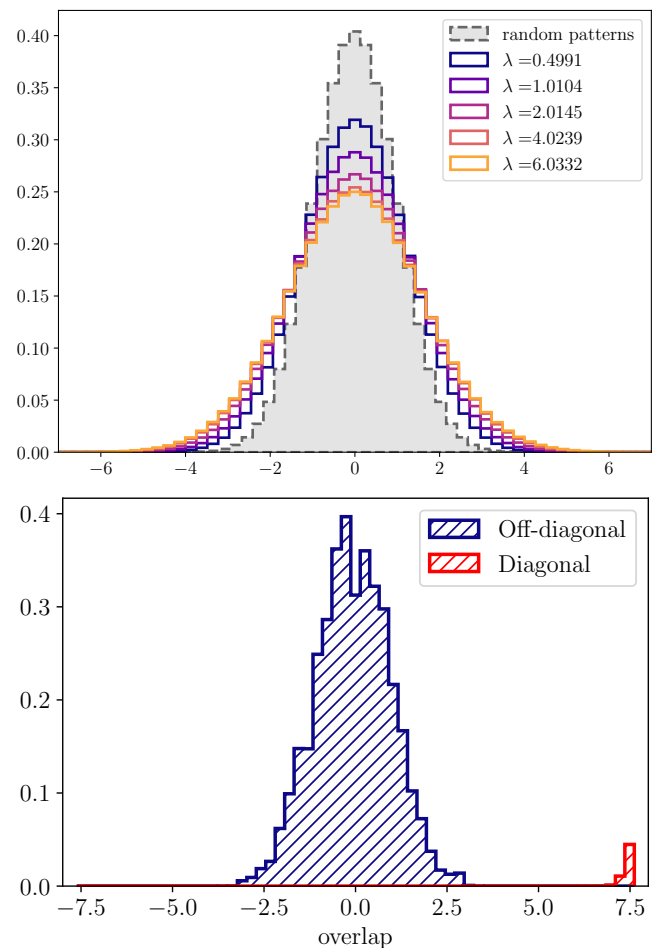


FIG. 11: Upper figure: Histogram of the entries of $\sqrt{N}\mathbf{Q}$ in the denoising phase for a single instance of (\mathbf{X}, \mathbf{Z}) with size $(N, M) = (60, 30)$ and Rademacher prior, obtained from $5 \cdot 10^3$ Monte Carlo samples after reordering of each sample columns. All entries are accumulated into each histogram, resulting in a sample size of $5 \cdot 10^3 M^2$ each. The gray histogram indicates the distribution of the overlap between two random Rademacher patterns of size N , which approaches a standard normal distribution as $N \rightarrow +\infty$. Lower figure: Histogram of $\sqrt{N}\mathbf{Q}$ for $\lambda = 7.96$ which lies at the start of the factorisation phase given that size, see FIG. 8. In that case, outliers emerge and so we have separated the diagonal and off-diagonal contributions. The diagonal one is peaked around $\sqrt{N} \approx 7.7$. The off-diagonal histogram resembles again a normal distribution, and its variance is very close to 1.

$(Q_{\mu\nu})_{\mu, \nu \leq M}$ are sufficiently weak to consider them independent. This allows us to estimate the average value of the diagonal of the squared overlap matrix under the null hypothesis that it is just due to the reordering.

According to the aforementioned independence and Gaussianity hypotheses on the overlap entries, the law

of the μ th diagonal square overlap element in FIG. 10 can be modeled as that of

$$\chi_\mu := \max_{\mu \leq \nu \leq M} Q_{\mu\nu}^2.$$

The cumulative distribution function of χ_μ is explicit:

$$\mathbb{P}(\chi \leq t) = \mathbb{P}(|Q_{11}| \leq \sqrt{t})^{M_\mu} = \text{erf}\left(\sqrt{\frac{Nt}{2\sigma^2(\lambda)}}\right)^{M_\mu}$$

for any $t \geq 0$, where $M_\mu := M - \mu + 1$, and $\text{erf}(z) := \frac{2}{\sqrt{\pi}} \int_0^z e^{-x^2} dx$. Furthermore, χ_μ being a positive random variable, the expectation of any function f of it can be computed via tail integration as

$$\begin{aligned} \mathbb{E}f(\chi_\mu) &= f(0) + \int_0^\infty f'(t)\mathbb{P}(\chi_\mu \geq t) dt \\ &= f(0) + \int_0^\infty f'(t)\left(1 - \text{erf}\left(\sqrt{\frac{Nt}{2\sigma^2(\lambda)}}\right)^{M_\mu}\right) dt. \end{aligned}$$

We are interested in evaluating the mean and order of the fluctuations of the average of the diagonal elements

$$\bar{\chi} := \frac{1}{M} \sum_{\mu=1}^M \chi_\mu. \quad (60)$$

Following our assumptions, the χ_μ 's are independent random variables so the variance of their sum is simply the sum of their variances:

$$\mathbb{V}(\bar{\chi}) = \frac{1}{M^2} \sum_{\mu=1}^M \mathbb{V}(\chi_\mu).$$

Therefore, if the empirical dominant diagonal in FIG. 10 was just an artefact of the reordering, its average value should be compatible with

$$\bar{\chi} \approx \mathbb{E} \bar{\chi} \pm \frac{2}{M} \sqrt{\sum_{\mu=1}^M \mathbb{V}(\chi_\mu)},$$

considering two standard deviations as confidence interval. Recall that both values on the r.h.s. depend on the SNR trough $\sigma^2(\lambda)$.

FIG. 12 compares the value of $\bar{\chi}$ with its uncertainty (orange) to the arithmetic mean of the diagonal elements of the averaged squared overlap $N^{-2}\langle(\mathbf{X}^\top \mathbf{x})^{\odot 2}\rangle$ (blue). There is an evident agreement in the denoising phase: the curve obtained via MCMC never detaches from $\bar{\chi}$ by more than two standard deviations. This suggests that our assumptions on the overlap elements $Q_{\mu\nu}$'s are effective, and above all that the diagonals in FIG. 10 for $\lambda \leq 6.723$, i.e., in the denoising phase for that size are compatible with the diagonal-amplifying effect of the reordering procedure. This entails that the posterior patterns \mathbf{x}_μ are diluted in the quasi basis of the ground truth patterns \mathbf{X}_μ . On the contrary, after the transition the

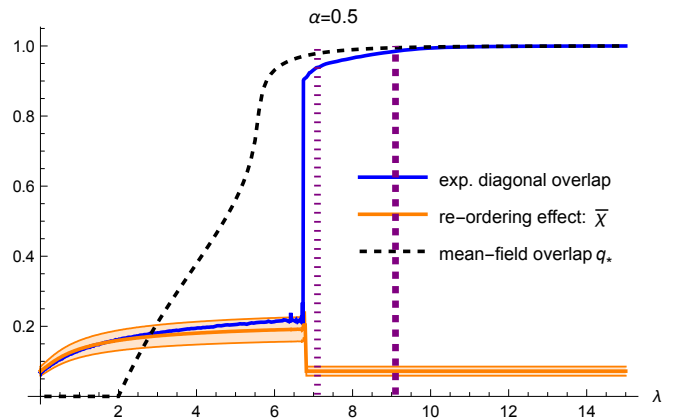


FIG. 12: Experimental average diagonal of the squared overlap as a function of λ obtained via Monte Carlo after reordering of each sample columns for a single instance (\mathbf{X}, \mathbf{Z}) with Rademacher prior and $(N, M) = (60, 30)$ (blue), as in FIG. 10. It is compared to the effect of the re-ordering of the columns of the posterior samples estimated by $\mathbb{E}\bar{\chi}$ (orange curve), with two standard deviations confidence interval (band). We also display the equilibrium diagonal overlap q_* predicted by the mean-field theory (44), (45). The asymptotic theory predicts a transition at $\lambda_c(\alpha = 0.5) \approx 9.1$ is the vertical purple dashed curve, which can be corrected for finite size effects yielding ≈ 7.1 , see caption of FIG. 7.

values of $\bar{\chi}$ are clearly incompatible (further than 5 standard deviations) with the empirical curve, signaling that the values in the diagonals of the bottom center and right panels in FIG. 10 are not only due to reordering, but a real effect happening in the factorisation phase. Note that the sudden decrease in $\mathbb{E}\bar{\chi}$ in FIG. 12 is related to the collapse of the blue histogram at the bottom of FIG. 11 onto a variance one normal law right after the transition, while it was more spreaded just before it, i.e., it is a manifestation of the transition through $\sigma^2(\lambda)$. As last comment, we can show that the effects $\mathbb{E}\bar{\chi}$ of the re-ordering vanish as $O(2\sigma^2(\lambda) \ln(2M)/N)$ (as it is a mean of maxima of i.i.d. Gaussians, see [129]).

In conclusion, from the evidence we gathered we expect that the seemingly bright diagonals in FIG. 10 for $\lambda \leq 6.723$ disappear in the thermodynamic limit. Consequently, in the denoising phase it is more plausible that factorisation is *not* possible, in contrast with the factorisation phase, and only denoising of $\mathbf{X}\mathbf{X}^\top$ is. This aligns with the fact that one cannot extract an estimator of \mathbf{X} from the RIE output, which we think is Bayes-optimal in that phase (or at least we do not see how to do so).

We have argued that non-trivial estimation of \mathbf{X} is impossible in the denoising phase. In order to clarify what is inferred about it that allows denoising of $\mathbf{X}\mathbf{X}^\top$, consider

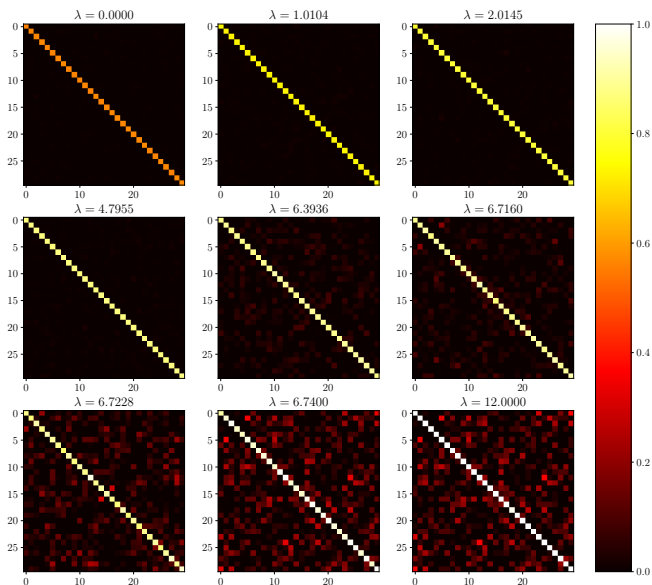


FIG. 13: Average overlap $N^{-1} \mathbf{X}^\top \langle \mathbf{xO}_*(\mathbf{x}) \rangle$ computed by Monte Carlo after reordering of each sample columns for a single instance of (\mathbf{X}, \mathbf{Z}) with Rademacher prior and size $(N, M) = (60, 30)$.

the following rotation for a given posterior sample:

$$\mathbf{O}_*(\mathbf{x}) := \underset{\mathbf{O} \in \mathbb{R}^{M \times M} : \mathbf{O}^\top \mathbf{O} = \mathbf{I}_M}{\operatorname{argmin}} \|\mathbf{X} - \mathbf{xO}\|^2. \quad (61)$$

In FIG. 13 we then plot the overlap matrix between “optimally rotated” posterior samples and the ground truth, averaged over Monte Carlo samples, i.e., $\mathbf{X}^\top \langle \mathbf{xO}_*(\mathbf{x}) \rangle / N$. As clear from the plot, in the denoising phase the profile of this matrix is diagonal, but with the diagonal now remaining order one as N increases, and whose intensity grows with λ . Note that there is a finite diagonal overlap even when $\lambda = 0$, as two random M -dimensional subspaces of \mathbb{R}^N always have a common subspace of dimension $O(N)$. This demonstrates two points: on one hand the denoising phase can be understood as the regime where the ground truth is estimated but only up to a random unknown rotation of the basis in which the patterns (\mathbf{X}_μ) are expressed. On the other hand, this also reveals that it is not sufficient to break the permutation symmetry of the columns in order to see a non-trivial overlap appear (as was done in FIG. 10). One instead needs to break the much larger symmetry group of rotations, which further requires an oracle already knowing the planted matrix. This “effective rotational invariance” is what we believe to be the source of universality in the denoising phase, and what prevents factorisation.

As last comment, solving the mean-field saddle point equations (44), (45) we get that the equilibrium overlap q_* is non vanishing in the denoising phase, see FIG. 12, which seems in contradiction with our negative conclusions concerning factorisation in this phase. However, we

argue that this is an artefact of the mean-field theory being applied in the “random matrix theory/RJE regime” where the necessary concentration-of-measure effects for it to hold are not present. As discussed in Section IV D, mean-field equations are reliable only after the transition $\lambda_c(\alpha = 0.5) \approx 9.1$, as manifest from the figure.

B. Connections to other models

The present matrix denoising problem bears several similarities with the celebrated Hopfield model [93] of associative memory. Its phenomenology is well understood (at least at the replica symmetric level) thanks to the seminal work [94]. The key idea is that samples from the Boltzmann-Gibbs measure cannot have extensive projections on all memorized patterns, but only on a finite subset and typically $O(1/\sqrt{N})$ projections onto the others. These infinitesimal contributions, being extensively many, give rise to a contribution that can be treated as effective noise called *pattern interference*. Its intensity depends on the load of the memory $M/N \approx \alpha$. There exists a retrieval phase for low α and temperatures, where an algorithm sampling from the Boltzmann-Gibbs distribution with informative initialisation “recalls” a pattern. Out of this region, the samples have instead $O(1/\sqrt{N})$ overlap with all the patterns.

This phenomenology reminds that of matrix denoising. We observe that for matrix denoising too, in the denoising phase, the overlap matrix presents $O(1/\sqrt{N})$ entries. In particular, the diagonal of the overlap matrix is not special w.r.t. the off-diagonals. However, instead of treating these elements as noise as done in Hopfield, here they actually give a fundamental contribution to decreasing the MMSE as illustrated in FIG. 9. This is the main difference with the Hopfield model: the sum of spurious alignments of the posterior sample columns \mathbf{x}_μ onto other patterns of the ground truth is exploitable as information when denoising $\mathbf{X}\mathbf{X}^\top$, and it is not a disturbance. The term $\operatorname{Tr}(\mathbf{x}\mathbf{x}^\top)^2$ in the Hamiltonian (13) certainly contributes to this phenomenology, generating a caging effect preventing posterior patterns to overlap and that helps reconstruction. Furthermore, our theory and its agreement with experiments in the factorisation phase is indicating that this effect becomes strong enough to cleanse almost completely the system from pattern interference, yielding an MMSE akin to that of many quasi decoupled rank-1 problems.

Another stretched, yet potentially fruitful comparison, is that with Anderson localization [130]. The phenomenon is different as being quantum by nature and is not a thermodynamic phase transition. Yet, the similarity is striking due to both transitions being linked to localization, i.e., macroscopic pairwise alignment of two bases of vectors: the eigenvectors of the energy operator of the quantum system at hand localize in lattice basis when tuning the amount of disorder, while in the present problem the quasi basis of posterior patterns (\mathbf{x}_μ) local-

ize at the transition in the quasi basis of planted ones (\mathbf{X}_μ) which manifests itself by the abrupt increase of the overlap diagonal in FIG. 10. It would be interesting to explore how far this analogy can be pushed.

VI. CONCLUSION AND PERSPECTIVES

In this paper we have first conducted numerical experiments to grasp features of the phase diagram of matrix denoising in the challenging regime of extensive-rank beyond the rotational invariant setting. We have clarified the rich phenomenology of the model. We have shown that a first order phase transition is separating a regime akin to a random matrix theory one where strong universality properties hold and the RIE is a Bayes-optimal denoising algorithm, from a fundamentally different phase where it is not anymore due to universality breaking, and which is more amenable to mean-field techniques. The free entropy (11) seen as a function of the SNR λ thus interpolates between a matrix model solvable by the HCIZ integral (the denoising phase) and a mean-field spin model (the factorisation phase).

We have then proposed an effective mean-field theory based on a combination of spin glass approaches which is able to correctly predict the transition and the values of the main information theoretic quantities (mutual information and minimum mean-square error). Interestingly, we have shown that our theory is equivalent to the replica method in [3, 78–80]. It was believed to be incorrect for a long time. But we have clarified through our independent analysis in which regime it is reliable –the factorisation phase– or not –the denoising phase–, and have shown how to correct it when not accurate thanks to universality, also conjectured by Semerjian [67] but for the whole phase diagram. The final theoretical predictions are in good quantitative agreement with the numerical experiments, up to unusually large finite size corrections which we were able to quantify.

Both the numerical and theoretical evidence suggested that optimal denoising is information theoretically solvable beyond the transition point, but it remains algorithmically hard due to the presence of the universal RIE state at all signal-to-noise ratios. We have experimentally confirmed that this state prevents Monte Carlo algorithms to outperform the RIE.

There are many directions to pursue from here. Concerning our present setting, we have proven that beyond a certain SNR universality cannot hold. It would be interesting to rigorously confirm that the universality breaks precisely at the predicted transition $\lambda_c(\alpha)$, and that the mean-field theory does become asymptotically exact beyond that point.

Concerning generalisations, the most natural one is to re-consider the non-symmetric version of the problem, with more general noises, as considered in [3, 78–80]. Another potentially fruitful extension we are pursuing is about associative memories. As discussed earlier, our

setting shares similarities with the Hopfield model, but mimics a memory which attempts to recall *all* patterns (see the recent related work [131] where multiple, but finitely many, patterns are jointly recovered). However, the phenomenology looks different from the one illustrated in [91, 94], especially regarding the load that the memory can withstand. From our theory it seems that it is possible to retrieve all the patterns even for α 's sensibly larger than the critical load $\alpha_c \approx 0.138$ for binary patterns, provided an informative initialisation is available and the signal-to-noise ratio is sufficiently high.

Concerning the denoising-factorisation transition, we argue that a similar phenomenon may occur also in the (Bayesian) learning of neural networks, such as in [132] where the authors computed the Bayesian-optimal generalization error of an extensive-width neural network. This model can be mapped to a matrix inference problem very similar to ours. The hidden matrix in their case is precisely a Wishart matrix $\mathbf{X}\mathbf{X}^\top$ with $X_{i\mu}$ standard Gaussians. It is plausible that the universality with respect to the distribution of \mathbf{X} argued in the mentioned paper breaks down there too. This suggests the existence of a broader set of models experiencing a universal regime followed by another one where prior details matter. We plan to explore this in greater generality with the hope to shed new light on learning transitions in neural networks.

Finally, it would be interesting to compare known Bayesian algorithms for matrix inference to our predictions, such as BIGAMP [133], the AMP algorithm of [80] or Unitary AMP [134]. Given our results on the hardness of denoising using Monte Carlo algorithms in the symmetric case, we think that these algorithms adapted to the present setting may, too, face a hard phase and be outperformed by the RIE without additional information on \mathbf{X} . We plan to look into this in a future work.

ACKNOWLEDGMENTS

J.B. and F.C. were funded by the European Union (ERC, CHORAL, project number 101039794). Views and opinions expressed are however those of the authors only and do not necessarily reflect those of the European Union or the European Research Council. Neither the European Union nor the granting authority can be held responsible for them. J.K. was funded by the Natural Sciences and Engineering Research Council of Canada (RGPIN-2020-04597). K.O. was funded by JSPS KAKENHI Grant number 22KJ1074, JST CREST Grant number JPMJCR1912, and Grant-in-Aid for Transformative Research Areas (A), “Foundation of Machine Learning Physics” (22H05117). Computational resources of the AI Bridging Cloud Infrastructure (ABCI) provided by the National Institute of Advanced Industrial Science and Technology (AIST) were used. Part of the work of K.O. was done while visiting the International Center for Theoretical Physics in Trieste.

-
- [1] O. Ledoit and S. Péché, *Probability Theory and Related Fields* **151**, 233 (2011).
- [2] J. Bun, R. Allez, J.-P. Bouchaud, and M. Potters, *IEEE Transactions on Information Theory* **PP** (2015).
- [3] A. Sakata and Y. Kabashima, *Europhysics Letters* **103**, 28008 (2013).
- [4] J. Mairal, F. Bach, J. Ponce, and G. Sapiro, in *Proceedings of the 26th Annual International Conference on Machine Learning, ICML '09* (Association for Computing Machinery, New York, NY, USA, 2009) p. 689–696.
- [5] I. Tošić and P. Frossard, *IEEE Signal Processing Magazine* **28**, 27 (2011).
- [6] Y. Bengio, A. Courville, and P. Vincent, *IEEE Transactions on Pattern Analysis and Machine Intelligence* **35**, 1798 (2013).
- [7] B. A. Olshausen and D. J. Field, *Nature* **381**, 607 (1996).
- [8] B. A. Olshausen and D. J. Field, *Vision research* **37**, 3311 (1997).
- [9] K. Kreutz-Delgado, J. F. Murray, B. D. Rao, K. Engan, T.-W. Lee, and T. J. Sejnowski, *Neural computation* **15**, 349 (2003).
- [10] E. J. Candès, X. Li, Y. Ma, and J. Wright, *Journal of the ACM (JACM)* **58**, 1 (2011).
- [11] A. Perry, A. S. Wein, A. S. Bandeira, and A. Moitra, *Annals of Statistics* **46**, 2416 (2018).
- [12] B. Hajek, Y. Wu, and J. Xu, *IEEE Transactions on Information Theory* **63**, 4729 (2017).
- [13] A. Belouchrani, K. Abed-Meraim, J.-F. Cardoso, and E. Moulines, *IEEE Transactions on signal processing* **45**, 434 (1997).
- [14] E. J. Candès and B. Recht, *Foundations of Computational mathematics* **9**, 717 (2009).
- [15] E. J. Candès and T. Tao, *IEEE Transactions on Information Theory* **56**, 2053 (2010).
- [16] E. Abbe, *The Journal of Machine Learning Research* **18**, 6446 (2017).
- [17] M. Lelarge and L. Miolane, *Probability Theory and Related Fields* **173**, 859 (2019).
- [18] F. Caltagirone, M. Lelarge, and L. Miolane, *IEEE Transactions on Network Science and Engineering* **5**, 237 (2017).
- [19] J. Mairal, M. Elad, and G. Sapiro, *IEEE Transactions on Image Processing* **17**, 53 (2008).
- [20] A. Mnih and R. R. Salakhutdinov, in *Advances in Neural Information Processing Systems*, Vol. 20, edited by J. Platt, D. Koller, Y. Singer, and S. Roweis (Curran Associates, Inc., 2007).
- [21] I. Johnstone, *The Annals of statistics* **29**, 295 (2001).
- [22] I. Johnstone and A. Lu, Unpublished manuscript (2004).
- [23] H. Zou, T. Hastie, and R. Tibshirani, *Journal of computational and graphical statistics* **15**, 265 (2006).
- [24] I. Johnstone and A. Lu, *Journal of the American Statistical Association* (2012).
- [25] J. Baik, G. B. Arous, and S. Péché, *Annals of Probability* , 1643 (2005).
- [26] J. Baik and J. W. Silverstein, *Journal of multivariate analysis* **97**, 1382 (2006).
- [27] F. Benaych-Georges and R. R. Nadakuditi, *Advances in Mathematics* **227**, 494 (2011).
- [28] T. Lesieur, F. Krzakala, and L. Zdeborová, in *2015 53rd Annual Allerton Conference on Communication, Control, and Computing (Allerton)* (2015) pp. 680–687.
- [29] T. Lesieur, F. Krzakala, and L. Zdeborová, *Journal of Statistical Mechanics: Theory and Experiment* **2017**, 073403 (2017).
- [30] J. Barbier and N. Macris, *Journal of Physics A: Mathematical and Theoretical* **52**, 294002 (2019).
- [31] J. Barbier, F. Camilli, M. Mondelli, and M. Sáenz, *Proceedings of the National Academy of Sciences* **120**, e2302028120 (2023).
- [32] J. Barbier, J. Ko, and A. A. Rahman, in *International Zurich Seminar on Information and Communication (IZS 2024)* (2024) p. 16.
- [33] D. Alberici, F. Camilli, P. Contucci, and E. Mingione, *Journal of Statistical Physics* **182**, 1 (2021).
- [34] D. Alberici, F. Camilli, P. Contucci, and E. Mingione, *Communications in Mathematical Physics* , 1 (2021).
- [35] Y. Zhang and M. Mondelli, arXiv preprint 2405.13912 (2024).
- [36] S. Korada and N. Macris, *Journal of Statistical Physics* **136**, 205 (2009).
- [37] Y. Deshpande, E. Abbe, and A. Montanari, *Information and Inference: A Journal of the IMA* **6**, 125 (2017).
- [38] J. Barbier, M. Dia, N. Macris, F. Krzakala, T. Lesieur, and L. Zdeborová, in *Proceedings of the 30th International Conference on Neural Information Processing Systems, NIPS'16* (Curran Associates Inc., Red Hook, NY, USA, 2016) p. 424–432.
- [39] J. Barbier and N. Macris, *Probability Theory and Related Fields* **174**, 1133 (2019).
- [40] J.-C. Mourrat, *The Annals of Applied Probability* **30**, 2234 (2020).
- [41] H. Chen, J.-C. Mourrat, and J. Xia, *Annales Henri Lebesgue* **5**, 1161 (2022).
- [42] G. Reeves, *IEEE Journal on Selected Areas in Information Theory* **1**, 777 (2020).
- [43] V. A. Kazakov and A. A. Migdal, *Nuclear Physics B* **397**, 214 (1993).
- [44] J. Ambjørn, B. Durhuus, and T. Jonsson, *Quantum Geometry: A Statistical Field Theory Approach*, Cambridge Monographs on Mathematical Physics (Cambridge Univ. Press, Cambridge, UK, 2005).
- [45] P. Francesco, P. Ginsparg, and J. Zinn-Justin, *Physics Reports* **254**, 1–133 (1995).
- [46] J. Verbaarschot and T. Wettig, *Annual Review of Nuclear and Particle Science* **50**, 343–410 (2000).
- [47] V. A. Kazakov, *Physics Letters A* **119**, 140 (1986).
- [48] V. A. Kazakov, M. Staudacher, and T. Wynter, *Communications in Mathematical Physics* **179**, 235–256 (1996).
- [49] D. V. Boulatov and V. A. Kazakov, *Physics Letters B* **186**, 379 (1987).
- [50] V. A. Kazakov, *Nuclear Physics B - Proceedings Supplements* **4**, 93 (1988).
- [51] E. Brezin, C. Itzykson, G. Parisi, and J. B. Zuber, *Commun. Math. Phys.* **59**, 35 (1978).
- [52] A. Zvonkin, *Mathematical and Computer Modelling* **26**, 281 (1997).
- [53] V. A. Kazakov, arXiv (2000), hep-th/0003064 [hep-th].
- [54] A. A. Migdal, *Sov. Phys. JETP* **42**, 413 (1975).

- [55] V. A. Kazakov, M. Staudacher, and T. Wynter, Nuclear Physics B **471**, 309 (1996).
- [56] Harish-Chandra, American Journal of Mathematics , 87 (1957).
- [57] C. Itzykson and J.-B. Zuber, Journal of Mathematical Physics **21**, 411 (1980).
- [58] A. Matytsin, Nuclear Physics B **411**, 805–820 (1994).
- [59] A. Guionnet and O. Zeitouni, Journal of functional analysis **188**, 461 (2002).
- [60] A. Guionnet, Communications in mathematical physics **244**, 527 (2004).
- [61] E. Marinari and G. Parisi, Europhysics Letters **19**, 451 (1992).
- [62] K. Hukushima and K. Nemoto, Journal of the Physical Society of Japan **65**, 1604 (1996).
- [63] R. M. Neal, Statistics and computing **11**, 125 (2001).
- [64] https://github.com/darjeeling-0/MCMC_for_RademacherMF (2024).
- [65] D. Guo, S. Shamai, and S. Verdu, IEEE Transactions on Information Theory **51**, 1261 (2005).
- [66] F. Pourkamali, J. Barbier, and N. Macris, IEEE Transactions on Information Theory **70**, 8133 (2024).
- [67] G. Semerjian, Journal of Statistical Physics **191**, 139 (2024).
- [68] E. Troiani, V. Erba, F. Krzakala, A. Maillard, and L. Zdeborová, in *Mathematical and Scientific Machine Learning* (PMLR, 2022) pp. 97–112.
- [69] F. Pourkamali and N. Macris, in *2023 IEEE International Symposium on Information Theory (ISIT)* (IEEE, 2023) pp. 2081–2086.
- [70] F. Pourkamali and N. Macris, arXiv preprint arXiv:2403.04615 (2024).
- [71] I. D. Landau, G. C. Mel, and S. Ganguli, Physical Review E **108**, 054129 (2023).
- [72] A. Guionnet and J. Huang, Journal of Functional Analysis **285**, 110144 (2023).
- [73] M. Talagrand, *Mean Field Models for Spin Glasses: Volume I: Basic Examples* (Springer, 2010).
- [74] M. Mézard, G. Parisi, and M. A. Virasoro, *Spin-glass theory and beyond*, Lecture Notes in Physics, Vol. 9 (World Scientific, Singapore, 1987).
- [75] J. Barbier, M. Dia, N. Macris, F. Krzakala, and L. Zdeborová, arXiv e-prints (2018), 1812.02537.
- [76] M. Aizenman, R. Sims, and S. L. Starr, Phys. Rev. B **68**, 214403 (2003).
- [77] A. El Alaoui and F. Krzakala, in *2018 IEEE International Symposium on Information Theory (ISIT)* (IEEE, 2018) pp. 1874–1878.
- [78] A. Sakata and Y. Kabashima, 2013 IEEE International Symposium on Information Theory , 669 (2013).
- [79] F. Krzakala, M. Mézard, and L. Zdeborová, in *2013 IEEE International Symposium on Information Theory* (2013) pp. 659–663.
- [80] Y. Kabashima, F. Krzakala, M. Mézard, A. Sakata, and L. Zdeborová, IEEE Transactions on Information Theory **62**, 4228 (2016).
- [81] F. Krzakala, M. Mézard, A. Manuel, and L. Zdeborová, Unpublished work.
- [82] H. C. Schmidt, *Statistical Physics of Sparse and Dense Models in Optimization and Inference*, Ph.D. thesis, Université Paris Saclay (COMUE) (2018).
- [83] A. Maillard, F. Krzakala, M. Mézard, and L. Zdeborová, Journal of Statistical Mechanics: Theory and Experiment **2022**, 083301 (2022).
- [84] J. Barbier and N. Macris, Phys. Rev. E **106**, 024136 (2022).
- [85] T. Plefka, Journal of Physics A **15**, 1971 (1982).
- [86] A. Georges and J. S. Yedidia, Journal of Physics A: Mathematical and General **24**, 2173 (1991).
- [87] D. J. Thouless, P. W. Anderson, and R. G. Palmer, Philosophical Magazine **35**, 593 (1977).
- [88] F. Pourkamali and N. Macris, Advances in Neural Information Processing Systems **36** (2024).
- [89] A. Bodin and N. Macris, in *2023 IEEE Information Theory Workshop (ITW)* (IEEE, 2023) pp. 365–370.
- [90] F. Camilli, *New perspectives in statistical mechanics and high-dimensional inference*, Ph.D. thesis, University of Bologna and École Normale Supérieure - PSL (2023).
- [91] F. Camilli and M. Mézard, Physical Review E **107**, 064308 (2023).
- [92] F. Camilli and M. Mézard, Journal of Physics A: Mathematical and Theoretical **57**, 085002 (2024).
- [93] J. J. Hopfield, Proceedings of the National Academy of Sciences **79**, 2554 (1982).
- [94] D. J. Amit, H. Gutfreund, and H. Sompolinsky, Phys. Rev. Lett. **55**, 1530 (1985).
- [95] J. J. Hopfield, D. I. Feinstein, and R. G. Palmer, Nature **304**, 158 (1983).
- [96] J. Van Hemmen, L. Ioffe, R. Kühn, and M. Vaas, Physica A: Statistical Mechanics and its Applications **163**, 386 (1990).
- [97] M. Benedetti, E. Ventura, E. Marinari, G. Ruocco, and F. Zamponi, The Journal of Chemical Physics **156**, 104107 (2022).
- [98] D. Kunisky, A. S. Wein, and A. S. Bandeira, in *ISAAC Congress (International Society for Analysis, its Applications and Computation)* (Springer, 2019) pp. 1–50.
- [99] J. Bun, J.-P. Bouchaud, and M. Potters, Physics Reports **666**, 1 (2017).
- [100] F. Antenucci, S. Franz, P. Urbani, and L. Zdeborová, Physical Review X **9**, 011020 (2019).
- [101] M. Mezard and A. Montanari, *Information, physics and computation* (Oxford University Press, 2009).
- [102] G. W. Anderson, A. Guionnet, and O. Zeitouni, *An introduction to random matrices*, 118 (Cambridge university press, 2010).
- [103] M. Potters and J.-P. Bouchaud, *A First Course in Random Matrix Theory: For Physicists, Engineers and Data Scientists* (Cambridge University Press, 2020).
- [104] Z. Bai and J. W. Silverstein, *Spectral analysis of large dimensional random matrices*, Vol. 20 (Springer, 2010).
- [105] T. Tao and V. Vu, Communications in Mathematical Physics **298**, 549 (2010).
- [106] L. Erdős, B. Schlein, and H.-T. Yau, Inventiones mathematicae **185**, 75 (2011).
- [107] O. H. Ajanki, L. Erdős, and T. Krüger, Probability Theory and Related Fields **169**, 667 (2017).
- [108] L. Erdős, S. Péché, J. A. Ramírez, B. Schlein, and H.-T. Yau, Communications on Pure and Applied Mathematics: A Journal Issued by the Courant Institute of Mathematical Sciences **63**, 895 (2010).
- [109] Z. D. Bai, B. Q. Miao, and G. M. Pan, The Annals of Probability **35**, 1532 (2007).
- [110] L. Erdős, B. Schlein, and H.-T. Yau, Communications in Mathematical Physics **287**, 641 (2009).
- [111] F. Benaych-Georges, arXiv preprint arXiv:1104.1219 (2011).

- [112] S. O’Rourke, V. Vu, and K. Wang, *Journal of Combinatorial Theory, Series A* **144**, 361 (2016).
- [113] J. Baik, G. Ben-Arous, and S. Péché, *The Annals of Probability* **33**, 1643 (2005).
- [114] J. Barbier, N. Macris, M. Dia, and F. Krzakala, *IEEE Transactions on Information Theory* **66**, 4270 (2020).
- [115] M. Talagrand, *Mean Field Models for Spin Glasses: Volume II: Advanced Replica-Symmetry and Low Temperature*, Vol. 55 (Springer, 2011).
- [116] J. Barbier, F. Krzakala, N. Macris, L. Miolane, and L. Zdeborová, *Proceedings of the National Academy of Sciences* **116**, 5451 (2019).
- [117] D. Panchenko, *The Sherrington-Kirkpatrick Model* (Springer, 2015).
- [118] D. Panchenko, *The Annals of Probability* **41**, 1315 (2013).
- [119] F. Krzakala, M. Mézard, and L. Zdeborová, in *2013 IEEE International Conference on Acoustics, Speech and Signal Processing* (IEEE, 2013) pp. 5519–5523.
- [120] H. Sompolinsky, N. Tishby, and H. S. Seung, *Phys. Rev. Lett.* **65**, 1683 (1990).
- [121] M. C. Angelini and F. Ricci-Tersenghi, *Physical Review X* **13**, 021011 (2023).
- [122] A. Decelle, F. Krzakala, C. Moore, and L. Zdeborová, *Physical Review E—Statistical, Nonlinear, and Soft Matter Physics* **84**, 066106 (2011).
- [123] M. Mézard, *Journal of Physics A: Mathematical and General* (1989).
- [124] H. Nishimori, *Statistical Physics of Spin Glasses and Information Processing: an Introduction* (Oxford University Press, Oxford; New York, 2001).
- [125] J. Barbier, *Information and Inference: A Journal of the IMA* (2019).
- [126] J. Barbier and D. Panchenko, *Communications in mathematical physics* **393**, 1199 (2022).
- [127] F. Krzakala, M. Mézard, F. Sausset, Y. Sun, and L. Zdeborová, *Journal of Statistical Mechanics: Theory and Experiment* **2012**, P08009 (2012).
- [128] J. Barbier and F. Krzakala, *IEEE Transactions on Information Theory* **63**, 4894 (2017).
- [129] P. Embrechts, C. Klüppelberg, and T. Mikosch, *Modelling extremal events: for insurance and finance*, Vol. 33 (Springer Science & Business Media, 2013).
- [130] P. W. Anderson, *Physical review* **109**, 1492 (1958).
- [131] E. Agliari, A. Alessandrelli, A. Barra, M. S. Centonze, and F. Ricci-Tersenghi, *arXiv preprint arXiv:2409.08151* (2024).
- [132] A. Maillard, E. Troiani, S. Martin, F. Krzakala, and L. Zdeborová, *arXiv preprint arXiv:2408.03733* (2024).
- [133] J. T. Parker, P. Schniter, and V. Cevher, *IEEE Transactions on Signal Processing* **62**, 5839 (2014).
- [134] Z. Yuan, Q. Guo, Y. C. Eldar, and Y. Li, in *ICASSP 2024-2024 IEEE International Conference on Acoustics, Speech and Signal Processing (ICASSP)* (IEEE, 2024) pp. 9576–9580.
- [135] Y. Ogata, *Annals of the Institute of statistical Mathematics* **42**, 403 (1990).
- [136] M. Jerrum and A. Sinclair, *SIAM Journal on Computing* **22**, 1087 (1993).
- [137] S. Syed, A. Bouchard-Côté, G. Deligiannidis, and A. Doucet, *Journal of the Royal Statistical Society Series B: Statistical Methodology* **84**, 321 (2022).
- [138] J. Machta, *Phys. Rev. E* **80**, 056706 (2009).

Appendix A: Irrelevance of the diagonal of the data

Proposition 3 (Information irrelevance of the data diagonal components). *The diagonal part of the data $(Y_{ii})_{i \leq N}$ does not contribute to the MI in the high dimensional limit. Specifically, the inference problem*

$$\tilde{Y}_{ij} = \sqrt{\frac{\lambda}{N}} \sum_{\mu=1}^M X_{i\mu} X_{j\mu} + \tilde{Z}_{ij}, \quad \tilde{Z}_{ij} \stackrel{\text{iid}}{\sim} \mathcal{N}(0, 1), \quad 1 \leq i < j \leq N \quad (\text{A1})$$

has the same asymptotic mutual information density between data and signal as (1).

Proof. The proof is based on standard interpolation. The interpolating inference problem is

$$Y_{ij}^t = \begin{cases} \tilde{Y}_{ij} & i < j \\ \sqrt{\frac{t\lambda}{N}} \sum_{\mu=1}^M X_{i\mu}^2 + Z_{ii} & i = j \end{cases} \quad (\text{A2})$$

where $Z_{ii} \stackrel{\text{iid}}{\sim} \mathcal{N}(0, 2)$. The MI density for this problem is

$$\begin{aligned}
\frac{1}{MN} I(\mathbf{Y}^t; \mathbf{X}) &= \frac{\lambda}{4MN^2} \sum_{i \neq j} \sum_{\mu, \nu=1}^M \mathbb{E} X_{i\mu} X_{j\mu} X_{i\nu} X_{j\nu} + \frac{t\lambda}{4MN^2} \sum_{i=1}^N \sum_{\mu, \nu=1}^M \mathbb{E} X_{i\mu}^2 X_{i\nu}^2 \\
&\quad - \frac{1}{MN} \mathbb{E} \ln \int dP_X(\mathbf{x}) \exp \sum_{i < j} \left[\sqrt{\frac{\lambda}{N}} \tilde{Y}_{ij} \mathbf{x}_i \cdot \mathbf{x}_j - \frac{\lambda}{2N} (\mathbf{x}_i \cdot \mathbf{x}_j)^2 \right] \\
&\quad \times \exp \frac{1}{2} \sum_{i=1}^N \left[\sqrt{\frac{t\lambda}{N}} Y_{ii}^t \|\mathbf{x}_i\|^2 - \frac{t\lambda}{2N} \|\mathbf{x}_i\|^4 \right] \\
&= \frac{\lambda(1 + \alpha t)}{4} - \frac{1}{MN} \mathbb{E} \ln \int dP_X(\mathbf{x}) \exp \sum_{i < j} \left[\sqrt{\frac{\lambda}{N}} \tilde{Y}_{ij} \mathbf{x}_i \cdot \mathbf{x}_j - \frac{\lambda}{2N} (\mathbf{x}_i \cdot \mathbf{x}_j)^2 \right] \\
&\quad \times \exp \frac{1}{2} \sum_{i=1}^N \left[\sqrt{\frac{t\lambda}{N}} Y_{ii}^t \|\mathbf{x}_i\|^2 - \frac{t\lambda}{2N} \|\mathbf{x}_i\|^4 \right] + O(N^{-1}). \tag{A3}
\end{aligned}$$

The last error term is uniform in $t \in [0, 1]$. The t -derivative of this interpolating MI thus reads

$$\frac{d}{dt} \frac{1}{MN} I(\mathbf{X}, ; \mathbf{Y}^t) = \frac{\lambda\alpha}{4} - \frac{1}{MN} \sum_{i=1}^N \mathbb{E} \left\langle \frac{1}{4} \sqrt{\frac{\lambda}{tN}} Z_{ii} \|\mathbf{x}_i\|^2 + \lambda \frac{\|\mathbf{X}_i\|^2 \|\mathbf{x}_i\|^2}{2N} - \frac{\lambda}{4N} \|\mathbf{x}_i\|^4 \right\rangle_t \tag{A4}$$

Now we can integrate the Z_{ii} 's by parts, taking into account that their variance is 2:

$$\begin{aligned}
\frac{d}{dt} \frac{1}{MN} I(\mathbf{X}; \mathbf{Y}^t) &= \frac{\lambda\alpha}{4} - \frac{1}{MN} \sum_{i=1}^N \mathbb{E} \left\langle \frac{\lambda}{2N} \|\mathbf{x}_i^{(1)}\|^4 - \frac{\lambda}{2N} \|\mathbf{x}_i^{(1)}\| \|\mathbf{x}_i^{(2)}\|^2 + \lambda \frac{\|\mathbf{X}_i\|^2 \|\mathbf{x}_i^{(1)}\|^2}{2N} - \frac{\lambda}{4N} \|\mathbf{x}_i^{(1)}\|^4 \right\rangle_t \\
&= \frac{\lambda\alpha}{4} - \frac{\lambda}{4MN^2} \sum_{i=1}^N \mathbb{E} \|\mathbf{X}\|^4 = O(N^{-1}), \tag{A5}
\end{aligned}$$

where in the last step we also used the Nishimori identity

$$\mathbb{E} \langle \|\mathbf{x}_i^{(1)}\|^2 \|\mathbf{x}_i^{(2)}\|^2 \rangle_t = \mathbb{E} \langle \|\mathbf{X}_i\|^2 \|\mathbf{x}_i^{(1)}\|^2 \rangle_t. \tag{A6}$$

and superscripts $\mathbf{x}^{(k)}$ denote replica indices, namely conditionally (on \mathbf{Y}) independent samples from the posterior measure. The error term is again uniform in t so the proof is complete by noticing that $\mathbf{Y}^{t=1}$ are the observations in (1) and $\mathbf{Y}^{t=0}$ is (A1). \square

The above proposition holds also if α is vanishing in the high-dimensional limit, i.e. for low rank settings.

Appendix B: Details of the Monte Carlo procedure

In this appendix, we elaborate on the numerical procedures necessary to evaluate the MI and MMSE for finite size systems. The target distribution is the posterior measure given by

$$P_\lambda(\mathbf{x}; \mathbf{X}, \mathbf{Z}) = \frac{P_X(\mathbf{x}) e^{-H_\lambda(\mathbf{x}; \mathbf{X}, \mathbf{Z})}}{\mathcal{Z}_\lambda(\mathbf{X}, \mathbf{Z})}, \quad -H_\lambda(\mathbf{x}; \mathbf{X}, \mathbf{Z}) = \sqrt{\frac{\lambda}{N}} \sum_{i < j, 1}^N (\mathbf{X}_i \cdot \mathbf{X}_j + Z_{ij}) \mathbf{x}_i \cdot \mathbf{x}_j - \frac{\lambda}{2N} \sum_{i < j, 1}^N (\mathbf{x}_i \cdot \mathbf{x}_j)^2, \tag{B1}$$

where \mathcal{Z}_λ is the partition function for SNR λ . Here, all expressions are explicitly rewritten using the quenched random variables \mathbf{X}, \mathbf{Z} , and the subscript for N, M are dropped for brevity.

Evaluating the MI numerically requires one to calculate $\ln \mathcal{Z}_\lambda(\mathbf{X}, \mathbf{Z})$ with high precision, which is difficult to perform with standard MCMC (Markov Chain Monte Carlo) samplers. Therefore, we use bridge sampling [135, 136], more popularly known as *Annealed Importance Sampling* [63]. Given a strictly increasing sequence of SNRs $0 = \lambda_0 < \lambda_1 < \dots < \lambda_R$, the logarithm of the partition function at λ_R can alternatively be expressed as a telescopic sum:

$$\ln \mathcal{Z}_{\lambda_R}(\mathbf{X}, \mathbf{Z}) = \ln \prod_{r=0}^{R-1} \frac{\mathcal{Z}_{\lambda_{r+1}}(\mathbf{X}, \mathbf{Z})}{\mathcal{Z}_{\lambda_r}(\mathbf{X}, \mathbf{Z})} = \sum_{r=0}^{R-1} \ln \left\langle \exp \left[H_{\lambda_r}(\mathbf{x}; \mathbf{X}, \mathbf{Z}) - H_{\lambda_{r+1}}(\mathbf{x}; \mathbf{X}, \mathbf{Z}) \right] \right\rangle_{\lambda_r}, \tag{B2}$$

Experiment No.	(N, M)	α	burnin MCMC steps	sampling MCMC steps	$R + 1$	No. of random instances
(1)	(10, 5)	0.5	2,000	8,000	72	128
(2)	(20, 10)	0.5	10,000	40,000	135	128
(3)	(40, 20)	0.5	10,000	40,000	261	32
(4)*	(20, 10)	0.5	10,000	40,000	29	128
(5)*	(40, 20)	0.5	10,000	40,000	29	128
(6)*	(60, 30)	0.5	40,000	160,000	29	128
(7)*	(40, 28)	0.7	10,000	40,000	29	128
(8)	(60, 30)	0.5	500,000	500,000	313	1
(9)	(60, 18)	0.3	40,000	160,000	256	32
(10)	(40, 28)	0.7	40,000	160,000	261	32

TABLE I: Specific parameters used to run each Monte Carlo experiment.

Figure reference	Experiment No.
1	(1,2,3)
2	(3, 10)
4	(4,5,6)
9	(1,2,3)
10, 11, 12, 13	(8)
8 ($\alpha = 0.3$)	(9)
8 ($\alpha = 0.5$)	(3) (for $\lambda < 8$) (6) (for $\lambda > 8$)
8 ($\alpha = 0.7$)	(10) (for $\lambda < 12$) (7) (for $\lambda > 12$)

TABLE II: Table of corresponding experiments used to generate each figure in this paper.

where $\langle \cdot \rangle_\lambda$ is the expectation with respect to $P_\lambda(\mathbf{x}; \mathbf{X}, \mathbf{Z})$. By taking λ_{r+1} and λ_r sufficiently close, and consequently taking $H_{\lambda_r}(\mathbf{x}; \mathbf{X}, \mathbf{Z}) - H_{\lambda_{r+1}}(\mathbf{x}; \mathbf{X}, \mathbf{Z})$ close to 0, the value in the brackets would yield low variance, allowing one to estimate its mean with high precision using samples generated from $P_\lambda(\mathbf{x}; \mathbf{X}, \mathbf{Z})$. To sample from a sequence of posterior measures with SNRs $\{\lambda_r\}_{r=0}^R$ in an efficient manner, we employ parallel tempering, or the replica exchange Monte Carlo method [61, 62]. This approach involves simultaneous execution of “local” MCMC samplers specifically simulating each of the $R + 1$ systems. In addition, configurations between adjacent SNRs are occasionally exchanged while satisfying the detailed balance condition for fast mixing time. More explicitly, given an adjacent pair of SNRs λ and λ' , with its current configuration of their corresponding sampler being given by \mathbf{x} and \mathbf{x}' , respectively, the exchange probability of the two configurations can be given using Metropolis’ method:

$$\min \left\{ 1, \exp \left[H_{\lambda'}(\mathbf{x}'; \mathbf{X}, \mathbf{Z}) - H_{\lambda'}(\mathbf{x}; \mathbf{X}, \mathbf{Z}) + H_\lambda(\mathbf{x}; \mathbf{X}, \mathbf{Z}) - H_\lambda(\mathbf{x}'; \mathbf{X}, \mathbf{Z}) \right] \right\}. \quad (\text{B3})$$

In our experiments, we use a single spin-flip Metropolis-Hastings algorithm as the local MCMC sampler for each SNR. A single MCMC step is defined as $30NM$ local spin flip moves on all $R + 1$ systems, followed by a replica exchange move between all adjacent pairs of SNR. Before each replica exchange move, the configuration of \mathbf{xx}^\top of each MCMC chain is recorded. After the the Monte Carlo procedure has finished, the thermal average appearing in the expression for the MI (B2) and MMSE (8) by the empirical average over these samples. This whole Monte Carlo procedure is executed for several instances of (\mathbf{X}, \mathbf{Z}) to then evaluate the average over the quenched randomness.

The specific number of MCMC steps, the number of replicas R , as well as the number of random instances of (\mathbf{X}, \mathbf{Z}) used for the simulations are given in Table I. Table II specifies which data was used to generate each figure in this paper. The precise values of $\{\lambda_r\}_{r=0}^R$ are chosen such that the exchange rate between adjacent SNRs is always finite (typically larger than 0.3) by using the adaptive algorithm given by [137]. This is with the exception of experiments designated with the star superscripts in Table I, whose SNR values are given by equispaced values in the range 8 to 15.

As indicated in Table II, the MCMC curves in FIG. 8 are obtained by augmenting data from two different types of experiments: one from the usual replica exchange MCMC ((3), (11)), and the other from MCMC specifically run under high SNR, (7) and (8). Note that with only the results from (3) and (11), the mean of the MMSE will become hidden in the statistical error from finite number of random instances. The results from high SNR, (7) and (8), are given to clarify the exponential decay of the MMSE, which have significantly lower statistical error due to the larger number of random instances we can afford to average over.

Experiments for FIG. 3. The experimental procedure to obtain FIG. 3 is very different from that to obtain the other ones. Unlike the other experiments, here we only consider MCMC without replica exchange moves, i.e. independent MCMC chains are simply run for each value of SNR. The informative points (black markers) are obtained by initializing a MCMC chain on the ground truth, and performing $50000 \times 30NM$ local spin flip moves for each SNR. This is repeated on 36 random realizations of (\mathbf{X}, \mathbf{Z}) to evaluate the disordered average. The uninformative points (red markers) are obtained by initializing each MCMC chain to a random configuration, and repeating the same process as that to obtain the informative points. Last, the averaged uninformative points, indicated by the blue markers, are obtained by running 32 individual MCMC chains with random initialization for each SNR and (\mathbf{X}, \mathbf{Z}) .

The estimator for $\mathbf{X}\mathbf{X}^\top$ is obtained by averaging over all 32 runs with different initializations. More concretely, for a given realization of (\mathbf{X}, \mathbf{Z}) , if we let $\mathbf{x}_i(t) \in \{-1, +1\}^{N \times M}$ be the configuration of the MCMC chain after $30NMt$ local spin flip moves were performed from a random initialization indexed by i , the estimate of $\mathbf{X}\mathbf{X}^\top$ is given by

$$\langle \mathbf{x}\mathbf{x}^\top \rangle_{\text{uninfo. averaged}} = \frac{1}{32 \times 4000} \sum_{i=1}^{32} \sum_{t=1001}^{5000} \mathbf{x}_i(t)\mathbf{x}_i(t)^\top. \quad (\text{B4})$$

This procedure is then repeated over 36 random realizations of (\mathbf{X}, \mathbf{Z}) to evaluate the disordered average. Note that for each initialization, only $5000 \times 30NM$ local spin flip moves were performed in total, since we found after performing the experiments for uninformative points (red markers) that the MCMC chains get stuck to a random spin configuration typically after $\sim 100 \times 30NM$ local spin flip moves for SNR larger than 7. Note that this is different from the procedure to obtain uninformative points (red markers), where for a given realization of (\mathbf{X}, \mathbf{Z}) , the estimate is given only by a single initialization:

$$\langle \mathbf{x}\mathbf{x}^\top \rangle_{\text{uninfo.}} = \frac{1}{40000} \sum_{t=10001}^{50000} \mathbf{x}_1(t)\mathbf{x}_1(t)^\top. \quad (\text{B5})$$

Initialization of the MCMC chains. In principle, given sufficient amount of Monte Carlo steps, the MCMC simulations are able to sample from the true equilibrium measure, irrespective of the configuration in which each chain was initialised. Here, the ground truth \mathbf{X} is chosen as the initial configuration, with the obvious exception of experiment (3). This is done for the following reason. As seen in FIG. 3, for low SNR the system converges to the RIE irrespective of initialisation, indicating a benign energy landscape explorable by local spin flips. On the other hand, under high SNR, an MCMC chain with random initialisation encounters a possibly glassy phase, where mixing time increases exponentially with respect to N . This resembles a ‘‘golf-course’’-type of energy landscape [138], where it consists of a large number of excited glassy states, and a small number of ground states, which correspond to the ground truth \mathbf{X} . An important observation is that while it is difficult to reach the ground truth from the excited states by using replica exchange and local spin flip moves, one can easily reach excited states from a ground state by exchanging configurations with replicas in low SNR. Therefore, given that the replicas exchange with finite probability in our simulations, replicas with a paramagnetic equilibrium will not remain trapped in the initial ground state for exponentially long periods; these replicas can access equilibrium states through exchanges with replicas in low SNR, or via local spin flip moves if the landscape is benign (which is the case in the denoising phase). Simultaneously, for the replicas within the factorisation phase, initialising on \mathbf{X} eliminates the effort to search for rare ground states across the entire configuration space. This enables efficient investigation of the problem without introducing significant bias towards informative states in the numerical results.

Appendix C: Mean-square error of the rotational invariant estimator when $\alpha \rightarrow 0$

Consider the usual problem,

$$\frac{\mathbf{Y}}{\sqrt{N}} = \frac{\sqrt{\lambda}}{N} \mathbf{X}\mathbf{X}^\top + \frac{\mathbf{Z}}{\sqrt{N}} \quad (\text{C1})$$

where we rescaled the observations so that they have $O(1)$ eigenvalues and a well defined spectral density ρ_Y . One can actually prove that $\rho_Y = \rho_{s.c.} \boxplus \rho_{\sqrt{\lambda}MP}(\cdot; \alpha)$ is the free convolution between the semicircular density and the spectral density of a Wishart matrix (Marchenko-Pastur distribution of parameter $1/\alpha$) multiplied by $\sqrt{\lambda}$. The shrinking procedure of [2] yields the eigenvalues of the RIE as:

$$\xi_i = \frac{\gamma_{Y,i} - 2\pi\mathbf{H}[\rho_Y](\gamma_{Y,i})}{\sqrt{\lambda}} \quad (\text{C2})$$

and

$$\pi\mathbf{H}[\rho_Y](\gamma_{Y,i}) = \text{P.V.} \int dy \frac{\rho_Y(y)}{x - y} = \lim_{\epsilon \rightarrow 0^+} \text{Re } g_Y(x + i\epsilon). \quad (\text{C3})$$

g_Y is the Stieltjes transform of the spectral density ρ_Y :

$$g_Y(z) := \int dx \frac{\rho_Y(x)}{z - x}, \quad z \in \mathbb{C} \setminus \text{Supp}(\rho_Y). \quad (\text{C4})$$

We consider the low-rank limit $\alpha \rightarrow 0$. For simplicity we set $M = 1$, but the argument below can be extended to any M finite, and we claim it can be extended to sub-linear regimes $M = \alpha N^\gamma$ with $\gamma < 1$. Under this hypothesis, $g_Y = g_Z$, since low rank perturbations are not enough to modify the spectral density of the noise. \mathbf{Y} then turns into a low rank perturbation of a full rank Wigner matrix. Hence, some eigenvalues (one for $M = 1$) will pop out of the bulk spectrum of the noise.

The eigenvalue(s) that pops out, for $\lambda > 1$, is located at $z^* = \sqrt{\lambda} + \frac{1}{\sqrt{\lambda}}$ according to our notation [113]. The Stieltjes transform of the observations evaluated at z^* is thus

$$g_Y(z^*) \xrightarrow{\alpha \rightarrow 0} g_Z(z^*) = \frac{z^* - z^* \sqrt{1 - 4/z^{*2}}}{2} = \frac{\sqrt{\lambda} + \frac{1}{\sqrt{\lambda}} - \sqrt{\lambda - 2 + \frac{1}{\lambda}}}{2} = \frac{1}{\sqrt{\lambda}}, \quad (\text{C5})$$

and hence

$$\pi \mathbf{H}[\rho_Y](z^*) \xrightarrow{\alpha \rightarrow 0} \frac{1}{\sqrt{\lambda}}. \quad (\text{C6})$$

From the above, we can infer the shrinkage of the leading eigenvalue:

$$\xi_1 = \frac{\sqrt{\lambda} + \frac{1}{\sqrt{\lambda}} - \frac{2}{\sqrt{\lambda}}}{\sqrt{\lambda}} = 1 - \frac{1}{\lambda}. \quad (\text{C7})$$

All other eigenvalues are flushed to 0. In fact, we can safely assume that under low rank perturbations of the noise bulk, all eigenvalues except the leading one lie inside the bulk. In that case, thanks to the identity

$$\text{P.V.} \int dy \frac{\rho_Z(y)}{x - y} = \frac{x}{2}, \quad x \in \mathbb{R}. \quad (\text{C8})$$

it is straightforward to see that (C2) yields 0 for all such eigenvalues.

Therefore the estimator given by the RIE in the low rank limit (recall $M = 1$) would read

$$\left\langle \frac{\mathbf{X}\mathbf{X}^\top}{N} \right\rangle_{\mathbf{Y}} = \mathbf{u}_Y \mathbf{u}_Y^\top \left(1 - \frac{1}{\lambda}\right), \quad (\text{C9})$$

where \mathbf{u}_Y is the eigenvector corresponding to the leading eigenvalue z^* of \mathbf{Y} . This estimator is also Bayes-optimal when the prior on \mathbf{X} is rotational invariant, and the MSE attained is

$$\text{MSE} = 1 - \left(1 - \frac{1}{\lambda}\right)^2. \quad (\text{C10})$$

This MSE is attained by the RIE regardless of the prior, and is equal to that of naive PCA [17]. This argument thus supports the sub-optimality of the RIE in the limit $\alpha \rightarrow 0$, unless there is a discontinuous behavior in α .

Appendix D: The Sakata and Kabashima replica approach to (53)

Here we adapt to our model the method of [3] developed originally for dictionary learning in an optimisation setting, then concurrently extended in [78–80] to the Bayesian case. In order to match notations, we consider the generic output channel

$$Y_{ij} \sim P_{\text{out}}\left(\cdot \mid \frac{\mathbf{X}_i \cdot \mathbf{X}_j}{\sqrt{N}}\right), \quad 1 \leq i < j \leq N. \quad (\text{D1})$$

The free entropy we are interested in computing, to be later connected to the MI, is

$$\tilde{\phi}_N := \frac{1}{MN} \mathbb{E} \ln \tilde{\mathcal{Z}}(\mathbf{Y}) - \frac{1}{MN} \mathbb{E} \ln \prod_{i < j} P_{\text{out}}(Y_{ij} \mid 0) \quad (\text{D2})$$

where

$$\tilde{\mathcal{Z}}(\mathbf{Y}) := \int dP_X(\mathbf{x}) \prod_{i < j, 1}^N P_{\text{out}}\left(Y_{ij} \mid \frac{\mathbf{x}_i \cdot \mathbf{x}_j}{\sqrt{N}}\right). \quad (\text{D3})$$

We proceed to the computation of the log partition function with the replica method:

$$\mathbb{E} \tilde{\mathcal{Z}}^n(\mathbf{Y}) = \int \prod_{i < j}^N dY_{ij} \int \prod_{a=0}^n dP_X(\mathbf{x}^a) \prod_{i < j, 1}^N P_{\text{out}}\left(Y_{ij} \mid \frac{\mathbf{x}_i^a \cdot \mathbf{x}_j^a}{\sqrt{N}}\right). \quad (\text{D4})$$

We now introduce a constraint on the overlaps

$$\mathbb{E} \tilde{\mathcal{Z}}^n(\mathbf{Y}) \propto \int \prod_{i < j}^N dY_{ij} \int \prod_{a=0}^n dP_X(\mathbf{x}^a) \int \prod_{a,b=0}^n dQ_{ab} \delta(NMQ_{ab} - \text{Tr}[\mathbf{x}^a \mathbf{x}^{b\top}]) \prod_{a=0}^n \prod_{i < j, 1}^N P_{\text{out}}\left(Y_{ij} \mid \frac{\mathbf{x}_i^a \cdot \mathbf{x}_j^a}{\sqrt{N}}\right). \quad (\text{D5})$$

Now we aim at identifying the joint law of the variables

$$z_{ij}^a = \frac{\mathbf{x}_i^a \cdot \mathbf{x}_j^a}{\sqrt{N}}, \quad 1 \leq i < j \leq N. \quad (\text{D6})$$

More precisely, let us introduce a delta function to isolate these variables

$$\int d\mathbf{Y} \int \prod_{a,b=0}^n dQ_{ab} \int \prod_{a=0}^n dP_X(\mathbf{x}^a) \prod_{a,b=0}^n \delta(NMQ_{ab} - \text{Tr}[\mathbf{x}^a \mathbf{x}^{b\top}]) \prod_{i < j, 1}^N \prod_{a=0}^n \delta\left(z_{ij}^a - \frac{\mathbf{x}_i^a \cdot \mathbf{x}_j^a}{\sqrt{N}}\right) P_{\text{out}}(Y_{ij} \mid z_{ij}^a) \quad (\text{D7})$$

and let us isolate their non normalised probability measure for a given value of the overlaps Q_{ab} :

$$\int \prod_{a=0}^n dP_X(\mathbf{x}^a) \prod_{a,b=0}^n \delta(NMQ_{ab} - \text{Tr}[\mathbf{x}^a \mathbf{x}^{b\top}]) \prod_{i < j, 1}^N \prod_{a=0}^n \delta\left(z_{ij}^a - \frac{\mathbf{x}_i^a \cdot \mathbf{x}_j^a}{\sqrt{N}}\right). \quad (\text{D8})$$

The key assumption is then to consider the z 's as a Gaussian family with zero mean and a covariance equal to

$$\mathbb{E}_z z_{ij}^a z_{kl}^b = \alpha Q_{ab}^2 \delta_{ik} \delta_{jl}. \quad (\text{D9})$$

This ‘‘Gaussian ansatz’’ allows to move forward with the replica approach. With the above covariance structure, coupled only in replica space, we can write

$$P_z((z_{ij}^a)_{a \leq n} \mid (Q_{ab})_{a,b=0}^n) = \frac{1}{\sqrt{(2\pi)^{n+1} \det \mathcal{T}}} \exp\left[-\frac{1}{2} \sum_{a,b=0}^n z_{ij}^a z_{ij}^b (\mathcal{T}^{-1})_{ab}\right] \quad (\text{D10})$$

with $\mathcal{T} := (\alpha Q_{ab}^2)_{a,b=0}^n$. Hence we can replace

$$\int \prod_{a=0}^n dP_X(\mathbf{x}^a) \prod_{a,b=0}^n \delta(NMQ_{ab} - \text{Tr}[\mathbf{x}^a \mathbf{x}^{b\top}]) \prod_{i < j, 1}^N \prod_{a=0}^n \delta\left(z_{ij}^a - \frac{\mathbf{x}_i^a \cdot \mathbf{x}_j^a}{\sqrt{N}}\right) \approx P_z((z_{ij}^a)_{a \leq n} \mid (Q_{ab})_{a,b=0}^n) e^{\ln V(Q)} \quad (\text{D11})$$

where

$$V(Q) := \int \prod_{a=0}^n dP_X(\mathbf{x}^a) \prod_{a,b=0}^n \delta(NMQ_{ab} - \text{Tr}[\mathbf{x}^a \mathbf{x}^{b\top}]), \quad (\text{D12})$$

is a normalisation. Therefore the replicated partition function reads

$$\mathbb{E} \tilde{\mathcal{Z}}^n(\mathbf{Y}) \propto \int \prod_{a,b=0}^n dQ_{ab} \exp(\ln V(Q)) \left[\mathbb{E}_{\mathbf{z} \sim \mathcal{N}(0; \mathcal{T})} \int dY \prod_{a=0}^n P_{\text{out}}(Y \mid z^a) \right]^{N^2/2}. \quad (\text{D13})$$

Letting N and M diverge we get the following expression by saddle point w.r.t. the integration variables $(Q_{ab})_{0 \leq a, b \leq n}$:

$$\frac{1}{MN} \ln \mathbb{E} \tilde{\mathcal{Z}}^n(\mathbf{Y}) = \text{extr}_+ \left\{ \frac{1}{MN} \ln V(Q) + \frac{1}{2\alpha} \ln \mathbb{E}_{\mathbf{z} \sim \mathcal{N}(0; \mathcal{T})} \int dY \prod_{a=0}^n P_{\text{out}}(Y \mid z^a) \right\} + o_N(1). \quad (\text{D14})$$

Now we specify our saddle point to the replica symmetric ansatz: $\mathcal{T}_{RS} = \alpha(1 - q^2)\delta_{ab} + \alpha q^2$, and we then send $n \rightarrow 0$. Here we have further imposed that $Q_{a0} = q = Q_{ab}$ for any $a \neq b$, and $v = Q_{aa}$ for all $a = 0, \dots, n$, which amounts to impose the Nishimori identities on the solution of the saddle point. This is justified by the the Bayes-optimal setting. The computation of $V(Q)$ also requires the introduction of Fourier delta representations. These steps are standard, and we defer the reader to [78] for this computation, since for what $V(Q)$ is concerned, it is identical. In the end one gets:

$$\frac{1}{MN} \ln V(Q) = -n \text{extr}_+ \left\{ \frac{rq}{2} + \mathbb{E} \ln \int dP_X(x) \exp \left[(\sqrt{r}Z + rX)x - \frac{r}{2}x^2 \right] \right\} + O(n^2) \quad (\text{D15})$$

where extremization is w.r.t. r . The other term is easily dealt with:

$$\begin{aligned} \frac{1}{\alpha} \ln \mathbb{E}_{\mathbf{z} \sim \mathcal{N}(0; \mathcal{T})} \int dY \prod_{a=0}^n P_{\text{out}}(Y | z^a) &= \\ &= \frac{n}{\alpha} \mathbb{E}_{u_0, \zeta} \int dY P_{\text{out}}(Y | \sqrt{\alpha(v^2 - q^2)}u_0 + \sqrt{\alpha q^2}\zeta) \ln \mathbb{E}_u P_{\text{out}}(Y | \sqrt{\alpha(v^2 - q^2)}u + \sqrt{\alpha q^2}\zeta) + O(n^2). \end{aligned} \quad (\text{D16})$$

We reach

$$\begin{aligned} \frac{1}{MNn} \ln \mathbb{E} \tilde{\mathcal{Z}}^n(\mathbf{Y}) &= \text{extr}_+ \left\{ -\frac{rq}{2} + \mathbb{E} \ln \int dP_X(x) \exp \left[(\sqrt{r}Z + rX)x - \frac{r}{2}x^2 \right] \right. \\ &\quad \left. + \frac{1}{2\alpha} \mathbb{E}_{u_0, \zeta} \int dY P_{\text{out}}(Y | \sqrt{\alpha(1 - q^2)}u_0 + \sqrt{\alpha q^2}\zeta) \ln \mathbb{E}_u P_{\text{out}}(Y | \sqrt{\alpha(1 - q^2)}u + \sqrt{\alpha q^2}\zeta) \right\} + o_N(1) + O(n), \end{aligned} \quad (\text{D17})$$

where extremization is always intended w.r.t. r, q . Specifying to Gaussian channel

$$P_{\text{out}}(y | x) = \frac{1}{\sqrt{2\pi}} \exp \left(-\frac{1}{2}(y - \sqrt{\lambda}x)^2 \right). \quad (\text{D18})$$

one gets

$$\text{extr}_+ \left\{ -\frac{rq}{2} + \mathbb{E} \ln \int dP_X(x) \exp \left[(\sqrt{r}Z + rX)x - \frac{r}{2}x^2 \right] - \frac{1}{4\alpha} \ln(1 + \lambda\alpha(1 - q^2)) - \frac{1}{4\alpha} \log 2\pi e \right\} + O(n) \quad (\text{D19})$$

and we can now subtract the term

$$\frac{1}{MN} \mathbb{E} \ln \prod_{i < j}^N P_{\text{out}}(Y_{ij} | 0) = \frac{1}{2\alpha} \mathbb{E} \ln P_{\text{out}}(Y | 0) + o_N(1) = -\frac{1}{4\alpha} \log 2\pi e - \frac{\lambda}{4}. \quad (\text{D20})$$

Putting altogether we get the free entropy

$$\tilde{\phi} = \lim_{N \rightarrow \infty} \tilde{\phi}_N = \text{extr}_+ \left\{ \frac{\lambda}{4} - \frac{rq}{2} + \mathbb{E} \ln \int dP_X(x) \exp \left[(\sqrt{r}Z + rX)x - \frac{r}{2}x^2 \right] - \frac{1}{4\alpha} \ln(1 + \lambda\alpha(1 - q^2)) \right\}. \quad (\text{D21})$$

For Gaussian channel, in order to obtain the MI it is sufficient to subtract $\lambda/4$ from the above and flip the sign:

$$\iota(\alpha, \lambda) = \text{extr}_- \left\{ \frac{rq}{2} + \frac{1}{4\alpha} \ln(1 + \lambda\alpha(1 - q^2)) - \mathbb{E} \ln \int dP_X(x) \exp \left[(\sqrt{r}Z + rX)x - \frac{r}{2}x^2 \right] \right\}, \quad (\text{D22})$$

where r and q have to be extremized. This formula matches (53).